2004

Behavior of Pile-Supported Integral Abutments at Bridge Sites with Shallow Bedrock

John Gordon DeLano
University of Maine - Main

BEHAVIOR OF PILE-SUPPORTED INTEGRAL ABUTMENTS AT BRIDGE SITES WITH SHALLOW BEDROCK

By

John Gordon DeLano

B.S. University of Maine, 2002

A THESIS

Submitted in Partial Fulfillment of the

Requirements for the Degree of

Master of Science

(in Civil Engineering)

The Graduate School

The University of Maine

May, 2004

Advisory Committee:

Thomas C. Sandford, Associate Professor of Civil Engineering, Co-Advisor

William G. Davids, Assistant Professor of Civil Engineering, Co-Advisor

Dana N. Humphrey, Professor of Civil Engineering

BEHAVIOR OF PILE-SUPPORTED INTEGRAL ABUTMENTS AT BRIDGE SITES WITH SHALLOW BEDROCK

By John Gordon DeLano

Thesis Co-Advisors: Dr. Thomas C. Sandford, and Dr. William G. Davids

An Abstract of the Thesis Presented
in Partial Fulfillment of the Requirements for the
Degree of Master of Science
(in Civil Engineering)
May, 2004

The advantages of constructing bridges with integral abutments are recognized by transportation agencies worldwide. However, pile supported integral abutments are limited to locations where the depth of overburden can provide fixed support conditions. In Maine, there are often cases where the depth to bedrock prohibits integral abutment bridges from being used. The goal of this research is to determine the feasibility of constructing integral abutments in conditions that cannot provide the fixed support conditions that are traditionally assumed.

A finite element model was created that incorporates realistic constitutive and surface interaction models. These models allow for a good prediction of the soil/structure interaction and the structural response. Three critical model responses were identified: pile stresses, pile kinematics, and pile/bedrock interaction. These responses were examined in later parametric studies, which investigated how changes in girder length,

pile length, loading, geometry, member properties, and subsurface conditions influenced the pile responses.

It was shown that for piles less than 4 m in length on bedrock, the tip of the pile rotates but does not translate horizontally or vertically. This is similar, in principle, to a column with a pinned support. Dead and live loading of the girder induces a rotation of the abutments, which causes pile head displacement. Typically, displacements due to thermal loading are the only lateral pile displacements considered in integral abutment design. Under cyclic live and thermal loading, plastic deformation of the pile did not accumulate if the strains in the head were kept below 125% of the yield strain (1.25 ε_y). Observations of behavior from the parametric study were used as a basis for a set of design guidelines for piles that did not meet the length criteria of the current Maine Department of Transportation procedure.

Using the criteria that pile head strains are kept below 1.25 ε_y, pile head moments based on data from the parametric studies are calculated from a relationship with the axial load. These relationships were created for various soil conditions and loadings, as well as pile sections. Forces at the pile tip are estimated from the moments at the head of the pile in order to determine if the pinned idealization is valid for the proposed pile/soil/load combinations. The ratio of shear forces and normal forces are compared to an equivalent coefficient of friction between the pile tip and bedrock, along with a factor of safety.

The proposed design procedure results in values of moments and shear forces that are higher than those obtained from the finite element model. This is due to the inherent conservatism built into the methods used to calculate pile forces, which presents a worst-case design scenario. The proposed method expands the application of integral

abutments to instances where an integral abutment supported by short piles is currently considered impractical. However, even with the expanded design criteria, finite element modeling indicates that there are cases where the combination of geometry, loading, and subsurface conditions may prohibit the use of integral abutments.

DEDICATION

This thesis is dedicated to my parents, John W. and Joan DeLano. Without their inspiration, love, and support, none of my accomplishments would have been (or ever will be) possible.

ACKNOWLEDGEMENTS

I would like to acknowledge the Maine Department of Transportation for providing the funding for this research. My appreciation goes to John Buxton and Dale Peabody for their continual support of this project. Special thanks goes to Laura Krusinski, who not only provided support from within MDOT, but also deserves credit for getting this project off the ground and headed in the right direction.

I would also like to thank Dana Humphrey for serving as the third member of my graduate committee.

Considerable thanks goes to my advisors and friends Tom Sandford and Bill Davids for having confidence in my abilities, even when I did not. They also deserve a lot of praise for being able to put up with my behavior, manners, and vocabulary, which was often times good, bad, bizarre, or anywhere in between. I feel truly fortunate to have had the opportunity to work with two exceptional people who could come at problems from totally different directions, and both arrive at the best solution.

Bill, thank you for being a guru for all things structural and numerical. I especially appreciate you not jumping over your desk and strangling with me when I asked you "stupid" questions, even when it was the same stupid question over and over again. Your guidance in finite element analysis and bridge engineering definitely helped me finish this research. However, the conversations about Zeppelin and the Stones, graduate school, and life in general will stick with after all the lines of code are long since forgotten.

Tom, I credit you with bringing me over from structural engineering to geotechnical. You showed me that while the shortest distance between two points is a straight line, sometimes a tangent (usually in the opposite direction) makes for a more interesting trip. I enjoyed how a simple question about soil properties or pile design would often turn into a half-hour discussion on the Red Sox. I have a feeling that in the future, if I just come walking into your office like I do now, I will still be greeted with an "Oh, there he is…" like you were expecting me any moment. Don't change, ever.

Finally, I wouldn't have seen this research through to the end without the help of my friends, fellow grad students, and family. Thanks to Scott, Bryan, Chris H. and even Sarah for giving me feedback, entertainment, and much needed diversions from research. My eternal gratitude to Dan Heathcote for helping me pull data off of a crashed hard drive in the 11^{th} hour. Extra special appreciation goes to my wife Nicole DeLano for her endless encouragement, optimism, and love.

Later, dudes.

TABLE OF CONTENTS

LIST OF TABLES

LIST OF FIGURES

LIST OF SYMBOLS AND ABBREVIATIONS

a ..... y-intercept of K_f line on a p-q diagram

A_{actual} ..... Cross-sectional area of actual bridge component

AASHTO ..... American Association of State Highway and Transportation Officials

AISC ..... American Institute of Steel Construction

AISI ..... American Iron and Steel Institute

A_{model} ..... Cross-sectional area of model bridge component

A_p ..... Cross-sectional area of pile

A_s ..... Gross effective area of column cross-section

AT ..... Alberta Transportation

b_f ..... Width of pile section parallel to flange

c ..... Cohesion yield stress

c' ..... Effective cohesion yield stress

C ..... Equivalent AASHTO moment factor

C_i ..... Inelastic rotation capacity reduction factor

C_u ..... Undrained shear strength

d ..... Depth of pile section parallel to web

d_m ..... Dimension of model pile along z-z axis

D_1 ..... Bending moment coefficient for determination of M_1

D_2 ..... Bending moment coefficient for determination of M_2

D_3 ..... Ductility coefficient

DOF ..... Degrees of Freedom

DOT ..... Department of Transportation

E_{actual} ..... Young's modulus of actual bridge component

E_g ..... Young's modulus of bridge girder

E_i ..... Initial tangent of Young's modulus for soil

E_{model} ..... Equivalent Young's modulus of model bridge component

E_p ..... Young's modulus of pile

E_u ..... Undrained Young's modulus

f_t ..... Tensile stress in girder flange

F_b ..... Allowable bending stress

F_{cr} ..... Critical buckling stress

F_e ..... Euler buckling stress

F_{ym} ..... Equivalent yield stress of model pile

FHWA ..... Federal Highway Administration

F_{yp} ..... Yield stress of pile

i ..... Angularity of rock joint peaks

I_{actual} ..... Moment of inertia of actual bridge component

I_g ..... Moment of inertia of bridge girder

I_{model} ..... Moment of inertia of model bridge component

I_p ..... Moment of inertia of pile

k_e ..... Equivalent lateral soil stiffness parameter

k_h ..... Horizontal stiffness of soil (modulus of horizontal subgrade reaction)

K ..... Modulus number

K_c ..... Correlation factor

K_f ..... Ratio of stress conditions at failure

l_c ..... Total length of equivalent cantilever (l_u+l_e)

l_e ..... Length of equivalent cantilever below ground surface

l_u ..... Length of pile above ground surface

L ..... Length of pile below ground surface

L_S ..... Length of bridge span

LRFD ..... Load Resistance Factor Design

M ..... Moment at pile head due to R_g

M_1 ..... End moment in pile due to Δ

M_2 ..... End moment in pile due to Δ and P

M_{AD} ..... Additional moment in girder required to produce M_y

M_D ..... Moment at head of pile due to P_D

M_{DL} ..... Moment at head of pile due to P_{DL}

M_{DLT} ..... Dead and live load moment at head of pile adjusted for thermal effects

MDOT ..... Maine Department of Transportation

M_{DT} ..... Dead load moment at head of pile adjusted for thermal effects

M_{D1} ..... Moment due to permanent loads on girder (w/o deck)

M_{D2} ..... Moment due to permanent loads on girder (w/ deck)

M_p ..... Plastic moment of pile section

MTO ..... Ontario Ministry of Transportation

M_u ..... Ultimate pile strength

M_y ..... Yield moment of girder or pile

n ..... Modulus exponent

p ..... x-coordinate of stress path

p_a ..... Atmospheric pressure

P ..... Applied axial pile load

P_D ..... Axial force in pile due to dead loading

P_{DL} ..... Axial force in pile due to dead and live loading

q ..... y-coordinate of stress path

R_g ..... End rotation of bridge girder

S_{actual} ..... Section modulus of actual pile

S_{LT} ..... Long-term composite section modulus

S_{model} ..... Section modulus of model pile

S_{NC} ..... Non-composite section modulus

S_p ..... Section modulus of pile

S_{ST} ..... Short-term composite section modulus

t_f ..... Thickness of pile flanges

V ..... Applied lateral load

V_{DT} ..... Shear at pile tip due to M_{DT}

V_{DLT} ..... Shear at pile tip due to M_{DLT}

W ..... Live load reaction in bridge piles

x_n ..... Distance from pile node to neutral axis

α ..... Coefficient of thermal expansion

β_1 ..... Shear factor for calculation of V_{DT}

β_2 ..... Shear factor for calculation of V_{DLT}

Δ ..... Lateral displacement of pile head due to temperature change

Δ_b ..... Lateral displacement of pile head at allowable bending stress

ε_y ..... Yield strain

ϕ ..... Internal angle of friction

ϕ' ..... Effective internal angle of friction

φ ..... Slope of K_f line on a p-q diagram

μ ..... Coefficient of friction

ν ..... Poisson's ratio

θ_1 .....Dead load rotation of non-composite and long-term composite sections

θ_2 .....Dead load rotation of short-term composite section

θ_3 .....θ_1 + live load rotation of short-term composite section

θ_4 .....θ_2 + live load rotation of short-term composite section

ρ ..... Mass density

σ_1 ..... Applied vertical stress

σ_3 ..... Confining stress

σ_a ..... Average normal stress

σ_p ..... Pile stress due to M

τ_e ..... Equivalent shear stress

τ_i ..... Shear stress at rock joint interface

ψ ..... Dilation angle

Chapter 1

INTRODUCTION

1.1. Background

Standard steel and concrete girder bridges require expansion joints and bearings at abutments and internal supports to accommodate movement and stresses due to thermal expansion. However, these joints and bearings are costly to maintain, and are subject to frequent damage. Hardware can be damaged by impact from heavy vehicles and by snow removal equipment in the winter. In addition, runoff can bring sand and deicing salts into contact with the bearings and joints. Many steel and Teflon bearings eventually freeze due to either corrosion, or excessive wear from grit. Malfunctioning joints and bearings can also lead to unanticipated structural damage. The presence of joints can allow for settlement of pile-supported abutments and overturning due to active earth pressures or surcharge forces (Wasserman & Walker, 1996).

In the early 1980s, the Federal Highway Administration (FHWA) issued a report titled "Tolerable Movement Criteria for Highway Bridges" (Moulton et al., 1985). This report examined 580 bridge abutments in the United States and Canada, of which three-quarters had experienced movement that was not accounted for in the design. The report states:

> "The magnitude of the vertical movements tended to be substantially greater than the horizontal movements. This can be explained, in part, by the fact that in many instances the abutments moved inward until they became jammed against the beams or girders which acted as struts, thus preventing further horizontal movements. For those sill type abutments that had no backwalls, the horizontal movements were often substantially larger, with abutments moving inward until the beams were, in effect, extruded out behind the abutments."

This account of the condition of the abutments leads to the conclusion that the use of expansion joints and bearings to account for thermal movements tends to exacerbate maintenance problems, rather than solve them (Wasserman & Walker, 1996). In the cases where the bearings were seized, and the abutment backwalls were able to contain the expansion of the girders, the structures acted similarly to integral abutment bridges.

Integral or continuous bridges are built without expansion joints, relying on the interaction between the structure and surrounding soil to accommodate lateral forces caused by thermal contraction/expansion and braking. They are single or multiple span bridges with the superstructure cast integrally with the substructure. Generally, these bridges include capped pile stub abutments. Piers for integral abutment bridges may be constructed either integrally with or independently of the superstructure. Semi-integral bridges are defined as single or multiple span continuous bridges with rigid, non-integral foundations. Their movement systems are primarily composed of integral end diaphragms, compressible backfill, and movable bearings in a horizontal joint at the superstructure-abutment interface (Mistry, 2000).

Allowance for seasonal thermal expansion or contraction is provided using an approach slab and a sleeper slab. A crack in the pavement forms at the termination of the approach slab, preventing pavement buckling, or bulging. Infiltration of runoff, or forces from vehicular impact is far less detrimental at this location. A typical configuration of an integral abutment bridge is shown in Figure 1.1.

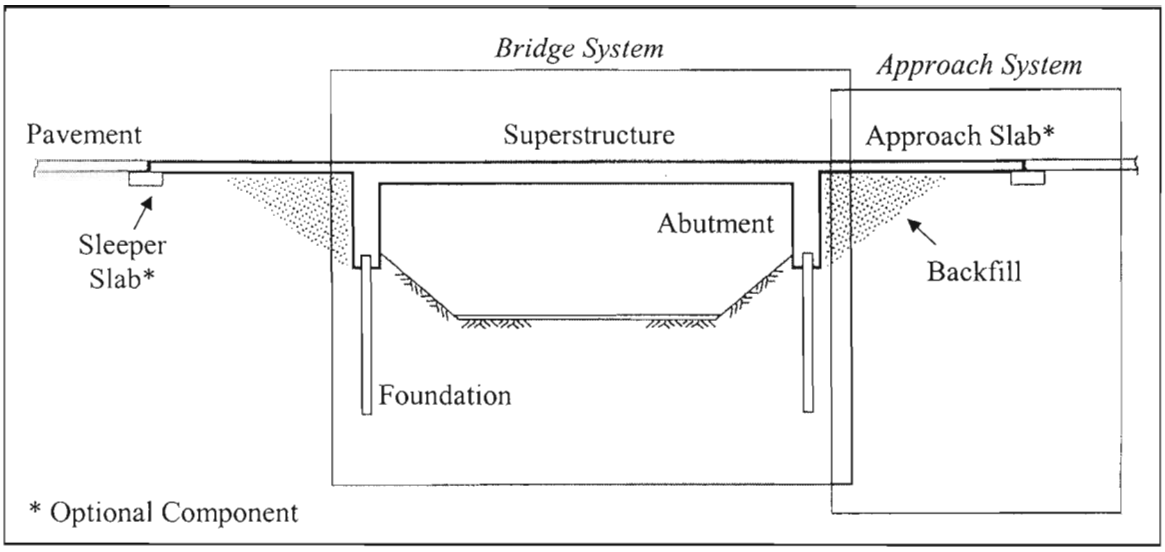

Figure 1.1. Typical components of an integral abutment bridge (Arsoy et al., 1999)

Integral abutment bridges have distinct advantages over standard bridges. Foremost, they have lower construction and maintenance costs due to elimination of joints. Construction is simple and rapid, because fewer piles are required for foundation support, and no battered piles are needed. Finally, since the superstructure is cast integrally with the foundations, bridges with integral abutments have improved seismic performance (Arsoy et al., 1999). In addition, the ratio of end-span to interior span length for girders cast integrally with the abutments can be smaller than traditional bridges, because the weight of the abutments counteracts the uplift of the girder when loaded (Wasserman & Walker, 1996).

Traditionally, the use of integral abutment bridges is limited by certain factors. Because of the unique stress and flexibility requirements of the foundations, steel H-piles are most commonly used (Burke, 1993). Limits on bridge geometry, such as length and skew are also imposed. Finally, restrictions are imposed on subsurface conditions to ensure that the foundation will be able to resist the lateral loading from the structure.

1.2. Research Objectives

Current design practices in Maine and other states limit the use of pile-supported integral abutments to sites where there is sufficient soil overburden to provide a full fixed condition for a driven pile (Krusinski, 2002). The objective of this research is to explore the feasibility and safety of pile-supported integral abutment bridges where the depth to bedrock is relatively shallow, considered in this study to be less than 4 m (13 ft) from the ground surface. If integral abutment bridges with short piles can be utilized successfully, their use in Maine could greatly increase, where bedrock is often close to the ground surface. The research objective will be accomplished in two phases.

Phase I:

a) Review of pertinent literature on the behavior and design of pile-supported integral abutments.

b) Parametric studies will be conducted using finite element analysis, to determine the effects of various design parameters, including pile length, on the bridge and foundation response.

c) Development of a preliminary set of design guidelines for short pile-supported integral abutment bridges.

Phase II:

a) Instrumentation and analysis of a short pile integral abutment bridge to be constructed in Coplin Plantation, Maine.

b) Finite element model verification using data from instrumented bridge.

c) Development of final design guidelines for short-pile integral abutment bridges, incorporating data from both the finite element model and an actual bridge.

1.3. Organization of this Thesis

This thesis deals with the work performed in conjunction with Phase I of the research. It will be organized according to the tasks listed for this phase. Chapter 2 contains a literature review that focuses on aspects of modeling and integral abutment pile design relevant to this project. Chapter 3 discusses the development of the finite element model used to perform the parametric studies. Details of the model that are covered include formulation of material properties, development of model geometry, and model/material verification. Chapter 4 describes the finite element parametric studies used to study the response of short-pile integral abutment bridges. The results of these studies are used to develop a set of preliminary design guidelines for short-pile integral abutment bridges, which are presented in Chapter 5. A summary of research findings, conclusions, and recommendations for future research is given in Chapter 6.

Chapter 2

REVIEW OF RELEVANT LITERATURE

Integral bridges are not a recent development and even occur naturally in the form of arches carved from bedrock by water and wind. For man-made integral structures, one need not look further than the unreinforced concrete arch bridges built by the ancient Romans (Burke, 1993). True integral abutment bridges with continuous beams began to appear after the 1940s. Since the early 1960s, the number of integral or continuous bridges constructed worldwide has increased dramatically. As of 1999, more than 30 American state and Canadian provincial transportation agencies have constructed over 9700 bridges with integral abutments (Kunin & Alampalli, 2000).

Although the benefits of constructing integral abutment bridges are clear, suitable methods for their design and analysis are somewhat uncertain. While the American Association of State Highway and Transportation Officials (AASHTO) Load Resistance Factor Design (LRFD) Bridge Design Specification (AASHTO, 1998) does not directly address specific methods of analysis, it recommends that "Integral abutment bridges shall be designed to resist and/or absorb creep, shrinkage, and thermal deformations of the superstructure." Many states have developed in-house design practices for bridges with integral abutments, and several researchers have proposed methods for design and analysis as well. Numerous papers have been published on the design of piles for the support of integral abutments. Increasingly, results from finite element models along with field data have been used to validate these design processes. It is unclear if the work that has been done on integral abutments to this point can be applied to integral abutments founded on short piles.

This literature review gives a brief overview of the current practice in the design and construction of bridges with integral abutments. It reviews research conducted thus far, including full-scale and field testing, mathematical models created for analysis, and some of the design procedures that have been developed. Knowledge garnered from this review will be put towards the creation of modeling and design methods for short-pile integral abutment bridges.

2.1. Planning, Design, and Construction of Integral Abutments

The results of several studies on integral abutment best practices are summarized in this section. This review focuses on surveys performed by transportation agencies in the United Kingdom (U.K.), Canada, and the United States (U.S.). The Canadian surveys focus on the practices employed by the provinces of Alberta and Ontario. The survey of U.S. transportation agencies performed by Kunin and Alampalli (2000) encompasses over 30 states and Canadian provinces, excluding Alberta and Ontario. Each section discusses the planning, design, and construction considerations of these world regions.

2.1.1. Current Practice in the United Kingdom

The construction of integral bridges in the U.K. is different from that in the U.S. or Canada, mainly due to the various forms of integral bridges used. Figure 2.1 depicts the six abutment configurations considered integral. Of these six structures, only the frame, embedded, and bank pad abutments, or slight variations of the three are used in the U.S. or Canada. In a paper titled "The Design of Integral Bridges", (Highways Agency, 1996) the British Highways Agency does not specifically limit the sites at which integral

bridges can be constructed as many agencies do. In this paper, the only general limitation is that the longitudinal movement of the abutments cannot exceed 20 mm (0.75 in).

The design of integral bridges in the U.K. is straightforward in that they are essentially designed in the same manner as jointed bridges, except that they must be able to accommodate thermal expansion and passive earth forces. Integral bridges in the U.K. must be stronger than their American counterparts, due to the higher design speeds and heavier design loading in the U.K. In certain cases, AASHTO design loads are 60% of the U.K. highway loading for bridges in the 40-60 m (130-200 ft) span range (Taylor, 1999). Integral bridges may be founded on piles or spread footings. Piles must be designed to accommodate displacement and support axial loads, as well as resist forces due to the movement of the pile or surrounding ground.

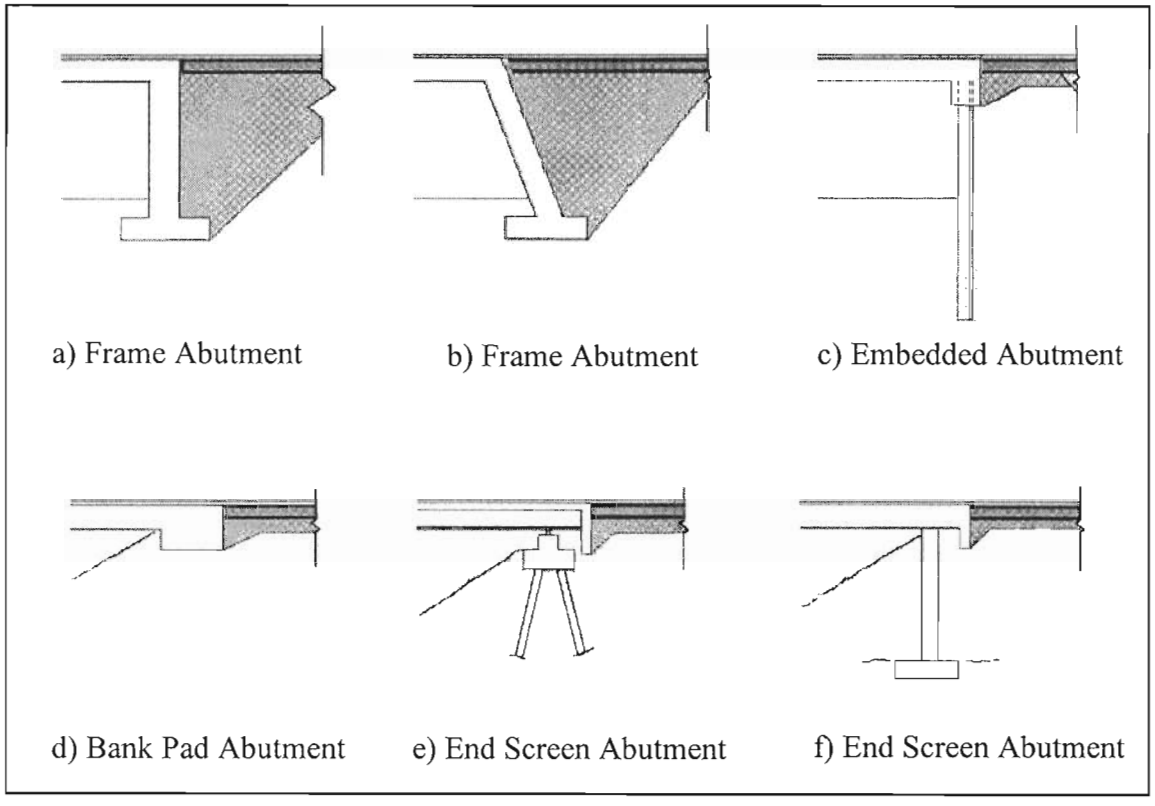

Figure 2.1. Types of integral abutments (Highways Agency, 1996)

The Highways Agency does not specify construction details such as approach, or run-on, slabs. Taylor (1999) describes a 1997 tour of integral abutments in the U.S. and Canada, which was attended by six engineers from the U.K. Department of Trade. They felt that the ride quality they experienced over displaced and settled run-on slabs would not be acceptable in the U.K. Instead of promoting or forbidding approach slabs, their recommendation was to rely on higher specification of backfill material and accept any pavement damage that occurs as a result of not having cycle control devices.

The abutment backfill is a designed material, with properties specified to provide a balance between stiffness and flexibility. In general, granular materials comprising compacted rounded particles of uniform grading can have a peak angle of internal friction, ϕ, as low as 35°, and may accommodate thermal expansion without high earth pressures. However, these soils are somewhat vulnerable to settlement. Fill of compacted, well-graded, hard angular particles can have a peak angle of internal friction as high as 55° with very high resistance to thermal expansion. These soils are less vulnerable to settlement (Highways Agency, 1996).

2.1.2. Current Practice in Canada

Alberta Transportation (AT) and the Ontario Ministry of Transportation (MTO) favor the use of semi-integral and pinned-integral bridges as opposed to the integral abutment bridges that are more commonly used elsewhere. Semi-integral abutment bridges have a deck and girder that is continuous with the approach slabs, thereby eliminating the need for an expansion joint. However, unlike full integral abutments, the superstructure unit is not continuous with the abutments. In a pinned-integral abutment,

the superstructure is embedded in a large concrete block called a diaphragm. The diaphragm is then connected to an abutment seat using a steel pin and bearing pad assembly. Both semi-integral and pinned configurations eliminate the transfer of moment between the abutments and girder ends. Semi-integral and pinned-integral abutment designs are not as cost effective and easy to construct as fully integral abutments. However, they can be used at sites where AT or MTO may not usually use a standard integral abutment, such as sites with large skew, long spans, or poor soil conditions. Examples of pinned and semi-integral abutment details are given in Figure 2.2.

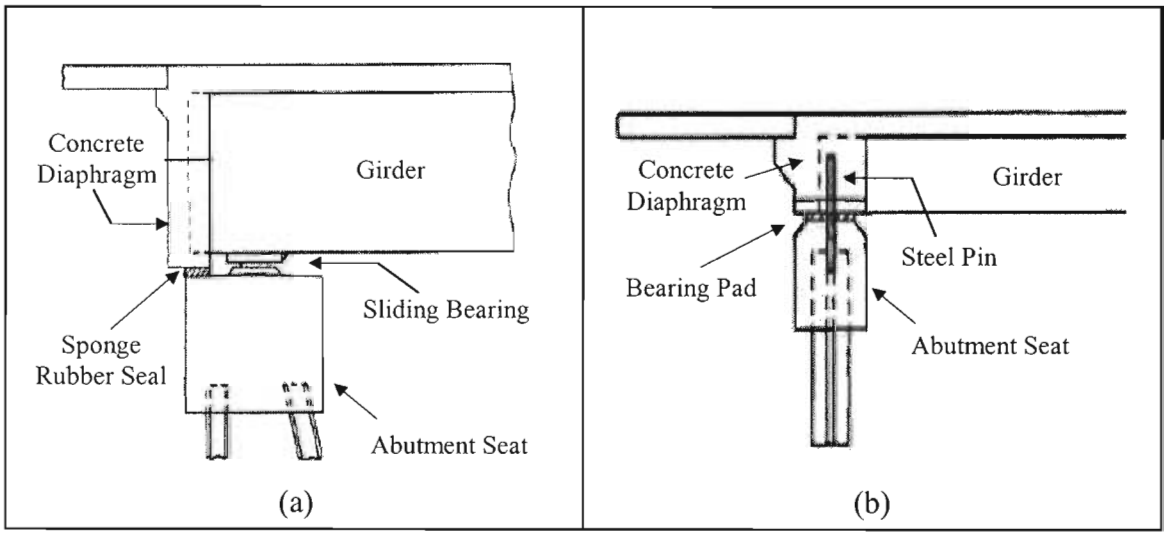

Figure 2.2. Examples of (a) Semi-Integral and (b) Pinned-Integral abutment configurations (Alberta Transportation, 2003)

2.1.2.1. Selection Criteria for Integral Abutment Bridges

During the planning stage, several factors are considered that determine the feasibility of using an integral abutment over a standard girder bridge. The length to be spanned is considered as a limiting factor. In Ontario, the total girder length is limited to 150 m (492 ft), which is based on the MTO's success and experience with integral

abutment bridges (Husain and Bagnariol, 2000). Integral bridges in Alberta are generally less than 50 m (164 ft) long, with a few bridges as long as 75 m (264 ft). In Appendix C of the AT Design Manual (2003), Yu notes that 95% of all bridges in Alberta are less than 100 m (328 ft) in length. Both agencies prefer to use concrete decks on steel girders, although prestressed concrete girders are also used.

The geometry of the bridge plays an important role in the feasibility of bridges with integral abutments. For full integral abutments, MTO prefers skew angles of less than 20°. Skews of up to 35° are allowed, but only if a thorough analysis is performed to determine the skew effects. The analysis must consider the effects of variables such as torsion, unequal load distribution, lateral torsion, etc. Semi-integral abutments do not have a limit on skew angle. Abutment height is limited to 6 m (20 ft), and wingwall length is limited to 7 m (23 ft) for all types of integral abutment bridges. While these provisions are intended to reduce the amount of soil pressure on the abutments, the minimum height of integral abutments should provide adequate protection from frost penetration. AT has geometric limits similar to MTO, however skews for all integral bridges are generally less than 30°. They advise that abutment heights should be kept as short as possible to reduce earth pressures.

MTO limits the use of integral abutments based on subsurface soil conditions. Sites where caissons or piles less than 5 m (16 ft) in length are planned for a foundation are considered unsuitable for integral abutment bridges. Integral abutments are not utilized at sites with soils susceptible to liquefaction, slip failure sloughing, or boiling. Sites with dense soil require piles to be installed in preaugured holes filled with loose sand. Use of semi-integral bridges are not as restricted and are subject to the same

general requirements as jointed bridges. It can be assumed that the AT restrictions on use of integral abutment bridges with regards to soil conditions are similar to that of the MTO, since the AT design guidelines draw in part from those of the MTO (Alberta Transportation, 2003).

2.1.2.2. Design and Construction of Integral Abutment Bridges

Once the decision to use an integral abutment is made, the design process begins. MTO Structures Office Report SO-96-01 by Husain and Bagnariol (1996) outlines a rational design method for integral abutments, which is used by both MTO and AT. This method is similar to the rational method proposed by Abendroth & Greimann (1988), which is discussed in Section 2.3. Husain & Bagnariol (2000) state, "In general, the analysis and design of semi-integral bridges are the same as those for conventional jointed bridges." MTO does not require any special design considerations for semi-integral bridges, except for the effect of the backfill pressure against the abutments and wingwalls. Both agencies specify that integral abutment bridges be founded on flexible piles, although AT does allow integral abutments to be constructed on shallow footings in some cases. The preferred pile type for the support of integral abutments is a steel H-pile oriented such that bending occurs about the weak axis. In skewed bridges, the web of the pile is oriented perpendicular to the direction of the girder.

The considerations for the construction of integral abutment bridges are virtually identical for both Ontario and Alberta. Both agencies are most concerned with the construction details and cycle control joints at the end of the approach slabs. Provisions are made to allow the bituminous pavement to better compensate for structural

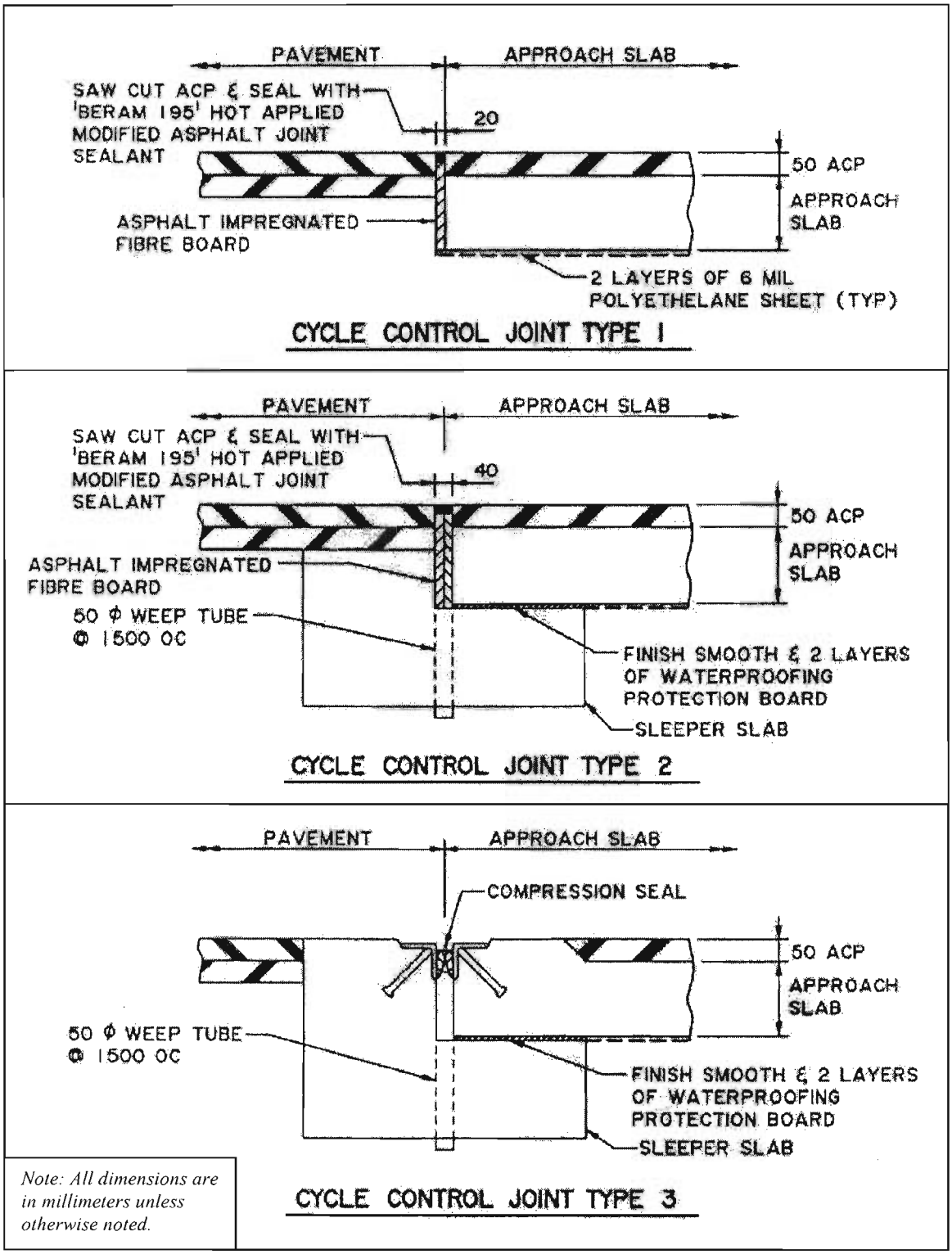

Figure 2.3. Typical expansion systems for steel and concrete girder integral bridges (Alberta Transportation, 2003)

movements, by controlling the location and depth of cracking. Typical cycle control joint details from the AT Design Manual are shown in Figure 2.3. The cycle control details for MTO are identical to the Type 1 and Type 3 joints of AT. The type of cycle control detail to be used is chosen based on the girder material, overall structure length, seasonal temperature variation, and capacity for movement of the structural system. Cycle control system recommendations for MTO and AT are given in Table 2.1.

Table 2.1. Suggested Joint Details for Various Span Lengths

Agency	Steel Girders	Concrete Girders	Joint Type
Alberta (AT)	< 40 m	< 50 m	Type 1
	40 m to 75 m	50 m to 100 m	Type 2 or Type 3
	> 75 m	> 100 m	Type 4
Ontario (MTO)	< 75 m	< 100 m	Type 1
	> 75 m	> 100 m	Type 3

After Alberta Transportation (2003) and Husain & Bagnariol (2000), 1 m = 3.281 ft

Drainage and construction sequence are the other major construction details considered by AT and MTO. Both agencies specify that adequate drainage of the abutment backfill must be provided to prevent damage. This damage is due to not only frost action but also degradation of the concrete and steel by water. Construction must be scheduled, such that tasks like pouring the deck or placing approach fill do not cause any undue stresses in the structure. Fill must be placed in nearly equal lifts at both ends of the structure. This prevents the occurrence of unequal earth pressures on the abutments, as well as minimizes differential settlement.

2.1.3. Current Practice in the United States

Practices regarding integral abutment bridges vary considerably from state to state. These practices are typically based on past local experience, making them

somewhat empirical. Of the 39 transportation agencies responding to the survey by Kunin and Alampalli (2000), eight said that they had no experience with integral abutment bridges. Overall, the general opinion of integral abutment bridges was high, with most agencies describing their performance as good or excellent. The survey reports that the Arizona Department of Transportation (DOT) was the only agency with a negative opinion, commenting that Arizona DOT built 50 integral abutment bridges, and they all required expensive repairs on the approaches. Therefore, they do not recommend the use of integral abutments. The survey does not mention the nature of the problems with the approach system, or any possible causes.

A summary of survey responses regarding the number, earliest and most recent construction of, and length of longest integral abutment bridges is given in Table 1 in the article by Kunin & Alampalli (2000). Integral abutment construction was reported as early as 1905, and as recently as at the time of survey. The longest precast concrete girder structure was a 358 m (1176 ft) bridge built in Tennessee. The longest steel and cast-in-place concrete girder bridges were both built in Colorado, measuring 318 m (1045 ft) and 290 m (953 ft), respectively. Typically, the integral abutments in the U.S. are the full integral type, with some states using pinned-abutment details with concrete girder superstructures, or integral abutments founded on spread footings. A typical integral abutment detail used by the Maine Department of Transportation (MDOT) is shown in Figure 2.4.

2.1.3.1. Selection Criteria for Integral Abutment Bridges

Similar to agencies in Canada, state transportation agencies consider several factors that determine whether an integral abutment is a viable choice for a certain

location. In order to control the thermal expansion and contraction, agencies in the U.S. limit either the length of the girders or the magnitude of thermal movements. While both measures aim to accomplish the same goal, agencies that limit the girder length tend to tolerate larger thermal movements. These thermal movements are based on the temperature ranges suggested for cold and moderate climates in Article 3.16 of the AASHTO Bridge Design Specifications (1998).

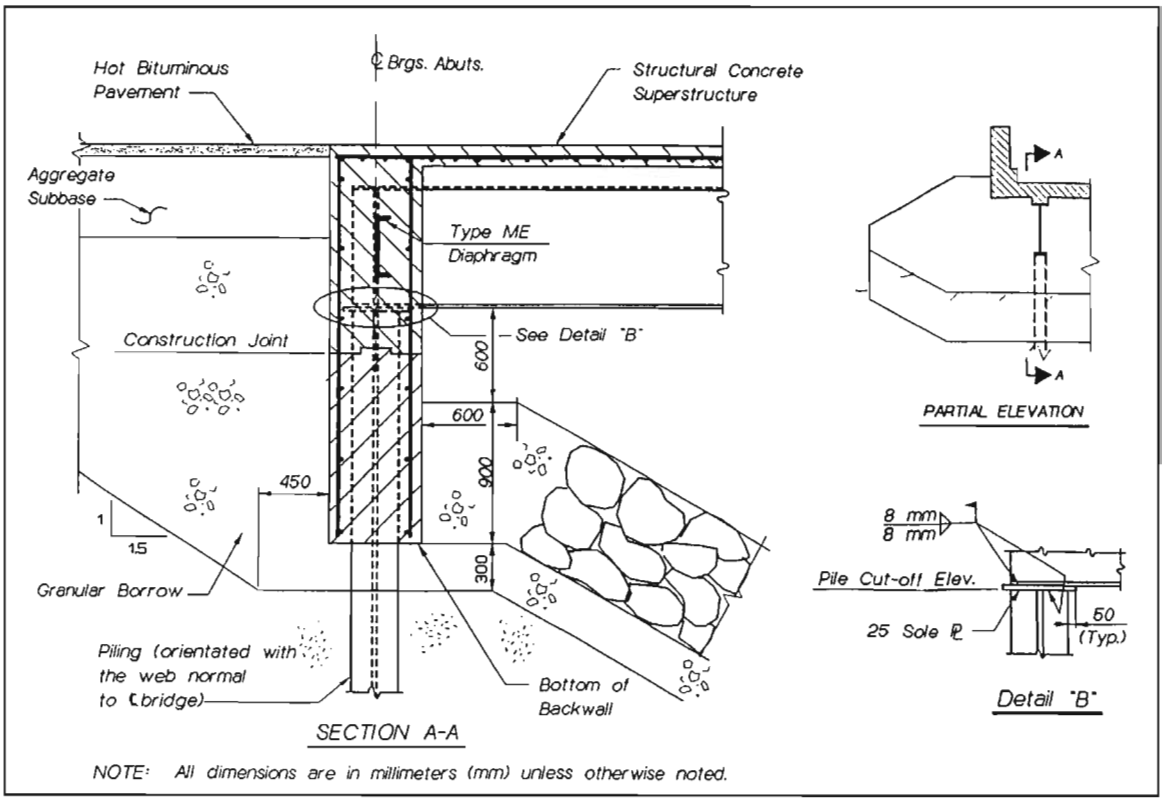

Figure 2.4. MDOT integral abutment detail (MDOT, 1999)

There are several other limiting factors considered by agencies in the U.S. According to the survey responses, skew is generally limited to 30°. However, one agency allowed no skew, while others have no skew limitations. There are various limits on abutment height and stem height as well. Kunin & Alampalli (2000) summarize the responses in regard to allowable limits in Table 2 of their article.

2.1.3.2. Design and Construction of Integral Abutment Bridges

The design process among state agencies is as varied as the limits imposed on geometry or thermal expansion. For the most part, passive soil pressure is used in abutment design, applied in distributions such as uniform or triangular. Massachusetts has started determining design earth pressures based on tests of an instrumented full-scale wall, while states such as North Dakota, California, and Alaska assume an ultimate passive soil pressure based on Rankine or similar methods.

Approximately 60% of the respondents answered that skew effects are not considered with respect to calculation of soil pressures, with three states indicating that they currently have no skewed integral abutment bridges. In Colorado, the soil pressure is assumed normal to the abutment, and battered piles are used by the department of transportation to accommodate transverse loading. Maine assumes that loads on skewed abutments induce transverse forces and translation to the piles. In their response to the survey, Oregon designers expressed concern that large skew angles can result in a large torque, with soil thrust loads not opposing one another (Kunin & Alampalli 2000).

Steel H-piles are the most frequently used foundation for integral abutment bridges, but respondents have also used cast-in-pace concrete, prestressed concrete, steel pipe, and concrete-filled steel pipe piles. About half of the respondents design piles solely for axial loads; the others conduct both axial and lateral analyses. Several agencies also analyze pile stresses using various methods. Some either consider the pile to be fixed at a certain depth, with a fixed, pinned, or free connection at the head, depending on the abutment connection detail. The computer program L-PILE (Ensoft, 2002), COM624P (Wang & Reese, 1993), or an equivalent program, are used by some agencies

to analyze the pile stresses. Maine uses an allowable stress design based on rotation of the girder ends, discussed further in Section 5.1.

Kunin & Alampalli (2000) summarize the various design criteria involving pile orientations in Table 3 of their article. Three U.S. agencies differ from those listed in the table. Washington State typically alternates orientation from pile to pile within an abutment, while North Dakota orients the weak axis parallel to the abutment face. Colorado typically places the weak axis parallel to the skew direction, however for larger movements, the weak axis is oriented in the direction of movement

Much like the rest of the world, agencies in the U.S. use construction details such as approach slabs and cycle control joints, which allow movement of the abutments without causing distress to the approach pavement. Most details are similar, with the slab resting on a lip or corbel built into the abutment. Typical approach slab problems include settlement, transverse or longitudinal cracking of the slab, and cracks in asphalt overlays at the ends of approach slabs. Washington State reports difficulties with approach slabs when bridge length is more than 105 m (345 ft) (Kunin & Alampalli, 2000).

Some agencies specify treatments to the abutment backwalls and backfill in order to reduce soil pressures. Wyoming has had satisfactory performance with a 50-100 mm (2-4 in) gap between the abutment and geotextile-reinforced backfill. Michigan has used high-density foam backing on one bridge. However, the performance of the foam is difficult to evaluate since the designers themselves questioned whether the foam backing was necessary. This is a sentiment echoed by agencies that have tried similar measures. Colorado typically uses a flowable fill with low-density foam and an expansion joint, providing for movements at the end of the approach slab via cycle control structures.

When Kunin & Alampalli asked if oversized holes are predrilled before pile driving and later backfilled with granular material, eighteen of 30 agencies said no. Some use predrilled holes if certain conditions are met, such as short fixed piles, difficult driving conditions, piles in fill sections, and bridge lengths of more than 30 m (98 ft). Several provided details for size of the pile hole, minimum hole depth, type of backfill, and required density limits; which are summarized by Kunin & Alampalli (2000) in Table 4 in their article. No agencies currently use a compressible material on piles to reduce earth pressure, in the same manner as with abutments. Colorado has used a bitumen coating to reduce downdrag on piles, but has not tried to reduce earth pressure.

2.2. Behavior of Integral Abutment Piles

Integral abutments are most commonly supported by pile foundations, due to the ability of a pile to resist lateral loading while maintaining its axial capacity. Studies on the behavior of integral abutment piles have been performed both in the laboratory and in the field. Published studies on the behavior of integral abutment piles are reviewed in this section. In the past, investigations into the behavior of integral abutment piles had been limited to field studies of in-service integral abutment bridges and driven test piles. Laboratory studies of integral abutment piles, using either full-size or scaled-down models, have become popular. Most of the experimental studies involve the use of steel H-piles as the foundation type, although the study performed by Arsoy, Duncan, and Barker (2002) examined steel pipe and prestressed concrete piles as well.

2.2.1. Field Studies

Integral abutment bridges equipped with instrumentation provide valuable insight into the behavior of integral piles due to loading from traffic, earth forces, and temperature change. Many of the field studies performed are concerned more about the behavior and performance of the structure as a whole. A study of the Cass County Bridge by Jorgenson (1983) focused primarily on the responses of piles due to the thermal movements of the bridge. The Cass County Bridge is located approximately two miles north of Fargo, North Dakota. It is a 137 m (450 ft) long prestressed concrete girder bridge with integral piers and abutments, supported by H-piles.

Measures were taken in this bridge to relieve the earth pressure on the piles and abutments, and to permit longitudinal movements. The measures on the abutment consisted of a void space created with corrugated metal supported by 100 mm (4 in) thick pressure relief strips. The pressure relief strips are made from a material that will recover 96% of its thickness after being compressed to 50% of its thickness according to the manufacturer (Jorgenson, 1983).

Similar measures were taken to allow for longitudinal movement of the piles without resistance. A 400 mm (16 in) diameter hole was bored through the soil to a depth of 6 m (20 ft). Piles were then placed in the holes and driven to an average final depth of 33.5 m (110 ft). A 50 mm (2 in) thick layer of compressible material was then glued to each side of the web for the first 6 m, and the hole was backfilled with sand. Figure 2.5 provides schematics of the details of the pressure relief systems incorporated on the abutments and piles of the Cass County Bridge.

To determine deflections and stresses, the piles were instrumented with slope indicators and strain gages. The slope indicators were installed in 10.5 m (35 ft) casings attached to the edge piles of each abutment. Readings were taken at 0.6 m (2 ft) intervals, with the instrument oriented in the plane of weak axis pile bending. Electric resistance strain gages were attached to the two edge piles of the north abutment. Stable instrument readings were obtained from installation in the fall of 1978 to the spring of 1979, when a flood caused the water level to reach a height above all of the strain gages. After this point, the readings were erratic, and the data from the strain gages was ignored.

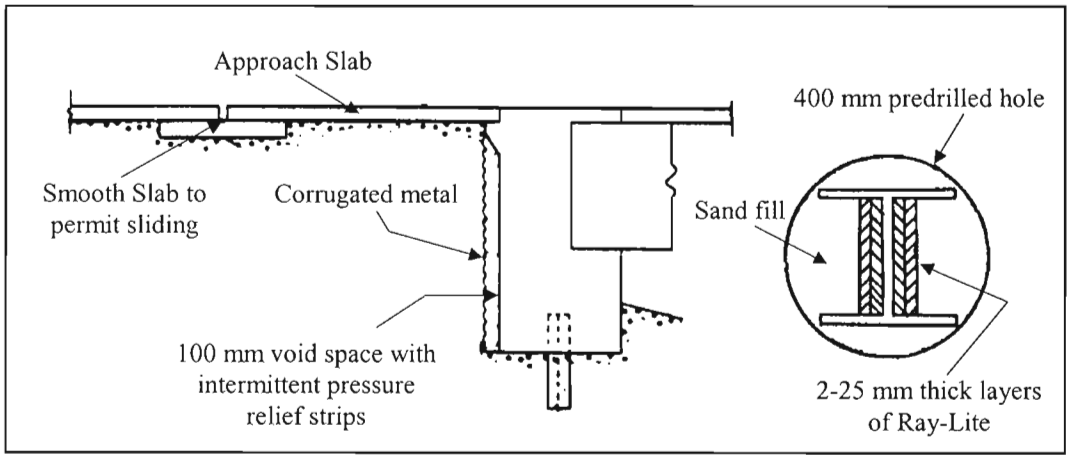

Figure 2.5. Pressure relief system details for abutments and piles (Jorgenson, 1983)

Since data from the strain gages could not be used, moments in the pile were calculated based on the deflection readings obtained from the inclinometers. The bending moment was then related to the bending stress in the pile through the section modulus. It was calculated that the moment induced by the maximum measured abutment movement of 49.8 mm (1.96 in) was sufficient to cause yielding within the top 305 mm (1 ft) of the pile. However, while strains exceeded the yield strain of the pile, the plastic hinge moment was not reached.

Data from the instrumentation was compared against an analytical model that predicted stresses in the piles due to movement of the abutments. However, it was found that the model predicted stresses that exceeded the yield stress of the pile by a factor of approximately three. This was attributed to the fact that the behavior of the pile in the model was incorrectly assumed elastic. However, the movements in the pile estimated using the model compared well to those measured by the inclinometers.

2.2.2. Laboratory Studies

The results of two laboratory studies of integral abutment piles are presented in this section. The first study is a test of scaled-down steel H-piles subjected to axial and lateral loading. The second study involves full-scale cyclic lateral load testing of three types of piles, steel H-piles, steel pipe piles, and prestressed concrete piles.

2.2.2.1. Small-scale Testing of Piles

Amde, Chini, and Mafi (1997) performed experiments on model steel H-piles driven into dry silica sand. The model H-piles underwent simulated thermal expansions and contractions of a bridge abutment to determine the influence of lateral displacement on the vertical load-carrying capacity of the piles. Because the cost of tests increases as the size of the pile increases, small-scale tests were performed. In most physical models, scaling correlations are necessary to determine the equivalent full-scale values from experimental data. In the case of soil, which behaves non-linearly, model soil would require increased unit weight. In addition, if complete similitude is desired, the model piles must be tested under increased gravitational acceleration in a centrifuge to match stresses present at full-scale. For a model with a scale of 1/60, a radial acceleration of

sixty times the acceleration of gravity is applied (Lock, 2002). However, since the model test results were compared with finite element models that used actual geometric and material properties existing in the model piles and soil, scaling relations were not required.

The model H-piles used in this study were fabricated from A36 structural steel, with the width-to-thickness ratios of the web and flange conforming to American Institute of Steel Construction (AISC) specifications for 'compact sections'. This was done to allow the sections to develop their plastic moment without any local buckling of the compression flanges occurring. Consideration of the height and diameter of the soil test tank led to the sizing of the H-piles to minimize the effect of clearance between piles and clearance between the pile and tank.

The testing apparatus is depicted in Figure 2.6. The tank was filled with dry silica sand in 15 layers. The first two layers were compacted to maximum density, and the other layers of soil were placed, leveled, and compacted to a unit weight of 16 kN/m^3 (102 lb/ft^3). To model end bearing conditions, a piece of steel plate was added at the pile locations during the filling of the tank. Each test pile was marked in 25 mm (1 in) increments, placed over the desired position, plumbed, and driven to the required depth. In the locations that end-bearing tests were performed, the pile was driven until it encountered the steel plate. The number of blows required for driving the pile each increment using a 3.7 kg (2.2 lb) hammer dropped from 305 mm (1 ft) was recorded.

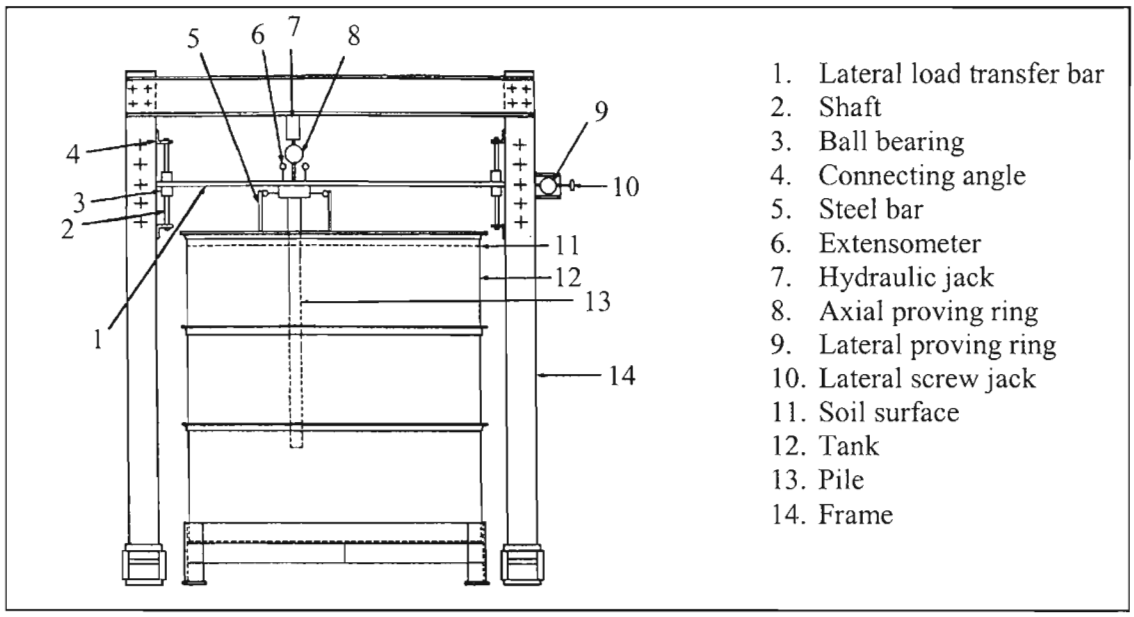

Figure 2.6. H-pile testing apparatus (after Amde et al, 1997)

The axial load test consisted of a vertical load applied to each model test pile in 445 N (100 lb) increments. Settlement and strain were recorded for each load increment by means of dial and strain gages. The displacement was the average of measurements from two dial gauges located on the pile cap. The loading continued until the change in displacement increased rapidly over a small change in the applied load.

Lateral load testing consisted of a load applied in 133.5 N (30 lb) increments. Displacement was measured by two lateral deflection gauges installed on the pile cap, and flexural strains were measured through strain gauges installed on opposite sides of the web. There was no mention as to whether the piles were subjected to weak or strong axis bending. As in the case for the axial test, failure was considered as the point where displacement began to increase rapidly over a small change in the applied load. The combined load tests were a combination of both the axial and lateral testing procedures. The procedures discussed for the lateral load test were used to displace the pile cap to the

required lateral displacement, and then the procedures of the axial load test were conducted until the ultimate pile capacity was reached. The lateral and vertical loads, and the displacement for each direction were recorded. The test on the end bearing pile was run to the limit of the test set-up for vertical load, which was equal to 4.45 kN (1000 lb).

The experimental data was compared to results from the finite element model. Curves for horizontal displacement versus lateral load for test pile A-3 obtained experimentally and from the finite element model are shown in Figure 2.7. The finite element model used for comparison is the same nonlinear model developed by Greimann et al (1986), discussed later in this chapter. Pile A-3 was 1143 mm (3.75 ft) long, and constructed from 3.2 mm (1/8 in) thick plates to a depth and width of 32 mm (1¼ in) . Although the finite element results are conservative, for small horizontal displacements the discrepancy between the two curves is smaller than at higher displacements. In addition, piles 1143 mm in length were found to have more resistance to lateral load than those that were 990 mm (3.25 ft) long. The thickness of the webs and flanges also has an effect on lateral resistance of the pile.

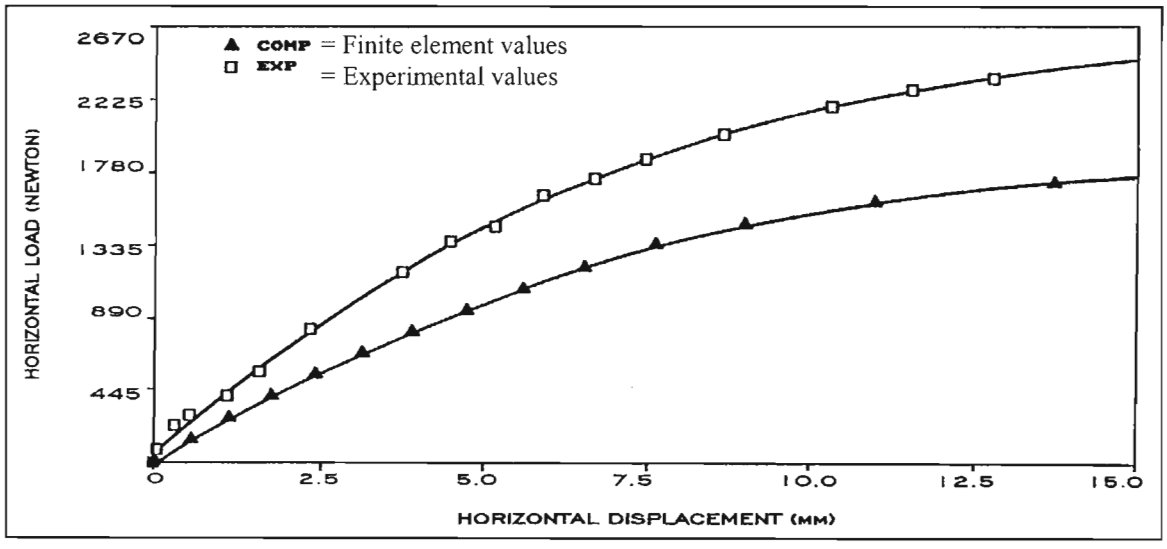

Figure 2.7. Horizontal load/displacement curves (after Amde et al, 1997)

A review of the vertical load-settlement data shows that all the piles failed through a vertical-type failure, occurring when the applied load exceeded the ultimate soil frictional resistance. The load settlement curves became horizontal as the load reached the ultimate pile load for all prescribed lateral displacements. When experimental data was compared to the results of the finite element program, the finite element model program underestimated the ultimate capacity of piles.

Amde, Chini, and Mafi (1997) concluded that the results show that all the model piles failed through a vertical-type failure, that is, the applied load exceeded the ultimate soil frictional resistance. In addition, no plastic hinges occurred during any of the load tests. The results from a nonlinear finite element computer program were found conservative when compared to the experimental results. The experimental results showed greater pile capacities and lower bending moments than were predicted by the finite element program.

2.2.2.2. Full-scale Testing of Piles

Arsoy, Baker, and Duncan (2002) investigated the performance of various types of piles used to support integral abutment bridges. Full-scale tests were performed on a steel H-pile, a steel pipe pile, and a prestressed concrete pile to determine the capability of each type of pile to withstand thousands of lateral thermal loading cycles with minimal distress. As shown in Figure 2.8, the soil-pile-bridge interaction is not modeled in the test setup. Rather, only the pile behavior under cyclic thermal displacements is under investigation.

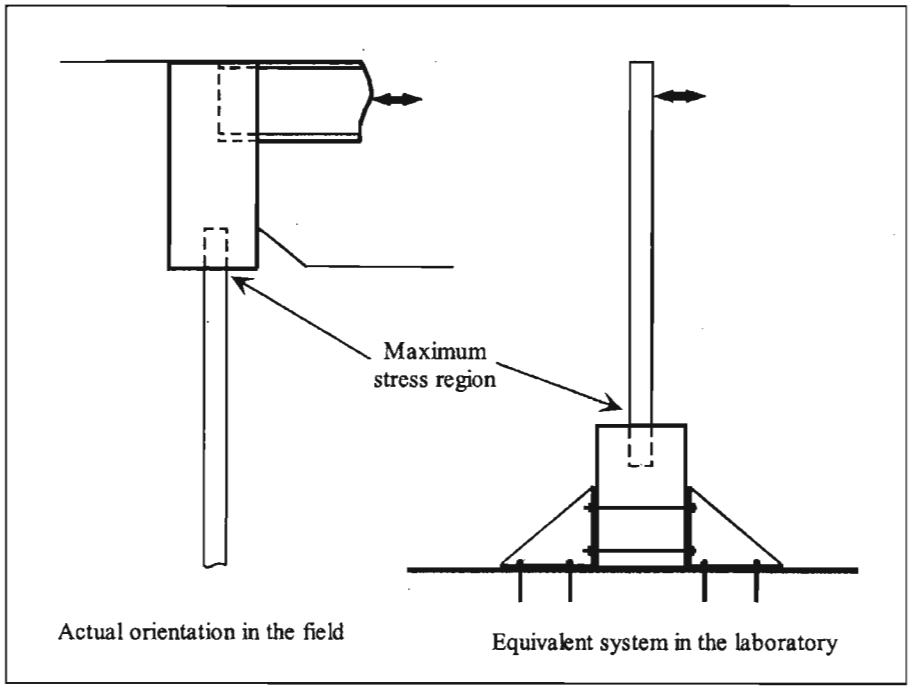

Figure 2.8. Equivalent laboratory test setup (Arsoy, Duncan, and Barker 2002)

The type of H-pile tested was an HP10x42 fabricated from grade A572-50 S50 steel. The pipe pile was made from ASTM A252 Gr. 3 steel, and had a 350 mm (14 in) outside diameter, with a 12.7 mm (½ in) wall thickness. The prestressed concrete pile was a 305 mm (12 in) square pile with five 12.7 mm diameter low relaxation steel strands, with a yield stress of 1.86 GPa (270 ksi). The prestress in the pile was 6 MPa (920 psi) (Arsoy et al, 2002). The piles were cast into pile caps constructed from Virginia DOT Class A4 concrete with a minimum 28-day strength of 27.6 MPa (4000 psi). Due to time constraints, early strength accelerators were added to achieve the 28-day strength in 7 days. Both the H-pile and prestressed pile were embedded 460 mm (18 in) into the pile cap, while the pipe pile was only embedded 150 mm (6 in). However, reinforcement of the pipe pile extended another 305 mm into the pile cap to achieve the same embedment as the other two piles.

The pile caps were fastened to a reaction floor beneath a load frame. A gravity load simulator was used to apply a constant vertical load to the pile as it deflected laterally. Approximately 27,000 cycles of lateral load were applied by a displacement-controlled actuator to simulate the thermal loading over a 75-year bridge life. Pile displacements were measured using wire pot transducers. Three transducers were affixed to the pile, while two were used to measure the lateral displacement and rotation of the pile cap. Load cells were used to monitor the vertical and horizontal loads being applied to the pile. Four strain gages were attached to the H-pile near the pile cap, at the tip of each flange. The pipe pile had two strain gages near the cap, one 1397 mm (55 in) above the pile cap, and one 1778 mm (70 in) above the cap. The prestressed concrete pile had only two gages, both at the pile cap, on opposite sides of the pile.

The H-pile bending about its weak axis exhibited the best behavior of the three piles tested. For the entire test, the maximum stress level was set to 50% of the nominal yield capacity of the pile. Overall, the H-piles sustained stresses in excess of 138 MPa (20 ksi) in cyclic loading and 241 MPa (35 ksi) in static loading without any sign of distress. The steel pipe pile was significantly stiffer than the H-pile. Consequently, the cap of the pipe pile rotated more than that of the H-pile. As was the case with the H-pile, the pipe pile did not sustain any damage during testing. The concrete pile was tested with no vertical load. In the first cycle, tension cracks developed at the interface with the pile cap. The tension cracks in the test pile developed progressively from the bottom (cap) towards the top (toe). The cracks gradually enlarged as the cycles continued. At the end of the test, it was observed that the contact area was only 20% of the original cross-sectional area of the pile.

Arsoy, Duncan, and Barker (2002) conclude that steel H-piles oriented in weak-axis bending are a good choice for support of integral abutment bridges. Pipe piles are less suitable for support of integral abutments, because they have significantly higher flexural stiffness than H-piles, for a given width or diameter. Because of this, stresses in an abutment supported by pipe piles will be higher than stresses in an abutment supported by steel H-piles in weak axis bending, leading to increased loading on the abutment. Concrete piles appeared to be the least suitable choice for support of integral abutments because tension cracks form and progressively worsen under cyclic thermal loading. This can greatly reduce their vertical load carrying capacity. While suitable integral abutment pile types are determined in this study, the results are lacking because they do not account for the soil/structure interaction, and the stress levels in the piles were relatively low.

2.3. Design Methods for Integral Abutment Piles

Because the AASHTO Specifications do not specifically address the design of piles for integral abutment bridges, there has been extensive research in this area. Many state transportation agencies use in-house methods, which are based on experience and are therefore highly empirical. The research into integral abutment pile design thus far has been aimed at using simplified structural models, or computer analysis, to account for the stresses and displacements in the pile created by thermal expansion of the superstructure. This section discusses the basis, procedures, and validity of two of the most widely accepted methods for integral abutment pile design. The first is referred to as a "rational design method" by Abendroth et al. (1989), which is in use by several state DOT's, and was part of an FHWA sponsored workshop on integral abutment bridges

(GangaRao, 1996). The other design method was prepared for the American Iron and Steel Institute (AISI) by the Tennessee Department of Transportation (Wasserman & Walker, 1996).

2.3.1. "Rational Design Method"

The "rational design method" presented by Abendroth et al (1989) is an evolution of a design procedure by Greimann and Wolde-Tinsae (1988). This procedure models the piles as equivalent cantilevers, based on the stiffnesses of the soil and the pile. Two alternatives are presented that address three AASHTO Specification (1993) design criteria: capacity of the pile as a structural member; capacity of the pile to transfer load to the ground; and the capacity of the ground to support the load. The first alternative is a conventional elastic approach, while the second is an inelastic approach that considers the redistribution principles of ductile piles.

The principle of this method is that a pile embedded in soil can be modeled as an equivalent beam-column without transverse loading between the ends, having a fixed base at a certain depth. The head of the pile can be modeled as either a fixed or a pinned connection, depending on the type of integral abutment detail specified, fixed for a full integral abutment, pinned for pinned or semi-integral. Figure 2.9 shows an idealization of the fixed cantilever, with both types of restraint at the head.

For a long pile embedded in soil, the length below which lateral displacements are relatively small (l_c) can be computed as

$$l_c = 4\left(\sqrt[4]{\frac{E_p I_p}{k_h}}\right) \qquad \text{(Equation 2.1)}$$

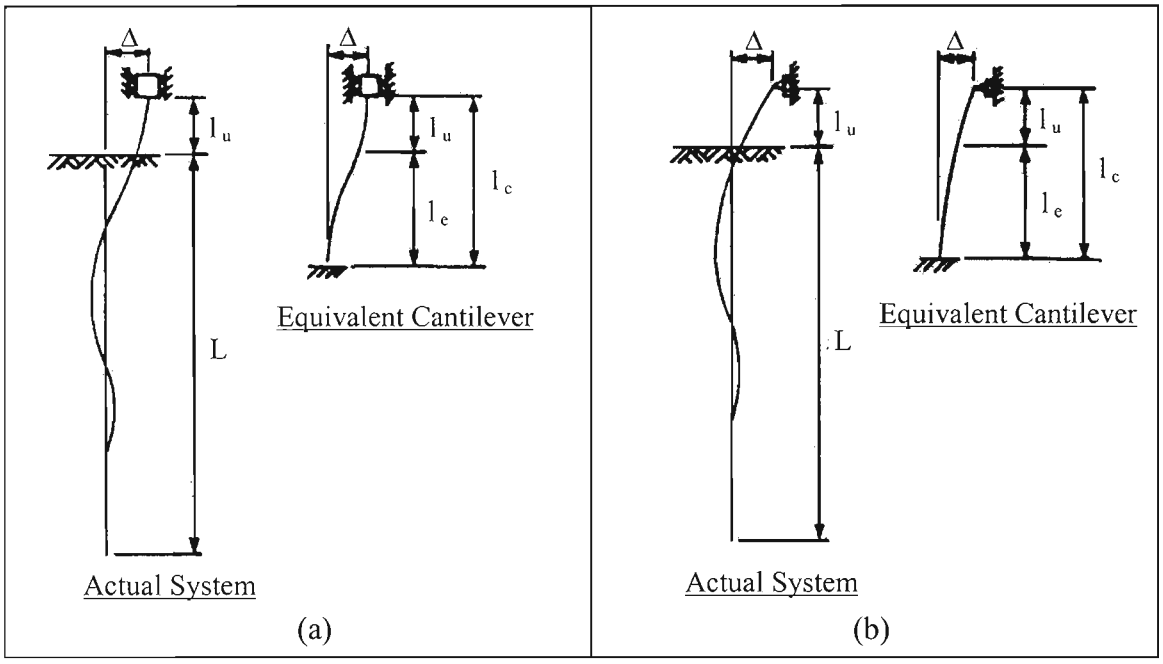

Figure 2.9. Equivalent cantilevers for: (a) fixed-head condition (b) pinned-head condition (Greimann et al., 1987)

The quantity k_h represents the lateral soil stiffness approximated by a linear Winkler soil model (Poulos and Davis, 1980), and E_p and I_p represent Young's modulus and moment of inertia of the pile, respectively. For non-uniform soil conditions, an iterative process is used to determine an equivalent lateral soil stiffness parameter, k_e, which is used in Equation 2.1 in place of k_h. Using the ratio of the calculated value of l_c to l_u, the equivalent embedment lengths, l_e, for moment, buckling, and horizontal stiffness are calculated using Figure 2.10. However, it should be noted that the equivalent cantilever defined in Equation 2.1 is a common, although imprecise, idealization of laterally loaded piles. Fleming et al (1992) comment that the pile is considered "fixed at some depth determined by folklore and ignoring the soil support above that depth".

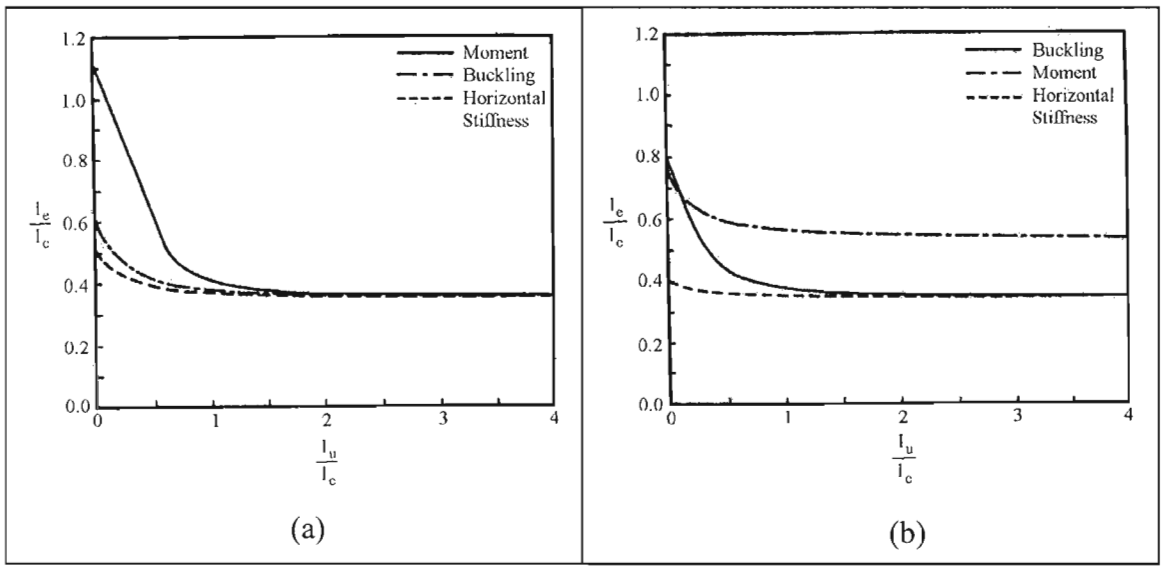

Figure 2.10. Length of embedment factors for: (a) fixed-head condition (b) pinned-head condition (Abendroth & Greimann, 1987)

Since this approach is based on elastic behavior and neglects any potential strength associated with the formation of plastic hinges, the redistribution of internal forces does not contribute to the ultimate strength of the pile. This design method is an elastic design procedure for the equivalent cantilever beam-column that considers all stresses developed in the pile. The lateral displacement, Δ, at the pile head, caused by thermal expansion and contraction of the bridge superstructure, produces an end moment, M_1, given as:

$$M_1 = \frac{D_1 E_p I_p \Delta}{(l_e)^2} \qquad \text{(Equation 2.2)}$$

The bending moment coefficient D_1 equals 6 or 3 for fixed or pinned-head piles, respectively. Abendroth and Greimann comment that this moment can dramatically affect the axial capacity of the pile.

A second approach used for ductile piles does not neglect the redistribution of forces due to the formation of plastic hinges. The stresses induced by the horizontal pile head movement are considered to not significantly affect the pile ultimate strength, as long as the corresponding strains can be accommodated through adequate pile ductility. Neglecting these thermally induced pile stresses is justified by first-order plastic theory involving small displacements (Abendroth and Greimann, 1989). However, for this case to be valid, local and lateral buckling must be prevented.

For the second alternative, the axial pile load, P, generates a bending moment due to the lateral displacement at the pile head. Abendroth and Greimann propose a conservative upper bound on this induced end moment as:

$$M_2 = D_2 P\Delta \qquad \text{(Equation 2.3)}$$

where the bending moment coefficient D_2 equals 0.5 or 1 for fixed or pinned head piles, respectively.

Using these thermally induced moments, combined with moments and axial loads produced by dead and live loads in the girder, the applied axial and bending stresses in the pile are calculated. For multi-span bridges, an axial force is induced in the pile by thermal expansion that must be considered as well. The axial and bending stresses are compared to allowable stresses using equations 10-42 and 10-43 in Section 10.36 of the AASHTO Standard Specification (1996).

In addition to strength and stability criteria, both design alternatives must satisfy local buckling and ductility criteria. For Alternative 1, the width-to-thickness ratios of the cross-sectional elements must be limited to prevent local buckling before the yield

moment is obtained. According to Article 1.9 of the AISC Specification (1980), standard rolled HP shapes satisfy these width-thickness criteria. Therefore, local buckling will not govern the pile capacity.

The second alternative requires additional ductility greater than that needed to satisfy the conditions of the first. This is to allow the pile to develop the inelastic rotation capacity associated with plastic hinge formations. Equation 2.4 expresses the ductility criterion in terms of the lateral displacement of the pile head.

$$\Delta \leq \Delta_b \, (D_3 + 2.25 C_i) \qquad \text{(Equation 2.4)}$$

D_3 is a ductility coefficient equal to 0.6 or 1.0 for fixed or pinned head piles, respectively, and C_i is an inelastic rotation capacity reduction factor, based on the flange width-to-thickness ratio and the yield stress of the pile. The expression for C_i is given as

$$C_i = \frac{19}{6} - \frac{b_f \sqrt{F_{yp}}}{60 t_f} \qquad \text{(Equation 2.5)}$$

An upper bound of 1.0 for C_i applies when $b_f / 2t_f \leq 65\sqrt{F_{yp}}$, and a lower bound of zero governs when $b_f / 2t_f \geq 95\sqrt{F_{yp}}$. Δ_b is the horizontal movement of the pile head at which the actual extreme fiber bending stress equals the allowable bending stress, F_b. The displacement Δ_b is given as:

$$\Delta_b = \frac{F_b S_p l_e^{\,2}}{D_1 E_p I_p} \qquad \text{(Equation 2.6)}$$

where S_p is the section modulus of the pile with respect to the plane of bending.

Abendroth and Greimann also determined that lateral displacement of the pile could affect the capacity of the pile to transfer load to the ground. However, this displacement should not affect the end bearing resistance of flexible piles, nor the capacity of the ground to support the load. Fleming et al. (1992) recommend that the maximum lateral displacement below which the frictional resistance is assumed to be unaffected by the movement is determined as 2% of the pile diameter. If the lateral displacement due to temperature change exceeds this value, the adjusted length of pile used in calculation of frictional resistance to axial load, l_n, is found using Figure 2.11.

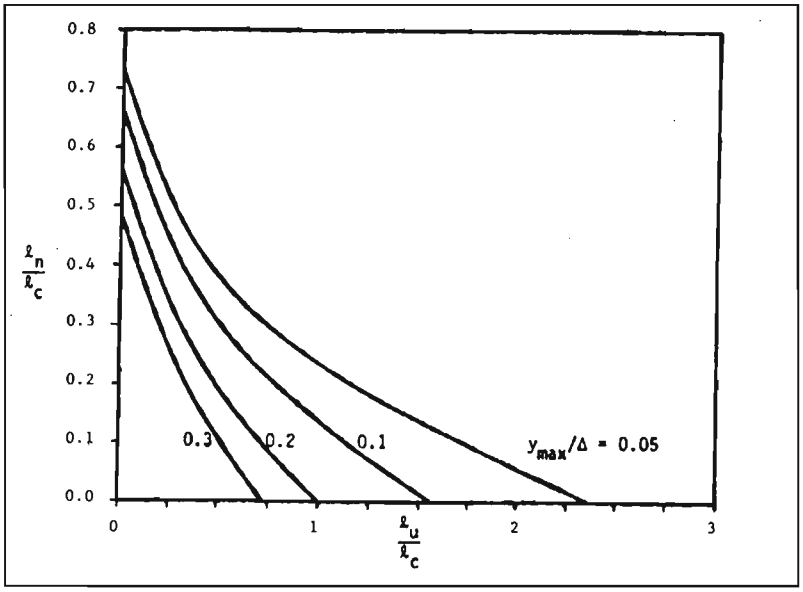

Figure 2.11. Adjusted pile lengths for frictional resistance of fixed-head piles in uniform soil (Abendroth et al, 1989)

The ultimate strengths predicted by both alternatives were compared to a finite element model as well as data from two bridges in Iowa (Girton et al, 1991). For a steel HP 10 x 42 pile, the results showed that both design alternatives were conservative, with Alternative 1 being overly conservative for small slenderness ratios where yielding controls over stability. Both the design alternatives and the finite element model predict

a decrease in the ultimate pile capacity as the horizontal displacement at the pile head increases. Detailed pile design examples using this method can be found in Abendroth & Greimann (1989) as well as in GangaRao (1996).

2.3.2. Lateral Analysis Design Method

Walker and Wasserman (1996) proposed a design procedure that incorporated a computer program for analysis of soil-pile interaction. The software used for this procedure was COM624P, which models and analyzes laterally loaded piles (Wang & Reese, 1993). The differential equation governing the bending of the pile is solved to obtain pile deflections. The pile response is obtained by an iterative solution of the fourth-order governing differential equation using finite difference techniques. The soil response is described by a series of non-linear relations that compute the soil pressure resistance, p, as a function of lateral pile displacement, y. Once the pile is analyzed with COM624P, interaction diagrams for the pile are developed and compared to the applied loads.

First, the movement at each abutment due to thermal expansion or contraction of the girder is calculated. The pile section that is chosen must be flexible enough to achieve double curvature within its design length under the thermal movement. Two calculations are performed to assess the adequacy of the abutment and pile system to function as needed. The first calculation determines whether the calculated thermal displacement is sufficient to cause a plastic hinge at the top of the pile, as plastic hinges can reduce the axial capacity of the pile. The second calculation determines if the

bearing strength of the concrete is adequate to apply M_p to the embedded length of pile without damage to the abutments.

After the ability of the HP section to develop the plastic-moment capacity at its top has been established, COM624P is utilized to develop the deflected shape of the pile under specified soil conditions. For the thermal displacements calculated initially, *p-y* curves are generated based on the soil properties. A thorough discussion of the procedure for the determination of *p-y* curves is given by Wang & Reese (1993). The pile is analyzed with the plastic moment and thermal displacement applied at the head of the pile. The unbraced length of the pile is determined from identification of the points of zero moment at varying depths of pile embedment, and the longest of these distances is used in subsequent calculations.

The pile is designed using the provisions for the design of compression members given in AASHTO Article 10.54 (1996). The resulting values are used to develop interaction diagrams using AASHTO Equations 10-155 and 10-156, given below as Equation 2.7 and Equation 2.8 respectively.

$$\frac{P}{0.85 A_s F_{cr}} + \frac{M C}{M_u \left(1 - \frac{P}{A_s F_e}\right)} \leq 1.0 \qquad \text{(Equation 2.7)}$$

$$\frac{P}{0.85 A_s F_y} + \frac{M}{M_p} \leq 1.0 \qquad \text{(Equation 2.8)}$$

The values of P and M are determined using the various applicable loading conditions as specified by AASHTO. It should be noted that the thermal movements and resulting factored loads are unique to the given soil profile and initial lateral displacements.

Ingram et al. (2003) recently investigated the applicability of using the AASHTO and AISC column design equations to design integral abutment piles. They specifically mention the use of COM624P to determine the distance between inflection points on the pile moment diagram, which is taken as the effective length of the column. Tests were performed on piles driven into soil to compare the ultimate strength to that computed using AASHTO and AISC column design equations. The results of the field study showed that these equations result in overly conservative values for the ultimate capacity of the piles. This is attributed to the fact that the column design equations only consider length effects. In addition, considering piles as unsupported between inflection points does not take into account the influence and support provided by the surrounding soil.

2.4. Finite Element Modeling of Integral Abutment Bridges

Numerous finite element models of integral abutment bridges have been developed by researchers in the past decade. Some of these models have been produced using commercially available software packages, while other models are comprised of original code written by the researchers. Both two-dimensional and three-dimensional models have been developed. In these models, the structure and soil are modeled using either continuum elements, or specialty elements, such as beams and springs. A review of several recent finite element models of different composition is provided in this section. Discussion of the models includes the goal of each model, the elements and numerical methods used, and the conclusions or recommendations of the researchers.

2.4.1. Two Dimensional Models

The two-dimensional (2D) finite element analysis of integral abutments is very popular, because 2D models require fewer computational resources. The soil response is most frequently modeled as a series of linear or non-linear spring elements. However, this approach is considered unrealistic by some, as these elements do not account for the fact that the springs are uncoupled, while the actual soil behaves more like a continuum. In addition, there is no widely accepted theory from which the spring constant, or modulus of subgrade reaction, can be derived (Krusinski, 2002). To this end, researchers have used continuum elements to model the soil using easily determined properties, such as internal angle of friction (ϕ), density (ρ), and cohesion (c).

2.4.1.1. Soil Response Modeled Using Specialty Elements

Greimann et al (1986) developed a nonlinear finite element algorithm (IAB2D) to study pile stresses and pile-soil interaction in integral abutment bridges. The piles, abutments, and girder were modeled using beam-column elements that incorporated geometric and material nonlinearities, such as yielding of steel. The soil was represented by vertical and lateral springs, as well as a spring supporting the tip of the pile. The soil springs and idealized structure are shown in Figure 2.12. The stiffness of these soil springs was determined using a modified Ramberg-Osgood cyclic model.

The model was calibrated using an actual integral abutment bridge, and data from the model was compared to data collected from pile load tests. These tests consisted of three separate tests. The first test was an axial load test on a steel H-pile, while the other two tests were a combined axial and lateral load test on a timber pile. When compared to

the test data for the different piles, the finite element models were found to give reliable results, although the program predicted a lower ultimate load than the load tests did.

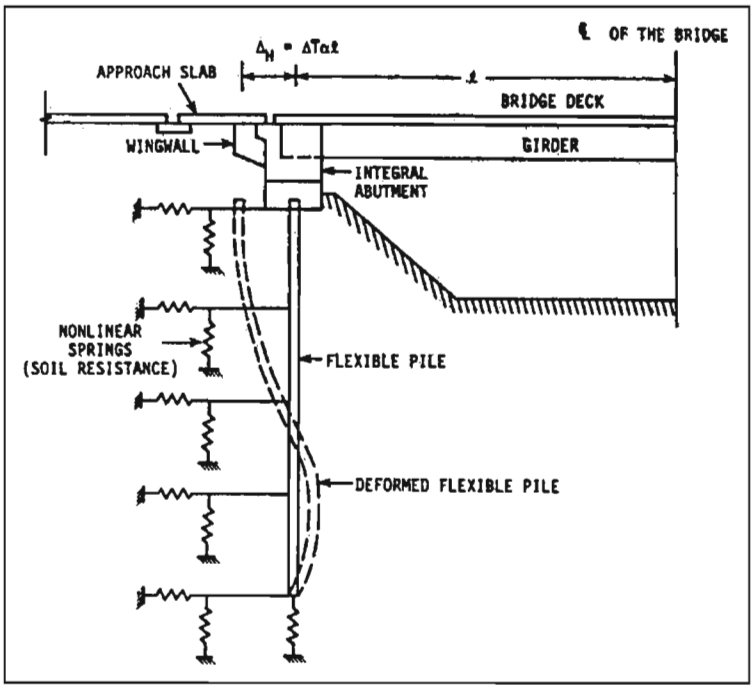

Figure 2.12. 2D model of integral abutment bridge (Greimann et al, 1986)

Thippeswamy et al (1994) performed a parametric study on the response of single-span integral bridges. The analysis was performed using the commercial software program ANSYS (1987). The girder and deck were modeled using ANSYS STIF 3 one-dimensional beam elements, with four degrees of freedom at each node of the element. The model bridge was founded on a shallow footing, not on piles. Three types of foundation support conditions were considered: hinged, fixed, and partially fixed. The partially fixed conditions were represented by means of rotational springs, with stiffness values assumed for the springs to represent different types of soils and foundations.

Effects of variation in span length, abutment height, ratio of superstructure to substructure stiffness (K), gravity load, thermal load, lateral load, soil settlement, and

their combinations were studied. The net moment developed at midspan due to thermal expansion in a jointed bridge was 1.8 and 1.9 times greater than that developed in an integral bridge with hinged and fixed foundation conditions, respectively. For thermal contraction, the net moment at midspan was 3 and 3.5 times greater than that for an integral bridge. It was determined that the stiffness ratio, K, and the boundary conditions have significant influence on the magnitude of the moments developed in an integral bridge. The thermally induced moment at the footing was found to be larger for smaller K values, and the moment at the footing associated with earth pressure was the highest for larger K values.

More recently, Diceli and Albhaisi (2003) performed a finite element study aimed at developing maximum length recommendations for integral bridges supported on H-piles in sand. The model was constructed using the finite element based software SAP2000 (1998). A bridge with three 40 m (131 ft) spans and a bridge with six 20 m (65 ft) spans were modeled in order to examine structures with varying deck and abutment stiffnesses. Only half of the actual structures were modeled due to their symmetrical configurations and nominally identical soil properties on each end of the bridge. An example of the structural model for the bridge with 20 m spans is given in Figure 2.13. The configuration for the larger-span bridge model is similar.

The composite slab-on-girder section was modeled using beam elements, with elastomeric bearings represented with roller supports. The abutment was also modeled using elastic beam elements, and the deck-abutment joint was modeled using a horizontal and a vertical rigid elastic beam element. In the model, the effective lengths of the piles were taken as 30 times the pile width. It was assumed that the portion of the pile below

this length has negligible effect on the pile-soil interaction. The pile was also modeled using beam elements with nonlinear frame-hinges to simulate the inelastic deformation of the steel H-piles under thermal effects. Approach slabs and wingwalls were not modeled because the frictional forces generated between these components and the backfill were found to have negligible effect on the movement of the structure.

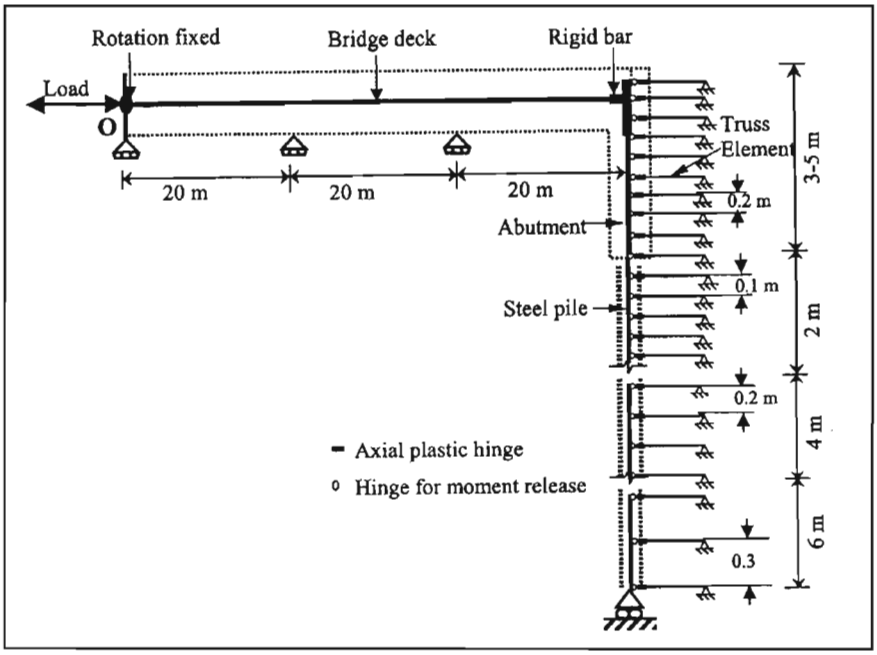

Figure 2.13. Nonlinear, symmetrical model of integral abutment (Diceli et al 2003)

The soil was modeled using truss elements with plastic axial hinges at their ends. The yield stress of the plastic hinges was calculated as the product of the ultimate soil resistance per unit length and the tributary length between nodes of the pile. The cross-sectional area of the truss elements were calculated using the coefficient of subgrade reaction, depth below surface, and arbitrary values of length and stiffness, 1 m and 1000 kPa (3.28 ft and 145 psi), respectively. These elements were attached at each node along the pile, and the spacing of the nodes increased along the length of the pile. The soil response at the bottom of the pile was represented with a roller support to provide

stability in the vertical direction. Backfill-abutment interaction behavior under thermal expansion was modeled in a similar fashion to that of soil-pile interaction. However, the soil-abutment interaction under thermal contraction conditions was not considered.

Diceli and Albhaisi (2003) define a limiting value of structural movement called the displacement capacity (Δ_D). The displacement capacity is reached when either: the pile fails due to moment fatigue, or the abutment fails in shear or flexure. They concluded that the displacement capacity of integral bridges decreases as the foundation soil becomes stiffer, or as the size of the bridge increases. In addition, they note that the flexural capacity of the abutment may control the displacement capacity of the bridge under positive thermal expansion. The backfill was found to restrain the displacement of the pile when the bridge expands, which allowed the piles to deform inelastically. It found that a pinned abutment-pile connection dramatically increases the displacement capacity of the bridge based on both the displacement capacity of piles and the flexural capacity of the abutment. The maximum recommended length of bridges in cold climates was 190 m (623 ft) for concrete girders and 100 m (328 ft) for steel girders. In moderate climates, the limits are increased to 240 m (787 ft) and 160 m (529 ft) for concrete and steel girders respectively.

2.4.1.2. Soil Response Modeled Using Continua

Lehane et al (1999) used a finite element model comprised of continuum elements to validate a simplified model for use in design of integral abutment bridges. The paper focused on the effects of thermal expansion on frame type bridges supported on shallow foundations (spread footings). The soil was modeled as an elastic continuum of uniform stiffness. This continuum was discretized with eight-noded quadrilateral elements. The

concrete structure, as well as the empty space spanned by the girder, was also modeled using these elements. A simplified plane frame model, was created using data from the finite element model. The equivalent abutment height and stiffnesses of the translational springs were calculated based on the horizontal and rotational restraint provided by the abutment and soil in the complex model.

Moments and axial forces predicted in the bridge deck by the analyses of Lehane et al (1999) were compared with that of the simplified model for various load cases. The results of both agree reasonably well. It was determined that the magnitudes of the induced moments and axial stresses in the deck are relatively small. In addition, the predictions were not overly sensitive to the choice of bridge geometry or material properties.

Duncan and Arsoy (2003) used the finite element analysis program SAGE (Bentler et al, 1999) to investigate the significance of the interactions among the abutment, the approach fill, the foundation soil, and the piles of integral bridges. Specifically, the effects of the stiffness of the approach fill and the foundation soil on the stresses in the piles supporting the abutment, as well as the effects of the type of abutment detail were examined. The finite element mesh is symmetric about the centerline of the girder. The bridge superstructure, the piles, and the dowels of the semi-integral abutments were modeled as beam elements with linear stress-strain properties only. The approach fill and the foundation soil were modeled using four-node quadrilateral and three-node triangular elements with hyperbolic stress-strain properties. As shown in Figure 2.14, the finite element mesh is refined near the abutment and coarse near the boundaries of the model.

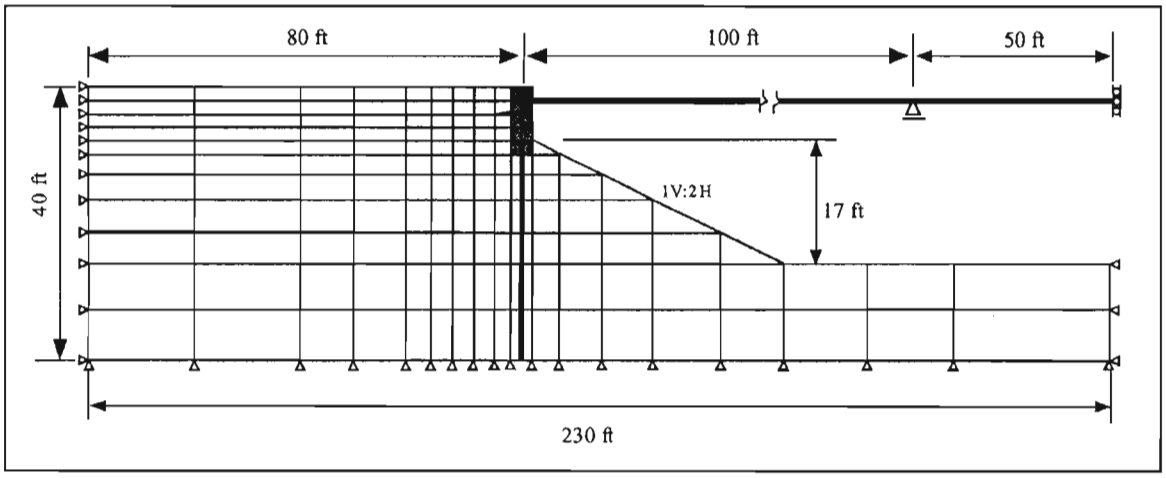

Figure 2.14. Finite element model with soil as a continuum (Duncan & Arsoy, 2003)

Parametric studies were conducted to study the effects of the approach fill for loose, medium and dense soils, and the effects of integral and semi-integral abutments on the pile stresses. The results from the finite element analyses indicated that semi-integral abutments offer benefits over integral abutments, such as reducing the pile stresses, especially those due to contraction of the bridge. In addition, interactions between the approach fill and the foundation soil creates favorable conditions with respect to pile stresses. Movement of the approach fill tends to cause the foundation soil to behave as if it were softer than it truly is.

The authors comment that it would be interesting to extend these studies, by using zero-thickness interface elements between the piles and the adjacent soil and between the approach fill and the foundation soil to allow for slip at these interfaces. In addition, a study on the effects of different weight and the stiffness of the approach and foundation soils would be very beneficial. They also comment that data from instrumented piles supporting integral bridges would help to validate the findings of this study.

2.4.2. Three Dimensional Models

Three-dimensional (3D) finite element models of integral abutment bridges are not as prevalent as two-dimensional models. This is due to their increased complexity as well as increased computational requirements. However, unlike 2D models, 3D models can account for skew effects, as well as effects of off-center loading.

A study by Mourad and Tabsh (1998) deals with the analysis of loads in piles supporting integral abutments. The load cases considered are composed of one or more side-by-side HS20 trucks, in accordance with AASHTO provisions (1996). A detailed finite element analysis is used to develop a simple, approximate procedure utilizing a two-dimensional frame model for computing pile forces from complex loading. The finite element model was created using the program ALGOR (1994).

The deck slab was modeled by both 3-node triangular and 4- node rectangular shell elements, with five degrees of freedom (DOF) at each node. The flanges of the steel girders were modeled using 2-node space beam elements with six DOF at each node, and the web of the girders was modeled with the 4-node rectangular shell elements used in the deck slab. Diaphragms composed of cross frames made from steel angles were modeled using space truss elements having three displacement degrees of freedom at each node. In addition, rigid beam elements were placed between all top flanges and deck elements to satisfy the compatibility of the composite behavior, and account for the thickness of the haunch. Abutments and wingwalls were modeled with 8-node brick elements with three DOF at each node. The steel H-piles were represented by 2-node space beam elements that span between the bottom of the abutments and the equivalent point of fixity of the piles.

The study resulted in several observations about the behavior of an integral abutment bridge. It was shown that the abutment/wingwall system did not behave as a rigid block, as opposed to the case of a footing supported on flexible piles. As expected, reducing the number of piles under the abutment greatly affected the axial load in the piles, but it did not significantly change the tension force in the piles under the wingwalls. The axial stresses in the piles were not affected by modeling the connection between the top of the piles and the abutment/wingwall as fixed or hinged.

Faraji et al (2001) created a 3D finite element model of an integral abutment bridge using the commercially available finite-element code GTSTRUDL (1991). They performed a small parametric study in which the compaction levels of cohesionless soils behind the abutment and adjacent to the piles were varied. The deck slab was modeled using shell elements, and stringers and diaphragms were modeled with linear beam elements. Rigid links were used between the stringers and deck slab to ensure strain compatibility and shear transfer between the deck slab and girder elements. The pier caps, reinforced concrete columns, and H-piles were all modeled using linear beam elements. Figure 2.15(a) shows the configuration of the model in its undeformed state.

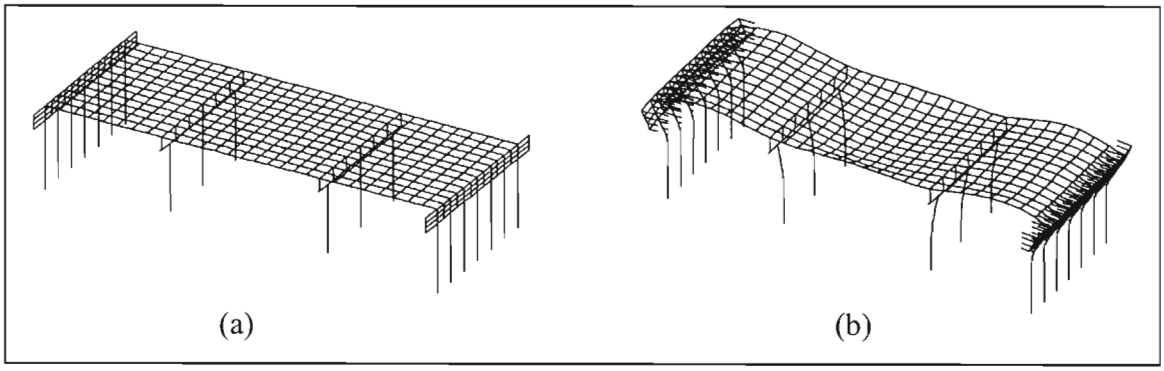

Figure 2.15. 3D Finite element model (a) in undeformed state (b) after thermal loading (Faraji et al, 2001)

The soil reactions adjacent to the piles and behind the abutment walls were modeled as nonlinear support springs. The force-deflection characteristics of the springs behind the abutments were derived from curves recommended in the National Cooperative Highways Research Program design manual. The nonlinear *p-y* design curves recommended by the American Petroleum Institute were used for the soil springs adjacent to the piles. For the parametric study, the soil conditions behind the abutments and next to the piles were varied as follows: loose/dense, loose/loose, dense/loose, and dense/dense, respectively.

The results obtained from the finite element analyses show that the composite action of the slab and stringers must be properly modeled. Failure to do so alters the relative stiffness of the deck compared with the abutment-pile-soil system, which results in dramatically different structural responses. Soil compaction behind the abutment wall was also found to be an important factor affecting the overall bridge behavior. The level of compaction behind the abutment affects the axial forces and moments in the deck, increasing both peak values by more than twice when the compaction is varied from loose to dense soil. The magnitude of the peak moments in the piles decreases by a factor of two when the compaction is varied from loose to dense. The level of soil compaction adjacent to the piles does not significantly influence bridge deck deflections or moments. However, the moment in the pile is considerably affected by the relative density of the soil both next to the pile and behind the abutment.

The authors plan to develop a 3D finite element model for a new fully instrumented bridge currently under construction, where field data such as lateral soil pressures behind the abutment walls and flexural strains in the H-piles will be

continuously collected. The reliability of the finite element model will be assessed by comparing finite element results with observed bridge behavior. Future studies will investigate the impact of preaugering holes for the piles and backfilling with loose granular fill as well as the impact of skew alignments.

2.5. Summary

Based on the studies of integral abutment bridges presented in this chapter, it is clear that they warrant further study. Transportation agencies worldwide each have slightly different design and construction methods, with no consensus on which ones are appropriate. Furthermore, limits are imposed on the geometry of integral abutment bridges based on experiences in one region that may not apply to other regions. To this date, very little work concerning the capabilities of integral abutments founded on short piles has been done. Existing design procedures preclude the use of piles below a certain length simply because the assumptions they are based on are generally only valid for longer piles. In addition, these methods generally do not take any interaction between pile and bedrock into account.

Finite element analysis seems to be the most preferred method for assessing the effect of changes in certain variables on the performance of integral abutment bridges. However, the large variety and limitations of existing models indicate that there is undoubtedly room for improved techniques. A large number of finite element models employ simplifications in modeling the soil and structure that may lead to only a partial understanding of the true behavior of the structure. The implementation of sophisticated and comprehensive methods of modeling may allow integral abutment bridges to be used in applications where simplified methods of modeling have concluded they cannot.

Chapter 3

DEVELOPMENT OF FINITE ELEMENT MODEL

This chapter describes the development and implementation of a finite element model created to simulate the behavior of a typical integral abutment bridge. Using plans of various integral abutment bridges proposed or constructed in the state of Maine, a series of two-dimensional models were developed using the computer program ABAQUS (HKS, 2001). These models were used to perform a parametric study, which is described in detail in Chapter 4. A materially and geometrically nonlinear, small-displacement analysis was used to capture the behavior of the structure, as well as model the soil-structure interaction.

3.1. Model Overview

Plans for a proposed integral abutment bridge called the Mill Pond Bridge over the Carrabassett River in Salem Township, Maine were used as a basis for this model. This bridge consists of four 35 m (115 ft) long steel plate girders supporting a cast-in-place concrete deck. The ends of each girder are welded to the top of a HP 360x108 (HP14x73) pile and cast within a 3 m (10 ft) high abutment. The spacing of the girders and piles is 2.7 m (9 ft). From these plans, a two-dimensional "slice" was taken through the three-dimensional structure. This "slice" contains five basic components: superstructure (girder and deck), piles, abutments, soil, and bedrock. A view of a typical model, showing the configuration of these components, is given in Figure 3.1.

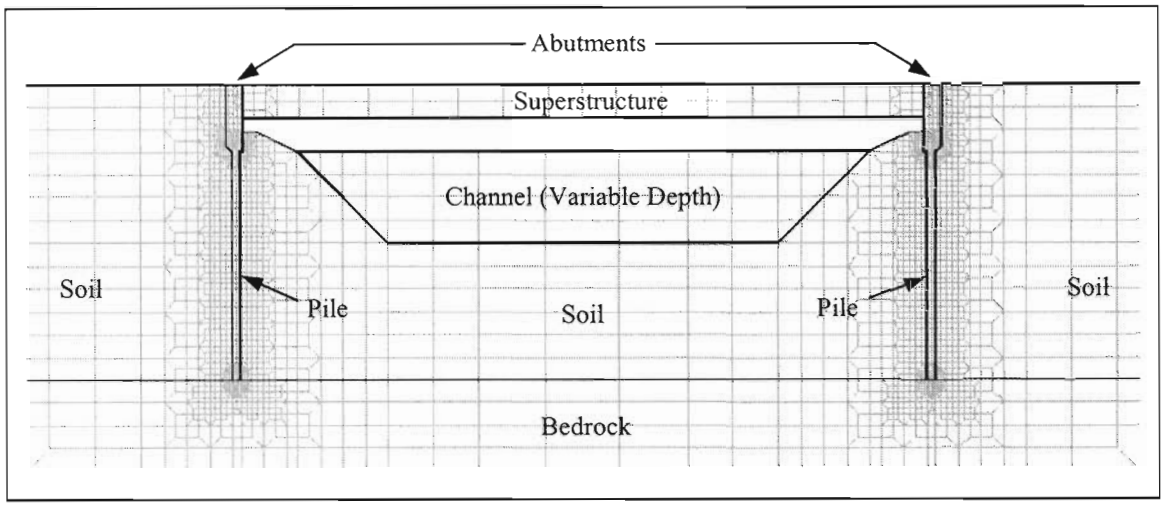

Figure 3.1. Typical finite element model of integral abutment bridge

All components of the bridge were modeled using continuum elements, as opposed to using specialty elements such as beams and springs. While the bridge plans specify wingwalls and approach slabs for each abutment, these were not included in the two-dimensional model. Many finite element models do not include approach slabs because they are not rigidly connected to the abutment. The finite element model studied by Diceli et al (2003) indicates that the effect of frictional forces between the approach slab and backfill and between the wingwalls and backfill on the behavior of the structure is negligible. The study preformed by Mourad & Tabsh (1998) found that the abutment/wingwall system does not behave as a rigid block, as a footing on flexible piles would behave.

This model accounts for both normal and tangential surface interactions between components. ABAQUS allows contact between elements to be defined using either surfaces or specialized contact elements. Surface-based contact was defined because it allows more complex interactions between the structure and soil than specialized elements will permit. Using surface-based contact in ABAQUS allows structural

elements to push against and deform soil elements, while simultaneously allowing the elements to slide against each other in opposite directions. A more detailed discussion of the development of the model is provided in the following sections.

3.2. Modeling Approach

A discussion of the techniques used in the creation of the finite element model is given in this section. Topics include a brief discussion of the types of elements used in the model, the constitutive models used to define the various material behaviors, and the use of surface based contact to model the soil-structure interaction.

3.2.1. Element Types

Because ABAQUS allows for the combination of different element types, the continuum that represents the soil and structure is comprised of both plane stress and plane strain two-dimensional solid elements. Although the elements in this model are two-dimensional, they have a nonzero out-of-plane thickness, the implications of which are discussed in Section 3.5.1.1. The structural components (piles, girder, and abutments) were modeled using plane stress elements. This is appropriate, because the components have a small thickness (z-component) compared to their dimensions in the x-y plane, and all of the loads applied to these elements act in plane (Logan, 1993). It may have been more appropriate to model the abutments with plane strain elements, because of their relatively large z-dimension. However, due to their large stiffness, there will be little change in the behavior of the system.

Conversely, the geotechnical components (soil and bedrock) were modeled using plane strain elements. Plane strain elements are well suited for geotechnical analysis,

because these problems generally have one dimension (usually the z-component) that is large in comparison with the others. In addition, ABAQUS only allows plane strain elements to be used with the elasto-plastic constitutive models that are used to represent soils.

As illustrated in Figure 3.1, the finite element mesh consists of both triangular and quadrilateral elements. The predefined ABAQUS element types used were: CPE6, CPS6, CPE8, CPS8, and CINPE5R. Elements with PE in the nomenclature are plane strain elements, while those with PS are plane stress. CPE6 and CPS6 types are 6-noded, second-order triangular elements that have three Gauss integration points per element. CPE8 and CPS8 types are also second-order elements, but they are 8-noded quadrilaterals with nine integration points per element. CINPE5R elements were used along the boundaries to represent soil and bedrock regions that extend a long distance away from the model. This element type is a 5-noded, second order infinite element, with four integration points per element. These elements are useful for modeling problems where the area of interest is small compared to the surrounding medium (HKS, 2001). General depictions of the elements used in this model are given in Figure 3.2.

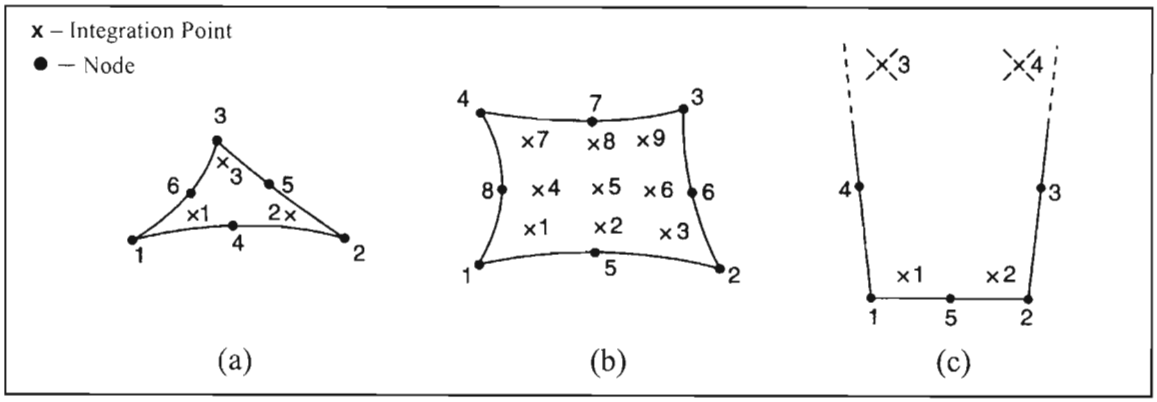

Figure 3.2. Examples of (a) 6-noded triangular, (b) 8-noded quadrilateral, and (c) 5-noded infinite elements (HKS, 2001)

3.2.2. Contact Modeling

Contact between elements in ABAQUS is defined in two different ways. Interaction between two materials can be defined with surfaces based on either nodes or element faces, or by using contact elements. In this model, the surface-based method was chosen because it was easier to implement and provided a more flexible method of contact modeling. The contact elements in ABAQUS are best suited for modeling large-sliding interaction between rigid bodies and small-sliding problems involving node-to-node contact (HKS, 2001). Use of contact elements in a model this large would require the definition of several thousand additional elements. In addition, advance knowledge of the kinematics of the two contacting bodies would be required to appropriately define their interaction. Surface based contact utilizes the faces of existing elements, and requires minimal advance knowledge of the behavior of the two bodies. Proper definition of contact surfaces allows the user to control deformation as well as frictional forces between surfaces.

The contact surfaces were defined by specifying the faces of the elements comprising the surfaces. ABAQUS uses a master/slave formulation to impose constraints on the interaction between the surfaces. The slave surface is usually defined as the surface with the finer mesh, to reduce the distance that nodes from one surface are allowed to penetrate into elements of the other. In this model, since the mesh densities across contact surfaces are equal, the slave surface was defined along the elements with the softer underlying material. This allows the structure elements and soil elements to push against each other, without allowing the nodes of the soil elements to penetrate into the pile and abutment elements.

Because the model considers geometric nonlinearities, and because the exact kinematics of the soil-structure interaction is not known, a finite-sliding formulation was used to account for the relative motion between the surfaces. Finite sliding allows for an arbitrarily large amount of relative motion between the surfaces, as well as arbitrarily large rotations and deformations. The surfaces may separate, unless they are joined using a tied constraint as required at the connection between the pile and abutment.

3.2.3. Constitutive Models

This model incorporates three constitutive models for the simulation of various materials. A linear elastic material model is used for the girders and abutments, as well as for soil and bedrock more than 2 m (6.6 ft) from the structure. The piles are modeled using an elastic-plastic constitutive model that ABAQUS calls classical metal plasticity. Soil and bedrock that is within 2 m of any part of the structure (abutments and piles) was modeled as a plastic material, using a Mohr-Coulomb failure criterion. A discussion of the determination of material properties needed to define these constitutive models is presented in Section 3.3.

In ABAQUS, stress-strain behavior for linear elastic materials is defined simply using Young's modulus and Poisson's ratio for the material. The girder was defined as a linear elastic material. This is reasonable since the model girder was based on the sectional properties of an actual girder, and the structure was analyzed under service loads. Thus, the girder strains will remain in the range of elastic material behavior. For the same reasons, the abutments were also modeled as linear elastic. Although the assumption of linear elasticity is unrealistic for soils, the soil and bedrock more than 2 m

away from structural elements were also modeled as linear elastic materials. This is because the soil and bedrock in these locations undergo very small strains and the material constitutive relationship has little effect on the bridge response. Furthermore, the computational complexity of the model is reduced significantly by assuming a linear elastic model. Finally, CINPE5R infinite elements may only be defined using linear materials, because the solution in the far field is assumed linear (HKS, 2001).

Classical metal plasticity is defined similarly to linear elasticity. However, an additional parameter indicating the yield stress of the material must be defined. Since one of the main principles of an integral abutment bridge is the redistribution of forces in the pile due to inelastic behavior, elasto-plastic behavior was necessary to realistically model the pile response. The additional computational cost of using such a constitutive model is negligible and is overshadowed by the benefit of more realistic behavior.

To achieve a higher degree of similitude with respect to the soil-structure interaction, the soil and bedrock adjacent to the abutments and piles were modeled using a Mohr-Coulomb plasticity model. This model is defined using the angle of internal friction (ϕ), the dilation angle (ψ), and the cohesion yield stress (c), in addition to the parameters used to define linear elastic behavior. The significance of these parameters is discussed in section 3.3.2. A popular simplification of this constitutive model is the Drucker-Prager material model. Unlike the Mohr-Coulomb yield function, the Drucker-Prager model does not have corners when plotted in principal effective stress space (Potts and Zdravković, 1999). These corners can result in singularities, which translate into the use of increased computer resources. Despite these drawbacks, Mohr-Coulomb plasticity was used to model the soil, because the parameters needed to define the material behavior

have more significance to a geotechnical engineer than those used to define the Drucker-Prager model.

3.3. Material Properties of Model Components

The development of material properties to be used for the various constitutive models in ABAQUS is discussed in this section. Two separate groups of components in the model are discussed herein. The first group is the structural components, which include the deck, girder, abutments, and piles of the bridge. The other group is the geotechnical components, comprised of soil and bedrock.

Methods used to develop material parameters for the model are discussed for each component of the model. Numerous papers and studies were reviewed in order to make sure that the proposed parameters were acceptable. The ultimate goal of the material property selection is to allow actual material test data to be correlated to the model parameters. Once model material parameters had been chosen, their behaviors were verified from the results of simplified finite element models.

3.3.1. Determination of Structural Properties

Since the model is a two-dimensional representation of a three-dimensional structure, certain geometric transformations of the structural elements had to be performed. This ensured that the model components retained the sectional properties and stiffnesses of the true components. Determination of superstructure (girder and deck) and substructure (abutment and piles) parameters is discussed separately, since slightly different methods and considerations were required for each.

3.3.1.1. Superstructure

For all variations of this model, the superstructure consists of a cast-in-place concrete slab supported by steel girders, similar to that of the Mill Pond Bridge. The properties of the steel girders and concrete deck are representative of the current design criteria of the MDOT. Bridge girders are typically constructed of ASTM A709 Gr. 345W structural steel plate. The concrete for abutments and the bridge deck is cast-in-place using MDOT Class P concrete, with a 28-day compressive strength of 41.3 MPa (6 ksi). Table 3.1 lists the material properties used in the model for the steel and concrete.

Table 3.1. Assumed Material Properties

	Steel	**Concrete**
Designation	*ASTM A709*	*MDOT Class P*
Yield/Compressive Stress	345 MPa (50 ksi)	41.3 MPa (6 ksi)
Young's Modulus	207 GPa (30000 ksi)	31 GPa (4500 ksi)
Density	7861 kg/m^3 (490 lb/ft^3)	2400 kg/m^3 (150 lb/ft^3)
Thermal Conductivity	1.17x10^{-5} 1/°C (6x10^{-6} 1/°F)	

As stated earlier, the span length of the Mill Pond Bridge is 35 m (115 ft). However, since the parametric study will cover a range of span lengths, it would not be reasonable to use a superstructure designed for a 35 m bridge for shorter spans. Therefore, a series of girders for various span lengths were derived from an elastic section analysis of a typical 35 m girder. The short-term, long-term, and non-composite section moduli of the girder were first calculated as required by the AASHTO LRFD Bridge Design Specification (1998). Short-term properties were calculated by considering the girder and slab as a composite section, transforming the concrete into steel using the ratio of Young's moduli of the materials. Long-term properties were calculated in a similar manner, except the modular ratio was multiplied by three. This

reduction in the modular ratio is intended to compensate for the effect of creep in the concrete deck. The non-composite section properties were simply the section properties of the steel girder, without considering the slab.

Three moments to be applied to the girder were then calculated. The first moment (M_{D1}) is due to the weight of the girder and slab. Weight of the crossframes and bracing was included by increasing the weight of the steel girder by 10% (Krusinski, 2002). The moment due to the weight of a 75 mm (3 in) thick bituminous concrete wearing surface (M_{D2}) was also calculated. Finally, the moment due to live loading (M_{AD}) was calculated using the HL-93 truck and lane load specified by AASHTO. The axle spacings of the truck were both 4.3 m (14 ft), and a distribution factor of 0.8 wheel lines/girder was applied to the live loads.

Using Equation 3.1, the tensile stress (f_t) in the bottom flange of the girder was calculated as:

$$f_t = \frac{M_{D1}}{S_{NC}} + \frac{M_{D2}}{S_{LT}} + \frac{M_{AD}}{S_{ST}} \qquad \text{(Equation 3.1)}$$

where S_{NC}, S_{LT}, and S_{ST} represent the non-composite, long-term, and short-term section moduli, respectively. The steel girder sections for other spans were sized such that the stress in the bottom flange was equal to this value under similar loading conditions. In addition, the span-to-depth ratios of all the girders were held constant. The thickness of the deck was also kept constant to simplify calculations. Section properties calculated for different spans are given in Table 3.2; these values compare well with section properties of actual girders used for bridges of similar lengths.

Table 3.2. Adjusted Composite Section Properties of Girders

Length (m)	Area (mm^2)	Moment of Inertia (mm^4)
15	108326	2.771×10^9
20	114319	6.336×10^9
25	120603	1.216×10^{10}
30	127595	2.070×10^{10}
35*	134800*	3.266×10^{10}*

**Actual values*

Since the model is a two-dimensional representation of a three-dimensional structure, special measures had to be taken to represent the stiffnesses of the components accurately. The solid elements used to model the girder and deck have a rectangular cross-section, while the true cross-section is more complex. As illustrated in Figure 3.3, the depth (h) of the model girder was set at the true depth of the actual girder, and the width of the girder elements was set at 1m along the z-axis. Using the short-term composite properties determined in the elastic section analysis, the moment of inertia of the model cross-section (I_{model}) was then calculated for each span length.

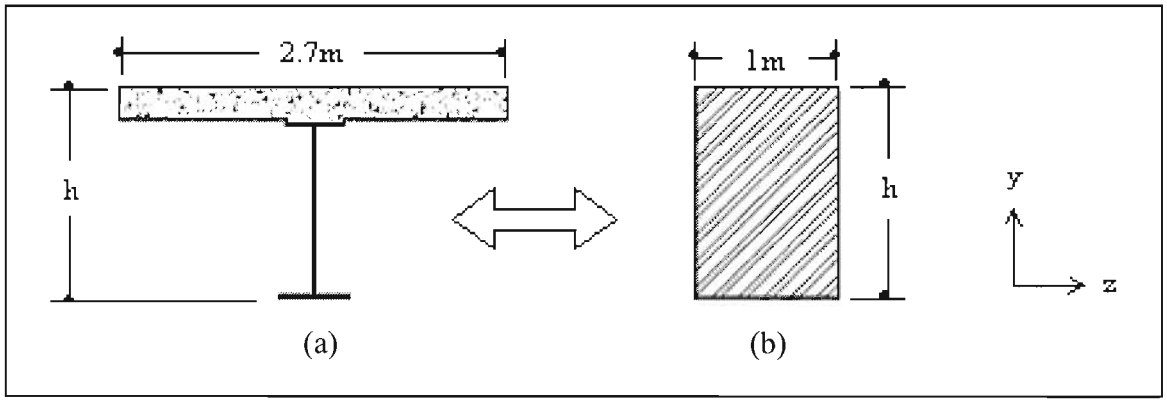

Figure 3.3. Cross-sections of (a) actual girder and (b) model girder

An equivalent Young's modulus (E_{model}) for the model girders was calculated using the following equation:

$$E_{model} = \frac{E\, I_{actual}}{I_{model}} \qquad \text{(Equation 3.2)}$$

where E_{actual} and I_{actual} are the modulus of elasticity and moment of inertia of the composite girder section, respectively. Values for the equivalent Young's moduli are given in Table 3.3. Axial stresses in the girder are not examined in this study, so it is not critical that the axial stiffness of the girder is not consistent with that of the model girder. In addition, the axial stiffness in the model was large enough to ensure that the superstructure is essentially inextensible, which is the actual case.

Table 3.3. Equivalent Young's Moduli for Model Girders

Length (m)	I_{actual} (mm^4)	I_{model} (mm^4)	E_{model} (GPa)
15	2.771×10^9	2.035×10^{10}	28.193
20	6.336×10^9	5.583×10^{10}	23.493
25	1.216×10^{10}	1.187×10^{11}	21.214
30	2.070×10^{10}	2.166×10^{11}	19.779
35	3.266×10^{10}	2.812×10^{11}	24.038

It should be noted that the moments of inertia given in Table 3.3 were based on the short-term composite section properties of the girder. Use of these properties is only strictly valid for cases involving the live loading. There are certain instances where the non-composite and long-term composite section properties must be considered. The long-term composite section properties are more appropriate for dead loading, because they will account for additional creep deflections. An explanation of how these

differences in section properties for various loadings were accounted for is given in Chapter 4.

To account for the increase in cross-sectional area of the superstructure, the densities for each girder were also modified to give the correct girder weight. The modified density is based on the weight of both concrete and steel in each girder section. Material properties such as the coefficient of thermal expansion (α) and the Poisson's ratio (ν) were unaffected by the transformation of the girder cross-section.

3.3.1.2. Substructure

Because the piles and abutments were also modeled using two-dimensional elements, cross-section transformations similar to those for the girder were performed. Unlike the girder, the cross-sections for the piles and abutments did not vary with span length. The abutment height was defined as 1.5 m plus the depth (height) of the girder. The pile section for all span lengths was chosen to be the same as that for the 35 m long Mill Pond Bridge. This was done to eliminate a variable in the parametric study, as this section is preferred by MDOT for integral abutment bridges with steel girder superstructures up to 36m (118 ft) long (MDOT, 1999). This pile may be oversized for smaller-span bridges, but as research by Arsoy et al (2002) shows that stiffer piles result in increased stresses for a given deflection. Therefore, use of a larger H-pile for smaller spans is thought to present a worst-case scenario in terms of pile stresses.

Since the H-piles are embedded into almost half of the height of the abutment, it was felt that the increase in flexural stiffness due to the pile needed to be accounted for. Therefore, the properties of the abutment cross section were calculated in a manner

similar to that used to determine the short-term composite properties of the girder, where the steel pile was transformed into concrete. The equivalent Young's modulus (E_{model}) that accounted for the presence of the embedded pile was found to be slightly larger than the value of E_{model} neglected the presence of the pile.

Unlike the unit thickness of the girder elements, the thickness of the abutment elements was set at 2.7 m (8.8 ft), which is the pile spacing and the tributary deck width used in the section property calculations for the girders. When this thickness is used in conjunction with the true width (x-dimension) of the abutments, the flexural stiffness ($E*I$) and axial stiffness ($E*A$) of the model and actual abutment are equivalent. The density and Poisson's ratio of the abutments were set equivalent to those of reinforced concrete, since the transformed abutment section was based on properties of concrete. Because the widths of the model and portion of the actual abutment considered were equal, no transformation of the density of the abutments was required.

Like other non-rectangular components, the properties of the piles had to be adjusted to account for the rectangular cross section of the elements. Because the pile material was homogenous, it was not necessary to transform materials to obtain composite cross-section properties. The piles in the Mill Pond Bridge were oriented for weak-axis bending, i.e., their webs were perpendicular to the direction of the span. Consequently, the thickness of the elements was set equal to the depth of the HP 360x108 section, or 0.346 m (13.61 in).

As with the abutments, it was critical that the flexural stiffness and axial stiffness of the model and actual pile be equal. However, if the x-dimension of the pile elements is set equal to the width of the pile flange, this cannot be accomplished. Therefore, it was

necessary to calculate a dimension that allows this condition to be met. As mentioned earlier, the equivalent model Young's modulus based on flexural stiffness can be calculated using Equation 3.2. Likewise, the equivalent Young's modulus can be calculated based on the axial stiffness of the pile, using:

$$\frac{I_{actual}}{I_{model}} = \frac{A_{actual}}{A_{model}} \qquad \text{(Equation 3.3)}$$

where A_{actual} and A_{model} are the areas of the actual and model piles, respectively. Setting both values of E_{model} equal results in:

$$E_{model} = \frac{E_{actual}\ A_{actual}}{A_{model}} \qquad \text{(Equation 3.4)}$$

Since the thickness of the model pile, as well as the area and moment of inertia of the true pile are known, the x-dimension of the pile can be calculated as:

$$x = \sqrt{\frac{12 \times I_{actual}}{A_{actual}}} \qquad \text{(Equation 3.5)}$$

This results in an element width of 0.308 m (12.1 in), compared to the flange width of 0.370 m (14.5 in). Equation 3.2 or 3.3 can then be used to solve for E_{model} of the pile.

Unlike the superstructure, the piles incorporate nonlinear behavior, and are able to yield at a specified stress. The change to the element width described previously will alter the section modulus, which will affects the value of the yield stress. A procedure similar to that for finding E_{model} can be used to determine an equivalent yield stress, F_{ym}, given in Equation 3.6 as:

$$F_{ym} = \frac{F_{yp}\ S_{actual}}{S_{model}} \qquad \text{(Equation 3.6)}$$

where F_{yp} is the yield stress (345 MPa), and S_{model} and S_{actual} are the section moduli of the model and actual piles.

The density of the model pile was adjusted to give the correct pile weight. The mass of the pile plus the mass of the volume of soil contained between the webs and flanges was used to obtain the model pile density. The density of the soil was assumed as 2000 kg/m^3, and was included to give a better representation of the pressure on the bedrock at the pile tip. Table 3.4 compares properties of the model and actual pile cross-sections. A summary of all structural element properties is provided in Table 3.5.

Table 3.4. Comparison of Actual and Model Pile Section Properties

	Actual	**Model**
Width	370 mm	308 mm
Depth	346 mm	346 mm
Moment of Intertia	109 x 10^6 mm^4	842.5 x 10^6 mm^4
Area	13800 mm^2	106600 mm^2
Section Modulus	5.87 x 10^5 mm^3	5.47 x 10^6 mm^3

Table 3.5. Summary of Structural Element Properties

Element Type	Girder / Deck	Abutment	Pile
Young's Modulus (E)	*see Table 3.3*	28.4 GPa	26.78 GPa
Poisson's Ratio (ν)	0.28	0.11	0.28
Density (ρ)	*Varies with span*	2400 kg/m^3	3172 kg/m^3
Yield Stress (F_y)	--	--	36.998 MPa
Thermal Conductivity (α)	1.17x10^{-5} 1/°C	--	--

3.3.2. Determination of Geotechnical Properties

A transformation such as the one performed on the structural elements was not necessary for the geotechnical elements, since the soil and bedrock were modeled with the assumption of plane strain conditions. Model soil properties were chosen to represent

a group of subsurface conditions commonly found in Maine, rather than specific soils. This approach helps to limit the number of variables in the parametric study, as well as simplify the design procedure.

Three general soil categories (granular, glacial till, and clay) were defined to represent subsurface conditions that could be encountered at bridge sites in Maine. The three categories were defined in a manner such that they each provide a different degree of support to the piles. It was desired that the granular material represent a dense sand and gravel, with high shear strength, to provide the most support to the foundation. On the other end of the spectrum, the clay material was defined as medium clay, offering less support to the piles. The properties of the glacial till were defined such that its behavior is somewhere in between that of the clay and granular materials. Properties for these soils are based mainly on published values and other empirical data. The properties of the bedrock were based on schist, which is a common type of bedrock in Maine.

As discussed earlier, a material obeying the Mohr-Coulomb plasticity model is defined using six parameters: Young's modulus (E), Poisson's ratio (ν), density (ρ), the angle of internal friction (ϕ), the dilation angle (ψ), and the cohesion yield stress (c). While the definition of the latter four parameters is relatively straightforward for soils, the definition of Young's modulus is not. Typical values for c, ϕ, and ρ were derived from values found in literature, and the remaining parameters were calculated using various correlations.

Parameters for the granular and glacial till materials were determined in the following manner. First, a range of representative values of ϕ and c were chosen from published works. For the granular material and glacial till, the drained strength

parameters ϕ' and c' were used, while undrained strength parameters were used for the cohesive material. Design values that are used in practice are generally conservative, having lower values for strength parameters. However, to predict performance, as is the case in this study, representative values measured in testing rather than overly conservative estimates are desired. According to Lambe & Whitman (1969), values of ϕ' range from 33° to 50° for gravel and sandy gravel, and from 33° to 45° for river sand to pebbles. Marsal (1973) gives values of ϕ' ranging between 32° and 53° for rockfill including sand and gravel. Lambe & Whitman (1969) note that larger values are appropriate for dense soils, for soil with angular particles, and for well-graded sand and gravel mixtures. Terzaghi, Peck, and Mesri (1996) give values of ϕ' ranging from 46° to 59° for the normal stresses expected in this project.

Most reported values of ϕ' are obtained by triaxial testing, whereas plane strain conditions usually prevail in most situations. Cornforth (1964) showed that ϕ' values for plane strain conditions were typically 4° higher than those obtained through triaxial testing. Terzaghi, Peck, and Mesri (1996) also report an average difference of 5° between plane strain and triaxial ϕ values. Therefore, the range of ϕ' for the granular material was chosen as 40° to 50°. Since the granular material is cohesionless, c should theoretically be zero. However, the use of a zero cohesion value causes solution problems in ABAQUS. Therefore, a small cohesion stress of 300 Pa (6 psf) was chosen to facilitate in solution convergence. As discussed later, verification of the model properties shows that this small amount of cohesion has negligible effects on the material behavior.

Values of ϕ' for glacial till were obtained from the proceedings of a research conference on shear strength of cohesive soils (Linell & Shea, 1961). In these proceedings, results of tests on various glacial tills from New England were presented. Results from consolidated-undrained triaxial tests, and consolidated-drained direct shear tests were used to develop the range of c' and ϕ' values. The range of ϕ' for the glacial till material was chosen as 30° to 40°, and the range of c values was chosen as 0.0 to 0.2 tsf (20 kPa).

After the ranges of ϕ' and c' were chosen, values for Young's modulus were determined. Duncan et al (1980) outline a procedure to determine stress-strain parameters based on the tangent value of Young's modulus. Values can be calculated using an equation proposed by Janbu (1963):

$$E_i = K \times p_a \left(\frac{\sigma_3}{p_a} \right)^n \qquad \text{(Equation 3.7)}$$

where σ_3 is the confining stress and p_a is atmospheric pressure, which is included for unit conversion purposes. The dimensionless parameters K and n are the modulus number and modulus exponent, respectively. E_i is the initial tangent to the hyperbolic stress-strain curve for soils. Duncan et al (1980) tested various soils under drained and undrained conditions to determine values of the modulus number and the modulus exponent. For each soil type, material properties such as unit weight, relative density, particle shape, ϕ', and c' are published. The range of confining stresses under which the test was performed in order to determine K and n values were also included.

Soils were selected that had ϕ and c values that fell within the range of values for the granular and glacial till materials. For the granular material parameters, well graded

gravels and sands as well as some poorly graded gravels were selected as a basis. In all cases, only soils with relative densities greater than 95% were considered. For the glacial till parameters, silty sands and sandy silts were selected. There was no relative density requirement for these soils. Equation 3.7 was solved using the values of the modulus number and exponent given for each soil, and p_a was taken as 101.3 kPa (1 atm).

An average value of the confining stress for the system was calculated at a depth of 5 m. This results in the values of Young's modulus above this depth being slightly higher than what would occur in the field, while values below this depth would be slightly less. This average confining stress was compared to the range of confining stresses given for the triaxial tests in Duncan et al (1980), and used to select appropriate values for K and n. The resulting E_i values, as well as the given values of c and ρ for each soil were averaged to give representative parameters for both the granular and glacial till materials. The calculated density of the glacial till was increased to reflect the densities for New England tills given by Linell & Shea (1961), as well as to reflect cobbles and boulders that are often present in Maine glacial tills.

The clays tested by Duncan et al (1980) did not have properties similar to those of clays of the Presumpscot formation, which is a "widespread blanket of glaciomarine silt, clay, and sand that covers most of southern Maine" (Thompson, 1987). Because of this, the method for determining representative values of E, c, and ρ described previously could not be used. Since extensive testing and research on the soils of the Presumpscot formation has been done in Maine, the material parameters are based on these values. It was assumed that the clay would be undrained, therefore the undrained friction angle (ϕ) was set to 0°. However, this value was changed to 0.001° because ABAQUS requires ϕ

to be a nonzero value. The density of the material was taken to be higher than normal for clays in the Presumpscot formation, in order to mimic a saturated unit weight. This also helps to account for the fact that in shallow conditions most of the clay will consist of a stiff crust.

Based on work by Amos (1987), Andrews (1987), and Devin (1990), some representative values for undrained shear strength, plasticity index, and overconsolidation ratio of typical Presumpscot formation clays were derived. The undrained shear strength was taken as 35 kPa (730 psf), which is somewhat high for the softer Presumpscot formation clays, but is a low value for the crust. Because the clay is assumed to be saturated, and ϕ is equal to 0°, the cohesion yield stress (c) is equal to the undrained shear strength. The overconsolidation ratio (OCR) was taken as 2.5. This value is an average of the OCR at the upper crust, which is approximately four, and the deeper deposits, which have an OCR closer to one. Finally, the plasticity index for Presumpscot formation clays was assumed as 20, based on test data of both brown and gray Presumpscot sediments (Amos, 1987).

Duncan & Buchignani (1976) and Mitchell (1993) suggest an empirical correlation between the undrained Young's modulus (E_u) and the undrained shear strength (C_u):

$$E_u = K_c \times C_u \qquad \text{(Equation 3.8)}$$

where K_c is a dimensionless correlation factor determined from Figure 3.4, using the OCR and plasticity index (PI) for the soil. For the given conditions, K_c was estimated as 850. This results in an undrained Young's modulus of approximately 30 MPa (4300 psi)

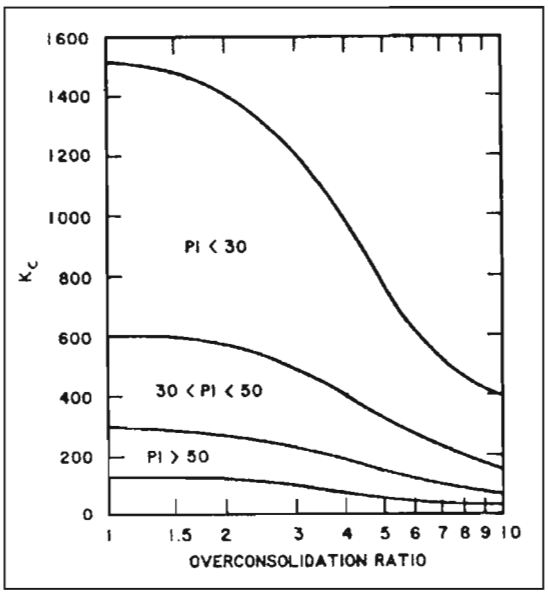

Figure 3.4. Chart for estimation of K_c constant (Army Corps of Engineers, 1990)

Parameters for the bedrock material based on schist were developed in the same manner as the parameters of the clay material. *E*, *c*, ϕ, and ρ were based on typical values for schist, laboratory test data, and values from case histories. The values for Young's modulus and cohesion yield stress were based on laboratory data for schist from Lama and Vutukuri (1978). However, this calculated value of Young's modulus was then decreased in order to allow the pile to be able to deform the bedrock, since the Young's modulus of the pile was decreased drastically from that of steel. The cohesion yield stress of the bedrock was taken as one-half of the unconfined compressive stress. Because of the reduced value of Young's modulus, larger unconfined compression strength values for the bedrock were used to prevent any premature yielding. Values for ρ and ϕ were based on the lower range of typical values for schist published in Bell (1992) as well as in Lama and Vutukuri (1978).

The meanings of Poisson's ratio (ν) and the dilation angle (ψ) for soils and rock are not as well understood as parameters such as E, c, and ϕ. In triaxial testing, ν can be calculated by measuring the axial compressive and lateral strains (Goodman, 1989). Head (1986) notes that it is common to use $\nu = 0.5$ for saturated soils, which is the theoretical value for an incompressible material. This represents a condition of no volume change, so in all cases Poisson's ratio is less than this value. Typical values for Poisson's ratio for numerous materials are given by Head (1986), Bishop & Hight (1977) and Goodman (1989). The value chosen for Poisson's ratio of the bedrock is somewhat high, compared to laboratory test data given by Lama and Vutukuri (1978). The higher value of Poisson's ratio was used in an attempt to capture any volume change of the bedrock due to deformation of the weathered upper layers.

The dilation angle of a material is defined as the ratio of the plastic volume change to the plastic shear strain. It describes the plastic flow potential of a material, and whether or not this potential is associated or non-associated. Associated plastic flow occurs when the friction angle is equal to the dilation angle (HKS, 2001). However, the use of associated flow leads to physically unrealistic volume changes. Non-associated flow occurs when $\psi < \phi$, and if $\psi = 0°$, no plastic dilation or volumetric strain occurs (Potts and Zdravković, 1999). Non-associated flow is preferred in most cases, because the vector of plastic strain is normal to the plastic potential, which is geometrically similar to the failure function (Rahim, 1998). This leads to better solution convergence, with more realistic volume change behavior with the application of stress.

Non-associated flow was desired for all of the materials in the model. Potts and Zdravković (2001) performed an analysis of a single pile in soil modeled using Mohr-

Coulomb plasticity, in which the value of ψ was varied from 0° to ϕ. They demonstrate that the analysis where ψ is equal to 0° the plastic volumetric strain in the soil reaches a limiting (constant) value faster than in the analysis performed where $\psi = \phi$ (associated flow). Furthermore, the analysis with associated flow conditions gave no indications of the plastic strains ever reaching a constant value with further displacement. Therefore, it was decided to set $\psi = 0°$ for all soils. The assumption of $\psi = 0°$ was valid for the clay material because the volume change of saturated undrained soils under stress is typically minimal. In addition, flow is still non-associated, since ψ is still less than ϕ (0.001°).

However, for the remaining geotechnical materials, the assumption of $\psi = 0°$ led to numerous solution convergence problems. Rahim (1998) also noted that numerical difficulties occur when the degree of non-associativity is high ($\psi << \phi$). Therefore, for the rest of the soils and bedrock, ψ was set equal to a value of ($\phi - 5°$). Better solution convergence was then obtained, while still incorporating non-associated plastic flow. A summary of the geotechnical material properties is presented in Table 3.6.

Table 3.6. Summary of Geotechnical Element Properties

Element Type	Granular	Glacial Till	Clay	Bedrock
Young's Modulus (*E*)	120 MPa	80 MPa	30 MPa	3.5 GPa
Poisson's Ratio (ν)	0.40	0.45	0.499	0.25
Density (ρ)	2000 kg/m^3	2200 kg/m^3	1800 kg/m^3	2660 kg/m^3
Friction Angle (ϕ)	45°	35°	0.001°	26°
Dilation Angle (ψ)	40°	30°	0°	21°
Cohesion (*c*)	0.3 kPa	9.0 kPa	35 kPa	82.7 MPa

3.3.3. Frictional Parameters

Surface contact in ABAQUS requires the input of various parameters that govern the behavior of the two bodies in contact. The first, as discussed in Section 3.2.3, is Young's modulus and density of the two materials. This keeps nodes of softer materials from penetrating the elements of harder materials. Interaction tangential to the surface is governed by a specified coefficient of friction, μ. Initially, the coefficients of friction between all dissimilar materials (soil/rock, soil/concrete, soil/steel, and steel/rock) were all set to 0.5. This translates into the forces acting parallel to the surfaces being one-half the magnitude of those acting perpendicular to the same surface. However, this coefficient of friction overestimates the forces in some cases and underestimates those in others.

Separate values for different material interactions were chosen in order to better capture the various surface-surface interactions around the model. The soil/rock coefficient remained at 0.5, because it was felt that this parameter would have very little effect on the behavior of the system. For interaction between soil/steel and soil/concrete, μ was chosen as 0.45. Separate coefficients of friction were not selected in order to reduce the number of variables in the parametric study. Although this value is high for steel on clay soils, it is a reasonable fit for the other soil types based on Table 1 of NAVFAC DM-7.02 (1986). This table lists friction factors, friction angles, and adhesion values for dissimilar materials.

Determining an appropriate value of μ for the interaction of steel and rock was more difficult than for the other interactions. Friction between smooth steel and smooth rock is generally quite low. However, the bedrock surface at a given bridge site would

most likely be weathered and broken, and the steel piles would have a hardened driving tip with jagged teeth welded to the end. Because of this, a representative friction factor was calculated using principles developed for the study of rock/rock and rock/concrete interaction.

Patton (1966a) presents the following equation used to determine the shear stress at a rough rock/rock interface:

$$\tau_i = \sigma_a \tan(\phi + i) \qquad \text{(Equation 3.9)}$$

where σ_a is the average normal stress applied to the joint, ϕ is the friction angle of the rock, and i is an angle that describes the roughness of the joint. In nature, rock/rock joints seldom have a regular saw-toothed pattern that would result in a constant value for i. Field measurements by Patton (1966b) show that a value of i between 10° and 15° is reasonable for the component of strength due to irregularities or in-situ discontinuities.

Figure 3.5 shows examples of driving shoes manufactured by Associated Pile & Fitting, LLC (2004). As can be seen in the figure, it can be conservatively estimated that the slopes (i) of the teeth on the bottom of a generic pile shoe are ±10°. Using Equation 3.12, μ can be calculated, since it is defined as the ratio of the shear stress to normal stress. With an i of 10°, a ϕ of 26°, and assuming that the surface of the bedrock is level, μ is calculated as approximately 0.7. A summary of coefficients of friction (μ) for all of the surface interactions included in this model is given in Table 3.7.

Table 3.7. Summary of Frictional Parameters

Interaction	Coefficient of Friction (μ)
Soil / Rock	0.5
Soil / Steel	0.45
Soil / Concrete	0.45
Steel / Rock	0.7

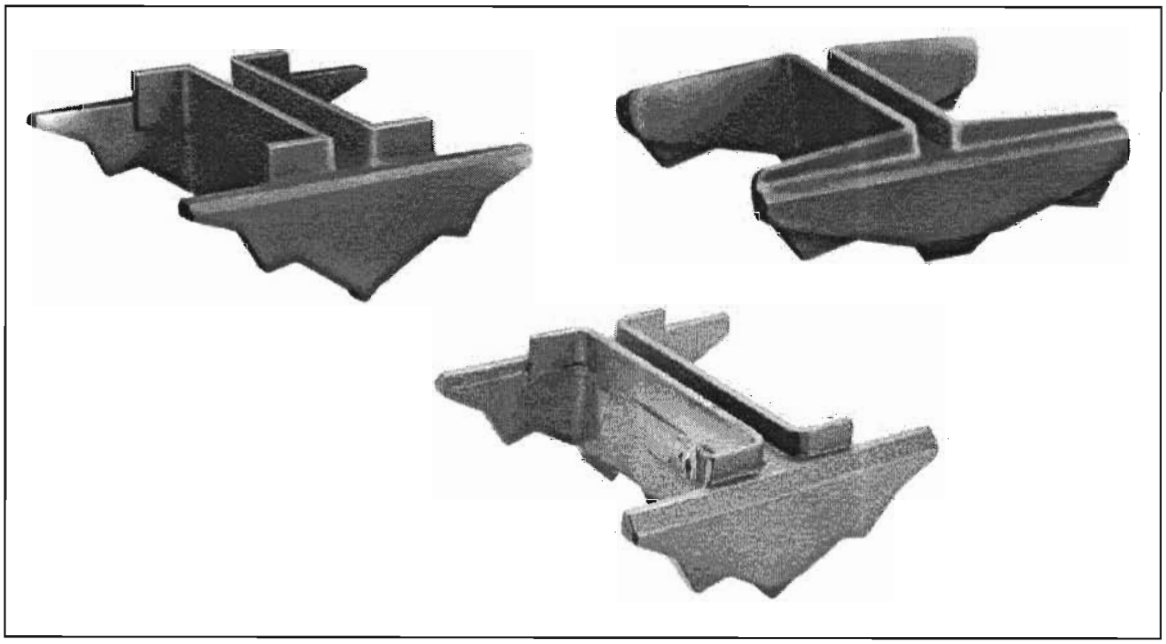

Figure 3.5. Examples of Hard-Bite™ H-pile points from Associated Pile (2004)

After changing the coefficients of friction for the various interactions in the model, several additional preliminary models were run to determine the effects of the changes. The results from these analyses showed improved behavior of the components of the model. However, it was determined that the frictional interface between the soil and structure was behaving improperly. Due to the incremented application of gravity loads discussed in section 3.4.2, the piles were experiencing downdrag forces from the soil 2-3 orders of magnitude greater than would be expected. When gravitational forces are applied to the soil, it settles while the positions of the piles and abutments remain

fixed in space, causing large initial differences in displacements. These large initial displacements result in increased shear stress along the surfaces of the pile, which cannot be equalized by the settlement of the pile alone.

This situation was resolved through the *CHANGE FRICTION command in ABAQUS, which allows for the user to modify the coefficient of friction for selected interactions at any time during the analysis. Initially, the coefficient of friction between all soil and structural elements was set to zero, meaning that no shear forces will develop, and the contact surfaces are free to slide (HKS, 2001). Gravity was then applied to the soil, which settled without generating any downdrag forces on the pile. The friction factor was then set to 0.45, and gravity was then applied to the abutments and pile. The shear forces generated with this procedure were not downdrag forces; rather they were similar to the side resistance generated during the driving of piles.

3.3.4. Verification of Material Properties

The behavior of the structural and geotechnical elements was verified using simple finite element models. For the structural elements, it was necessary to determine if the girders and piles with transformed rectangular cross sections behaved like their non-rectangular counterparts. As for the geotechnical elements, simple finite element analyses were performed to study their behavior as well as verify the values of parameters such as c and ϕ.

3.3.4.1. Structural Elements

Checks were performed on both the girder and the piles. For the girder, the deflections due to loading, as well as the amount of expansion under temperature changes

were examined. As for the piles, deflections and the stress at which the material yielded were reviewed. Simplified models were created, and results from these models were compared to hand calculations and theory.

The deflections at the midpoints of the model girders were compared to the values calculated using equations for a simply supported beam and a beam fixed at both ends, subjected to a uniform loading, in addition to a point load acting at the midpoint. The magnitude of the distributed load represented the dead load of the girder plus the weight of the crossframes, pavement, and railing; the point load was an arbitrary value of 145 kN (32.6 kips). Deflections predicted by the model girders compared well with calculated values. In most cases, the deflections predicted by the model were slightly higher than the calculated values, but differed by only 3% at the most.

Expansion and contraction of the model girders due to temperature change was also compared to theoretical values. The model girder was fixed at one end, and free to translate horizontally at the other. A temperature change of ±50°C (±122°F) was applied to the girder. Values predicted using the finite element model compared extremely well with theory, falling within 0.03% of each other. The higher degree of accuracy of the predicted thermal movement can be attributed to the fact that the weight and stiffness parameters of the girder were transformed as discussed in this chapter, while the coefficient of thermal expansion was not.

Deflections and the yield stress of the pile were verified by modeling the pile as a cantilever beam with the toe of the pile fixed, and applying a lateral load to the head of the pile. No soil was included, to allow for the comparison between the model results and the known solution for a cantilever beam. Piles 3m, 6m, and 9m in length were

studied to determine whether the load-displacement behavior of the model piles was affected by pile length.

Initially, the fixed condition at the base of the pile was modeled by restraining all of the nodes along the toe in both the x and y directions. However, it was found that this method overpredicted the loads that cause the yield moment (M_y) and the plastic moment (M_p) by artificially restraining the tip of the pile. To resolve this, the fixed condition at the pile tip was modeled by applying a shear force in the opposite direction of the applied force, distributed across the nodes of the pile toe as shown in Figure 3.6. Only the left-most node (node 80) in Figure 3.6 was restrained against movement in the x and y directions, while the rest of the nodes were restrained in only the vertical direction. The distribution of the shear reaction at the pile toe was taken as parabolic, in accordance with beam theory. The equivalent shear stress, τ_e , was calculated using the following equation (Gere & Timoshenko, 1997):

$$\tau_e = \frac{V}{2I_{model}}\left(\frac{d_m^{\,2}}{4} - x_n^2\right) \qquad \text{(Equation 3.10)}$$

where V is the value of the applied lateral load, I_p and d_m are the moment of inertia and depth (308 mm) of the model pile, respectively. The value of x_n is equivalent to the distance between the neutral axis of the cross-section, and the node at which the shear stress is calculated. The equivalent reaction force at each node is then given by the product of the shear stress, and 1/8 of the area of the model pile.

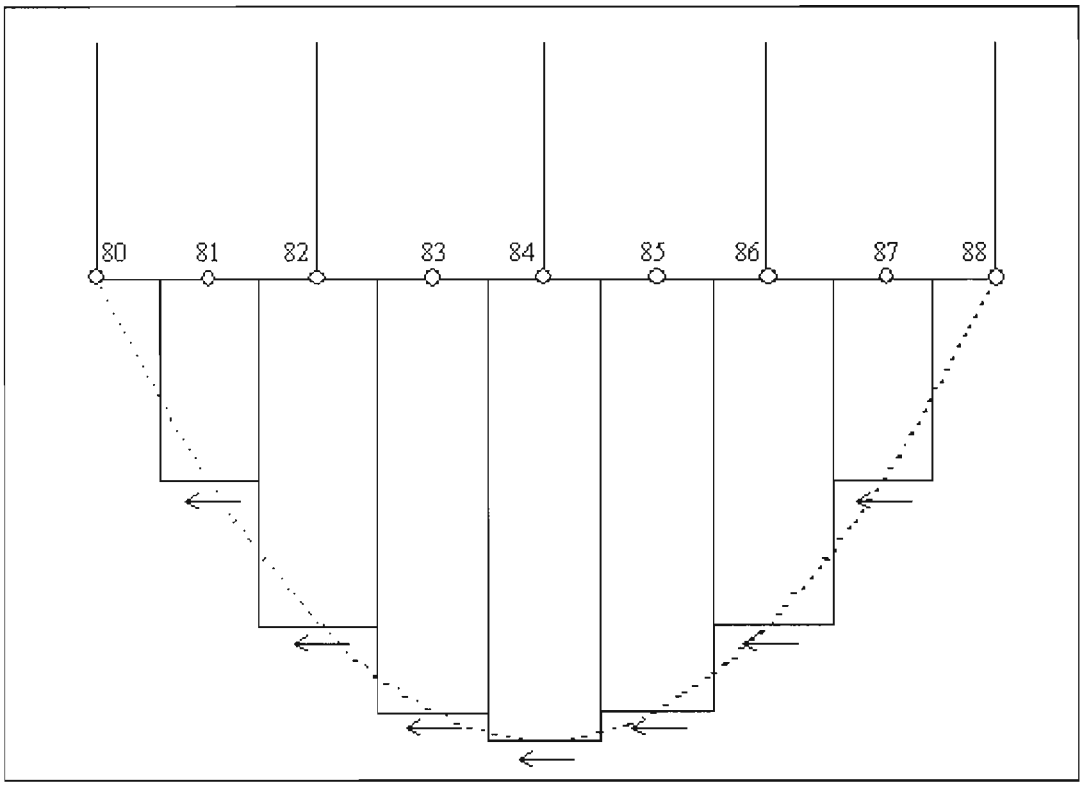

Figure 3.6. Distribution of equivalent reaction forces at pile toe

Load-displacement diagrams for the model piles utilizing the more compatible formulation at the pile tip are shown in Figure 3.7. The load-displacement behavior is linear up to the point where the applied load is sufficient to initiate yielding of the cross section. When the load is large enough to cause the entire cross section to yield, the diagram becomes a horizontal line. Thus, the finite element model predicts a curved transition between the loads causing the yield and plastic moments, which is due to the progression of yielding over the depth of the cross-section. The comparison between the finite element model results and the idealized elastic-plastic response is excellent.

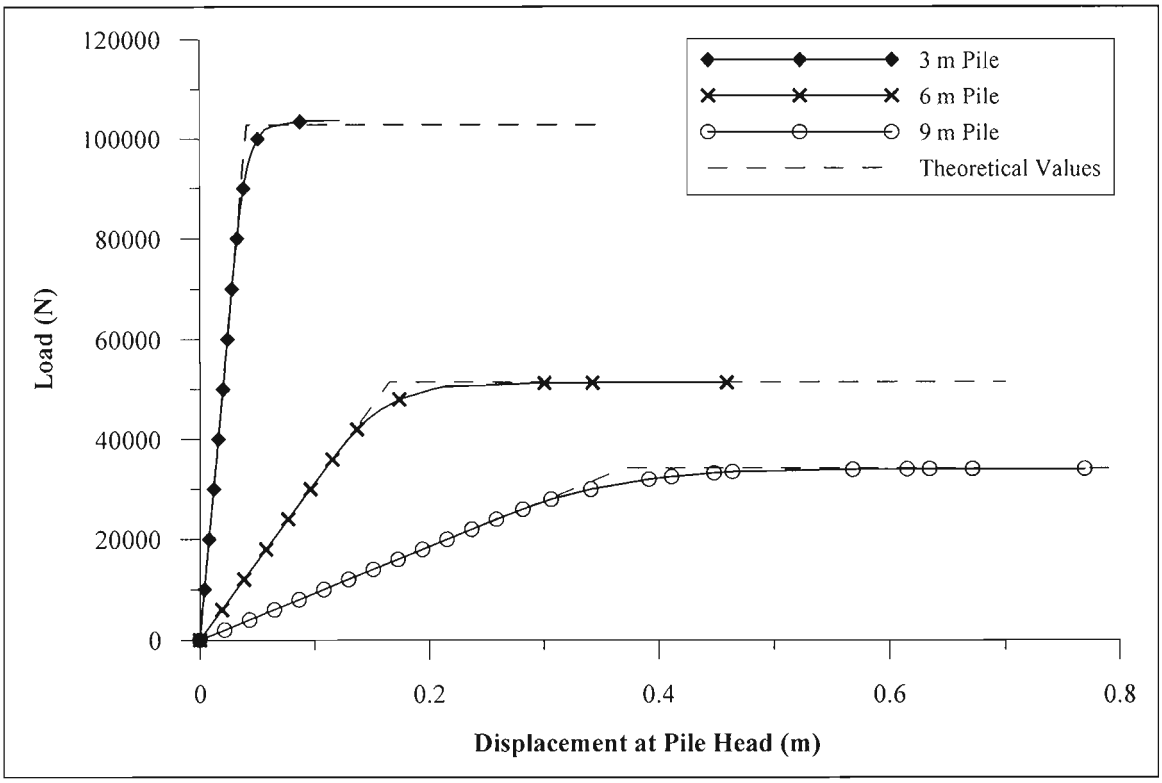

Figure 3.7. Load-displacement curves for model piles of various lengths

3.3.4.2. Soil Elements

Plane strain compression tests were modeled using the three soil types in order to determine whether they exhibited a response consistent with their assigned material properties. Using ABAQUS, a 100 mm (4 in) cube of soil was tested at confining pressures ranging from 20 kPa to 400 kPa (3 to 58 psi). Instead of applying a load to the top of the soil specimen, the nodes along the top of the sample were displaced uniformly in the y-direction to apply a constant rate of strain to the specimen, which better simulates a laboratory triaxial test. The bottom nodes were restrained against displacement in the y-direction, while a single node at the bottom center of the specimen was restrained in the horizontal direction. The magnitude of the deviator stress was determined by subtracting

the confining pressure from the vertical stresses in the soil elements given in the ABAQUS output. The model was run until the strain in the soil specimen reached 22%.

The volumetric strain of the soil sample was calculated in order to determine the effect of the value of ψ on the material behavior. As expected, volumetric strains in the soil specimen increased with larger values of ψ, with little to no volume change occurring when $\psi = 0°$. While the value of ψ significantly affected the volume change behavior of the material, there was little change in the stress-strain behavior, unless $\psi = 0°$. To examine the stress strain behavior, the principal stress difference ($\sigma_1 - \sigma_3$) was plotted versus the axial strain. For all soil types, the slope of the initial linear portion of the stress-strain curves matched the Young's modulus of the material. As would be expected, for increasing confining stresses, the soils reached a higher peak principal stress difference. A limitation of the Mohr-Coulomb material model in ABAQUS was observed, as the soils did not exhibit strain softening/hardening behavior past the peak principal stress difference. Overall, the stress-strain behavior of the model soils was satisfactory for this phase.

Values of the friction angle (ϕ) and cohesion (c) were verified using the data from the model plane strain tests. Based on the data, values of p and q were calculated using the following equations given by Holts and Kovacs (1981):

$$q = \frac{\sigma_1 - \sigma_3}{2} \qquad \text{(Equation 3.11)}$$

$$p = \frac{\sigma_1 + \sigma_3}{2} \qquad \text{(Equation 3.12)}$$

where σ_1 is the value of the applied vertical stress, and σ_3 is the value of the applied confining stress. Using the values of p and q at different confining stresses, a K_f line for each material was plotted, as shown in Figure 3.8. The slope (φ) and intercept (a) of the K_f line are related to the friction angle and cohesion of the material by the following equations:

$$\sin(\phi) = \tan(\varphi) \qquad \text{(Equation 3.13)}$$

$$c = \frac{a}{\cos(\phi)} \qquad \text{(Equation 3.14)}$$

Table 3.8 gives a comparison between the intended soil parameters, and the values of ϕ and c based on the test data. As was the case with the pile elements, the soil elements exhibit the behavior that was expected in their definition.

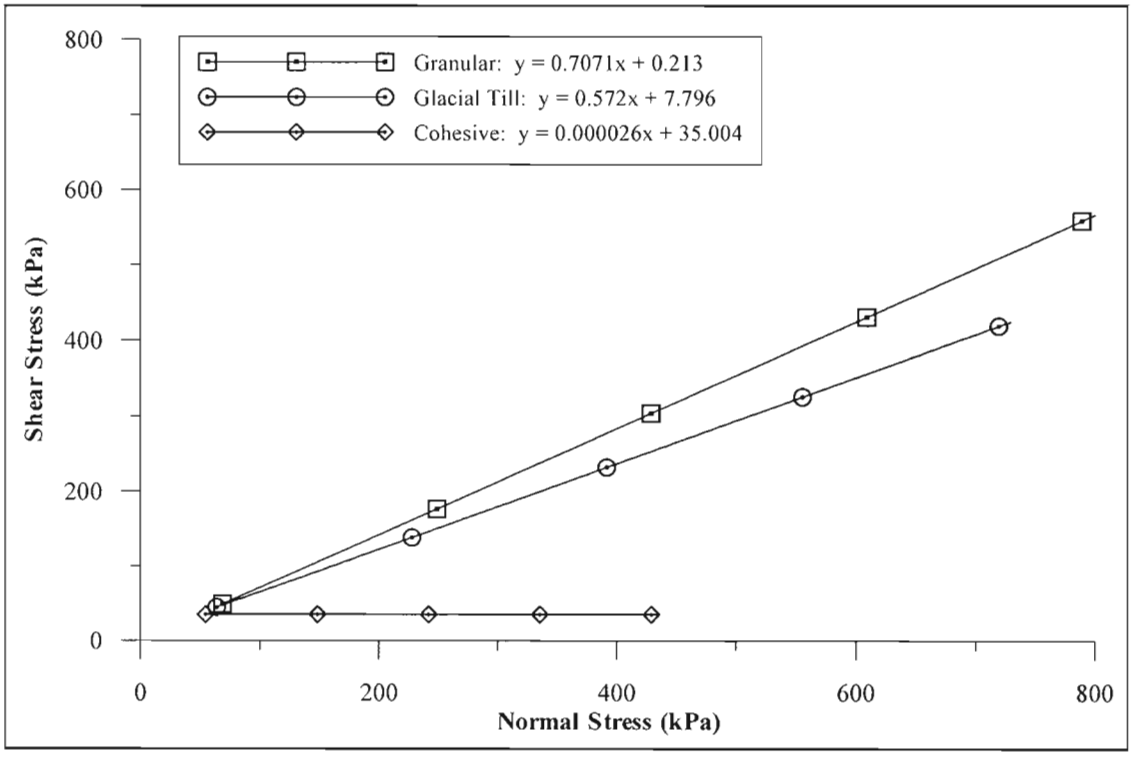

Figure 3.8. Mohr-Coulomb failure envelopes for model soil types

Table 3.8. Comparison of Intended and Actual Model Soil Parameters

		Granular	Glacial Till	Clay
Intended	**Friction Angle (ϕ)**	45°	35°	0.001°
	Cohesion (c)	0.3 kPa	9.0 kPa	35.0 kPa
Actual	**Friction Angle (ϕ)**	44.9°	34.8°	0.0028°
	Cohesion (c)	0.301 kPa	9.5 kPa	35.0 kPa

3.4. Loading and Boundary Conditions

This section deals with the application of gravity, thermal, and live loads to the structure, as well as some of the initial boundary conditions used to constrain the model during different loading stages. The application of the gravity and thermal loads is governed by amplitude curves that improve model convergence. Live loads are applied instantaneously, using only amplitude curves to load the structure cyclically.

3.4.1. Initial Conditions

As mentioned in Section 3.2.1, the outer boundaries of the model are represented with infinite elements. By fixing the perimeter nodes of these infinite elements, any stresses caused by this constraint would be in the far field, and have little impact on the soil near the structure. The nodes along the sides of the model were fixed in the horizontal direction, allowing the soil elements to compress vertically. The nodes along the bottom edge of the model were fixed in the vertical direction. The only other instance of a constraint being placed on nodes for the entire simulation is at the pile/abutment interface. A fixed constraint was placed on the nodes in this area relative to each other, keeping the bottom of the abutment from separating with the pile elements.

Two other initial conditions are applied to other elements in the model. A geostatic state of stress is applied to the bedrock elements in the initial step. This stress state varies linearly with depth based on the unit weight of the bedrock material. The purpose of the geostatic state of stress is to preload the bedrock elements before the weight of the soil above is applied to them. This was done rather than apply gravity load first to the soil and then bedrock, as this method would have caused separation between the surfaces of the soil and bedrock.

The only elements in the model that require the definition of an initial temperature state are the girder elements. The girder elements are given an initial temperature in order to define positive and negative temperature changes. In an actual structure, this initial temperature can be considered the ambient temperature at the time the girders are welded to the tops of the piles. This temperature is critical, because any change in temperature after this time will result in movement of the head of the pile. For this model, the initial temperature was chosen to be 20°C (68°F).

3.4.2. Dead Loads

The dead loading in this model can be broken down into two categories: dead loads due to gravity and supplemental dead loads. In ABAQUS, the gravity loads are applied as a distributed load over the entire element using the *DLOAD command. After the group of elements to which the distributed load is applied has been selected, the magnitude and direction of the gravity vector are defined using the GRAV option. ABAQUS uses the density of the elements together with this vector to calculate the loading due to gravity (HKS, 2001).

The supplemental dead loads represent loads that cannot be accounted for using the combination of the density and acceleration due to gravity. These loads are applied as a pressure distributed over the faces of elements using the *DSLOAD command. There are two instances of supplemental dead loading in this model. The first SDL accounts for the weight of the pavement, railings, bracing, and crossframes for each girder. Based on calculations done for the Mill Pond Bridge (Krusinski, 2002), the weight of the crossframes and bracing are taken as 10% of the weight of the steel in the girder. As discussed in Section 3.3.1.1, since there are different girders for each span length, the magnitude of this portion of the supplemental dead load also varies. From the same set of calculations, the weight of the railing is taken as 4 kN/m (274 lb/ft). This value is then divided by two, since there are two railings and four girders. The weight due to the pavement is representative of an 80 mm (3 in) thick wearing surface of bituminous concrete.

The other supplemental dead load accounts for bituminous pavement that would be installed on top of the soil leading up to the approaches of the bridge. The thickness of this pavement was assumed to be 150 mm (6 in) to account for wearing surface and binder courses. This load was included not only for the sake of completeness, but also to provide a small amount of confining pressure to the soil at the ground surface.

Both the gravity and supplemental dead loads are applied to the structure using an amplitude curve defined with the *AMPLITUDE command. The curve used to apply the loads is shown in Figure 3.9. As shown on the y-axis, the relative magnitude of the load ranges from 0 (no load) to 1 (full-load). The curve was defined in a manner that provides small changes in relative magnitude up until the value reaches 0.25. This results in fewer

convergence difficulties than would occur if the entire weight of hundreds of cubic yards of soil and structural elements were mobilized instantaneously.

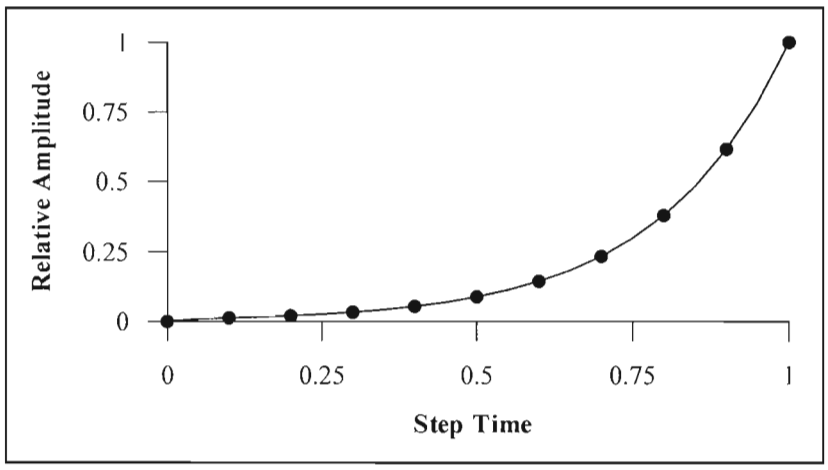

Figure 3.9. Amplitude curve for application of dead loads to model

In addition to being governed by the amplitude curve shown in Figure 3.9, gravity loads are also applied to different potions of the model at different stages in the simulation. This is done in order to attempt to duplicate some of the stresses created in the soil and structure by the construction loading sequence of an actual integral abutment bridge. Initially, gravity loads are applied to the soil and bedrock elements, in order for these elements to come to equilibrium. After this occurs, gravity is then applied to the piles, girder, and abutments. After gravity has been applied to the whole structure, the supplemental dead loads discussed earlier are applied, and the whole model is allowed to come to equilibrium once more. It is from this state of equilibrium, after the dead loads of the soil and structure have been applied, that further live and thermal loading of the structure commences.

3.4.3. Thermal Loads

Thermal expansion and contraction of the girder is governed by two separate thermal loads. These loads are based on the AASHTO requirements for structures in cold climates (1996). For metal structures, the design temperature range is from –30°F to 120°F (-35°C to 50°C). Because Maine has lower temperatures than many places in the country, the upper limit on the temperature range was reduced to 40°C (104°F). This results in a positive temperature change of 20°C (68°F), and a negative temperature change of 55°C (131°F). These temperature changes were applied to the nodes of the girder using the *TEMPERATURE command in ABAQUS for thermal loading of elements.

The temperature changes were achieved by modulating the initial temperature of the girder using amplitude curves. The amplitude curves for the thermal loads used in the model are shown in Figure 3.10. The linear "curve" is the temperature increase, while the second, linear "curve" is the temperature decrease. It should be noted that the temperature decrease amplitude curve has many more data points than the curve for temperature increase. This is mainly because the negative temperature change is much more drastic than the positive change. Better convergence of the model is achieved by using smaller steps between temperature change, rather than large jumps.

A third amplitude curve was created in order to model an annual temperature cycle that mimics the temperature changes a girder would see over an entire year. The curve shown in Figure 3.11(a) is a portion of an actual plot of annual temperature data recorded at The Forks Bridge in western Maine by Sandford (1997). The jagged peaks and spikes on the plot represent the day-to-day air temperature fluctuations. However,

for a given year, the temperature curve is generally sinusoidal. Figure 3.11(b) is the amplitude "curve" created for ABAQUS that approximates the shape of an actual annual temperature cycle. For the purposes of this model, an annual cycle starts at 20°C, increases to 40°C, returns to the original temperature, decreases to -35°C, and then returns to 20°C.

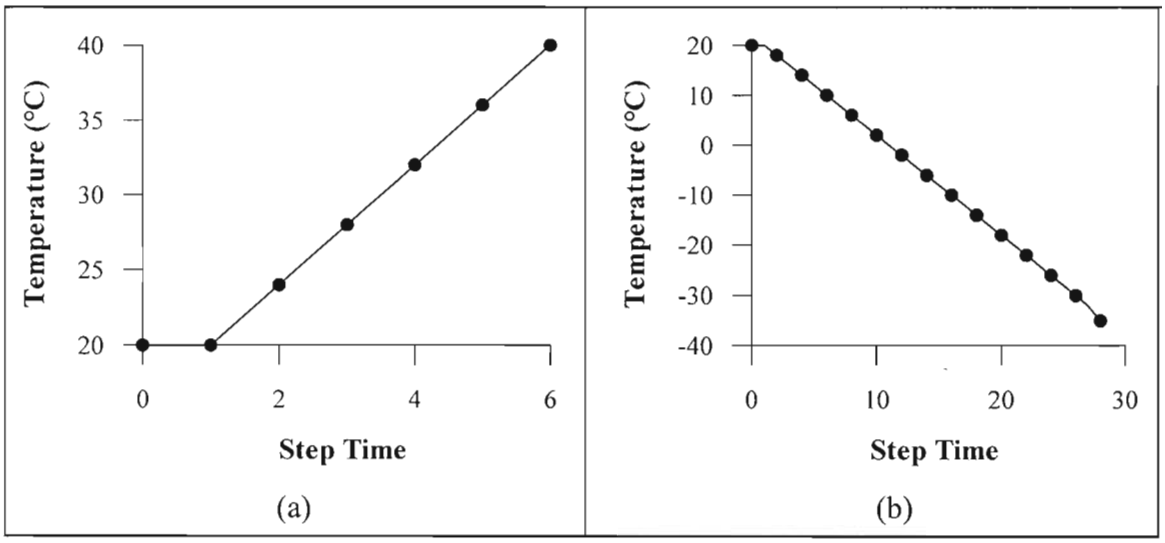

Figure 3.10. Amplitude curves for (a) positive and (b) negative temperature change

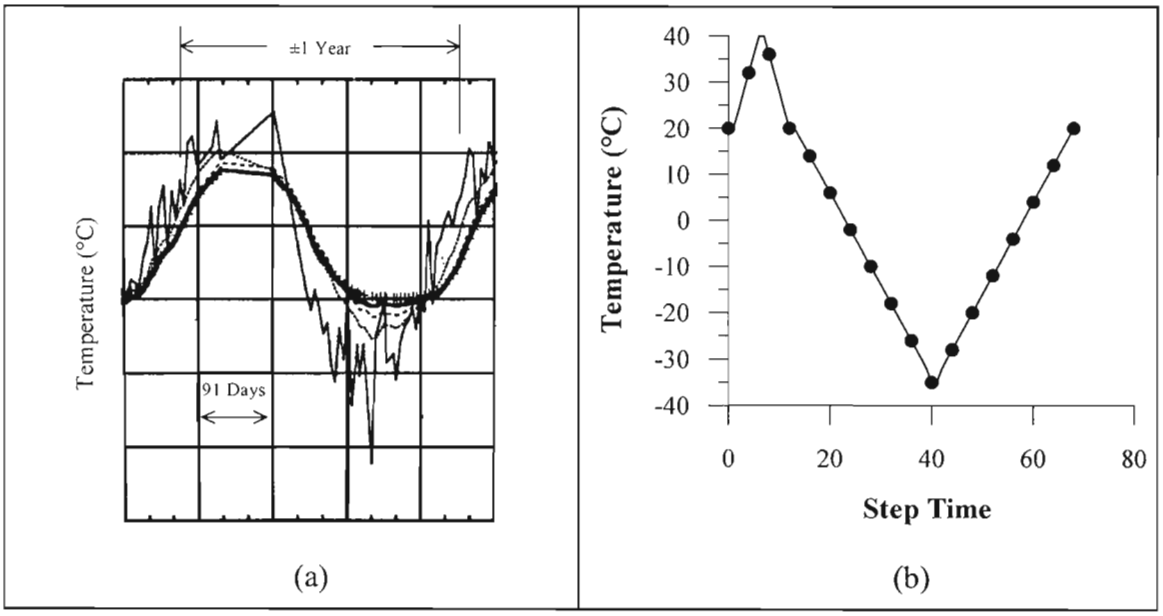

Figure 3.11. Annual temperature cycle curves for (a) actual bridge and (b) model

3.4.4. Live Loads

The live loading for this model consists of three axle loads of a design truck placed at various locations on the girder, in order to maximize or minimize certain effects. Two design trucks were used in the parametric study, an AASHTO (1998) HL-93 design truck, and the MDOT (1999) design truck. A representation of the HL-93 truck is shown in Figure 3.12. The MDOT truck is identical to the HL-93 truck in all respects, except for the axle loads, which are 25% higher. A distribution factor of 0.5 was used, as the bridge contains two lanes supported by four girders. AASHTO requires the addition of a distributed lane load of 9.4 kN/m, to which the 0.5 distribution factor was also applied.

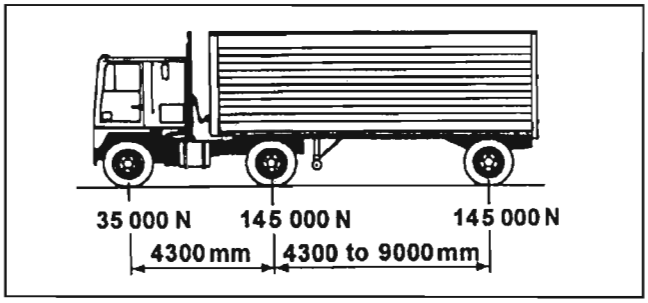

Figure 3.12. HL-93 design truck (AASHTO, 1998)

The axle loads were applied to the girder using the *CLOAD command, which allows for a force in any direction to be defined at a specified node. To maximize bending moment in the girder, a design truck was placed with its central axle at the centerline of the span, with the remaining axles located 4.3m away. If one of these axles did not fall at the location of a node, the load was split proportionately between adjacent nodes. Shear in the girder was maximized by placing the rear axle of a design truck at the location where the girder and abutment meet. As was done for maximum bending moment, the remaining axles were spaced at 4.3m.

Unlike the dead and thermal loading, the live loads were applied to the structure instantaneously, without the use of an amplitude curve. However, the amplitude curve shown in Figure 3.13 was implemented in the studies to examine the effect of a cyclic live load. The purpose of this curve is similar to that of the curve used for the dead load in that its function is to modulate the relative magnitude of the live load between 0 and 1. The curve was defined using a sine function that could be repeated for as many cycles as were desired.

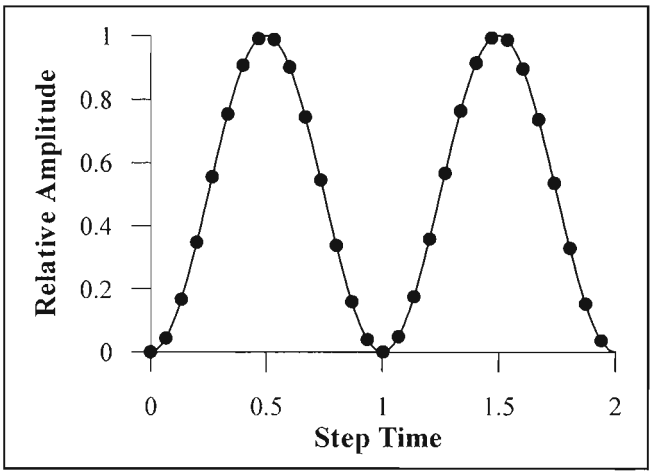

Figure 3.13. Amplitude curve for cyclic live load

The three categories of load (dead, live, temperature change) were combined into six separate load cases, to be applied to the models in the parametric study. Load Case 1 was simply the dead load of the structure, including all supplementary dead loads. Load Case 2 contained all of the dead loads in addition to the HL-93 truck and lane live loading. Load Cases 3 and 4 were a combination of the dead loading acting in conjunction with the 20°C (68°F) positive temperature change and 55°C (131°F) negative temperature change, respectively. Load Cases 5 and 6 were simply Load Cases 3 & 4, plus live load, respectively. A summary of the load cases to be used in the parametric studies is given in Table 3.9.

Table 3.9. Summary of Load Cases

Load Case	Abbreviation	Components
1	DL	Dead load of structure and attachments
2	DL+LL	Load Case 1 with HL-93 live loading
3	DL+ΔT	Load Case 1 with positive temperature change
4	DL-ΔT	Load Case 1 with negative temperature change
5	DL+LL+ΔT	Load Case 2 with positive temperature change
6	DL+LL-ΔT	Load Case 2 with negative temperature change

3.5. Preliminary Finite Element Model

After all of the material parameters had been settled upon and verified, a preliminary study was undertaken to determine whether the behavior of the model bridge was reasonable. Preliminary models consisted of an integral abutment bridge with a 25 m (82 ft) long superstructure, and pile lengths that varied between 2 m (6.5 ft) and 10 m (32.8 ft). Pile lengths up to 10 m were included in the study in order to determine at what length the behavior of the piles drastically changes. The length of superstructure was chosen as 25 m, because this value fell at the center of the range of lengths that would be examined in the parametric study. All material behavior was linearly elastic in order to improve solution times, and to eliminate the effect of material plasticity on the behavior of the model. As a result, all models were run with granular soil, since the linear elastic soil models would not account for the differences in c and ϕ in the soil behavior. The six load cases in Table 3.9 were applied to the models with the different pile lengths, resulting in 54 models examined in the preliminary study.

The results of the preliminary analyses were used to eliminate anomalous model behavior and make improvements to the performance of the model. A secondary goal of

the preliminary study was also to determine the critical model responses that warranted further examination in the parametric study. This section describes some of the factors that affected the behavior of the model, as well as the modifications made to the model in an attempt to mitigate their effect. The critical model responses selected for further study are also discussed. The mesh in the preliminary studies was coarse, in another attempt to reduce computational cost. Therefore, refinements were made in the areas of the model with critical responses in order to obtain a more accurate and convergent solution.

3.5.1. Factors Affecting Model Behavior

Two major factors that altered the behavior of the model are described in the following sections. The first factor relates to the out-of –plane thicknesses of the two-dimensional elements used in the model, and how of elements of varying thicknesses interact with each other. The second factor covered is the effect of the depth of the channel over which the bridge spans on the behavior of the piles. It was found that this factor, which is generally ignored in most simplified pile analyses, could have a significant effect on the behavior of the pile.

3.5.1.1. Variation of Element Thickness

As discussed in previous sections, the plane stress and plane strain elements in ABAQUS are defined with an element thickness in the z-direction. This thickness is used to determine magnitudes of forces applied over the surfaces of the element (contact forces, distributed loading) and forces distributed throughout the entire element (gravity). In ABAQUS, the default value of this thickness is a unit width, 1 m in the case of this model. As discussed in Section 3.3.1, it was necessary to change the thickness of the pile

and abutment elements in order to make their axial and flexural stiffnesses equal to those of the actual components. For the remaining elements, soil, bedrock, and girder, the default unit thickness was defined.

Nodes of elements involved in surface-surface interaction lie on a plane at one-half the defined element thickness. Because the elements of the various components of the model have different thicknesses, there are several instances where elements of one thickness are required to contact elements of a larger or smaller thickness. ABAQUS accounts for this by allowing the user to define the dimension out-of-plane thickness of each contact surface using the *SURFACE INTERACTION command. For the preliminary analyses, the surface thickness was set to the smaller thickness dimension of the two contacting sets of elements.

After examining output data from the preliminary studies, it was determined that this measure alone was not sufficient to solve all of the difficulties associated with having elements of a different thickness in contact with each other. Furthermore, in the case of the abutment/soil contact pair, it was not clear if the 1 m wide soil elements provided sufficient support to the 2.7 m wide abutment elements. However, it was felt that the 1 m wide soil elements provided a reasonable amount of resistance to the piles. Each pile is capable of mobilizing an area of soil up to three times the width of the pile. In the design of pile groups, a spacing of 2.5 to 3.5 times the pile diameter is therefore recommended to ensure that soil resistance is not affected by surrounding piles (Army Corps of Engineers, 1992; Chen & Poulos, 1993). The 1 m width of the soil elements is approximately 2.8 times the width of the pile, and therefore the resistance provided is not as questionable as in the case of the soil/abutment interaction.

To provide adequate resistance to the movements of the abutments, the width of the soil elements in contact with the abutment was increased to 2.7 m. This modification presented another problem, because in some cases the volume of the soil adjacent to the abutments was more than twice that of the soil adjacent to the piles. This not only resulted in unrealistic confining pressures on the soil at lower depths, but also brought about increased contact forces normal to the surface of the piles. To resolve this situation, a distributed load was applied upward to the bottom surface of the group of 2.7 m soil elements adjacent to the 1 m elements. The distributed load is equivalent to the increase in weight caused by increasing the element width by 1.7 m. This load also takes the increased amount of pavement loading into account.

3.5.1.2. Channel Depth

During the examination of preliminary data, it became apparent that the depth of the channel under the bridge (as shown in Figure 3.1) contributed more significantly to the amount of support provided to the piles more than was initially expected. In the initial studies, the channel depth varied with pile length, with channel depth being measured downward from the abutment/pile interface. The variation of channel depth with pile length is given in Table 3.10. Preliminary data showed that the lateral displacements at the pile tips were greater for longer piles than shorter, i.e., 10 m piles compared to 2 m piles. However, within groups of channel depth values, another trend was observed. It was shown that the longer pile within a group of channel depths had smaller displacements than a shorter pile with the same channel depth.

Table 3.10. Variation of Channel Depth with Pile Length

Pile Length	Channel Depth (below top of pile)
2 m	0 m
3-4 m	1 m
5-6 m	2 m
7-8 m	3 m
9-10 m	4 m

To quantify this trend, a simplified study was performed on a model bridge with 10m long piles, subjected to Load Case #2. The depth of the channel was varied from the top of the pile (0 m deep) to 10 m below the top of the pile. Figure 3.14 presents a plot of deflections along the length of the pile for three different channel depths. It can be seen from the plots that the deflections at the pile tip are greater for deeper channels than shorter. In addition, the deflection at the head of the pile for each channel depth is shifted towards the right (in the direction of the channel). The most notable effect of the varied channel depth is that the maximum positive deflection along the length of the pile increases dramatically with channel depth. For a channel depth increase of approximately 5 m (16.5 ft), the maximum deflection increases by approximately 1 mm (0.04 in). While a 1 mm change is small when compared to some of the dimensions of the model, it is much larger than the change in deflections at the head and toe of the pile caused by the change in channel depth.

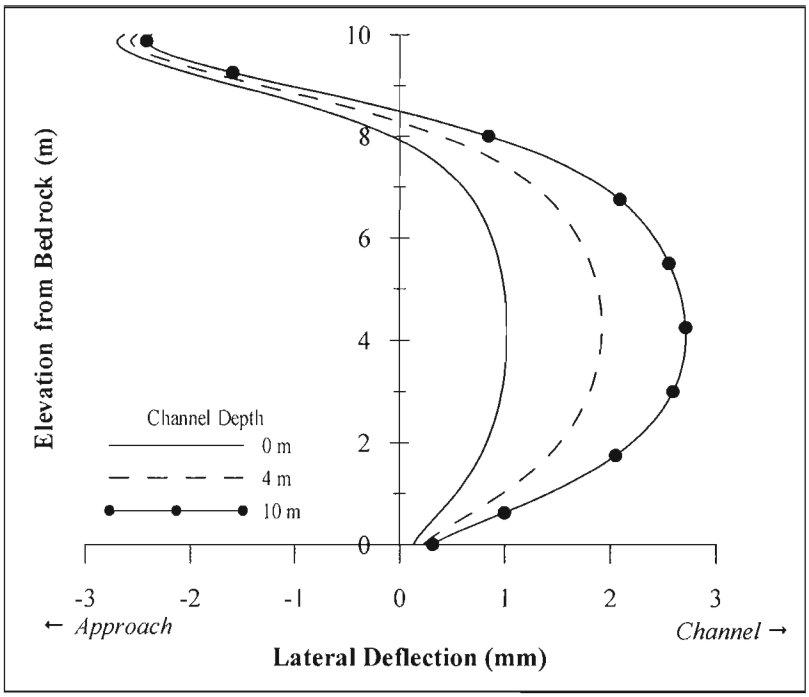

Figure 3.14. Comparison of pile deflections for varied channel depths

Because of the discrepancies in pile deflection caused by the varied channel depth, an attempt was made to minimize the effect the channel depth had on piles of varying length. It was decided that for piles with a length of 4 m or less, the depth of the channel would be equal to the length of the pile. This was done for two reasons, the first being after examinations of several bridge plans, the channel is often the same depth or deeper than the piles due to a sloping bedrock profile, or erosion by moving water. Furthermore, the effect on channel depth of piles shorter than 4 m was observed to be negligible. This solution also helps to present a worse case state of support for "short" piles, since that is the focus of this research. For piles 5 m and greater in length, the channel depth was set to a constant depth of 4 m. Although the effect of channel depth was reduced by this change, it was not completely eliminated.

3.5.2. Establishment of Critical Model Responses

The preliminary finite element model was used to determine the areas where changes in the loading and bridge geometry caused the greatest effects. It was quickly recognized that the piles were the most significant area of model behavior. Movements and stresses in and around the piles were the largest throughout the model. Based on the results of the preliminary analyses, three aspects of pile response were considered for closer analysis in the parametric studies: movement at the tip and head of the pile, stresses in the pile, and forces at the pile/bedrock interface. The abutment/girder interface was also considered an area of interest, because of relatively high stresses observed in the preliminary study. This area was also studied to try to determine whether the girder behaved as a simply supported beam, or a beam with fixed supports.

The preliminary models were discretized with a coarse finite element mesh in order to reduce computational costs. Elements in the model had a y-dimension of either 1.0 m or 0.5 m, which often resulted in aspect ratios greater than 2:1 in the areas of interest, especially in the piles. The number of elements in the model varied with the pile length, with a minimum of 392 elements in the models with 2 m long piles, and a maximum of 902 elements in the models with 10 m long piles. It has been shown that as the number of elements increases, and as the aspect ratios of the elements in the model decrease, the solution converges on a more accurate value (Logan, 1993). Therefore, it was decided to utilize a finer mesh in the areas of interest; the pile, soil and bedrock adjacent to the pile, the pile/bedrock, pile/abutment interfaces, and girder/abutment interfaces. This increased the number of elements to 1874 for the model with 2 m piles and 3315 for the 10 m model. The aspect ratios in the piles and other areas of interest

were reduced to a value of 1:1 or less. Figure 3.15 provides a comparison between the initial and refined meshes for a model with 3 m long piles.

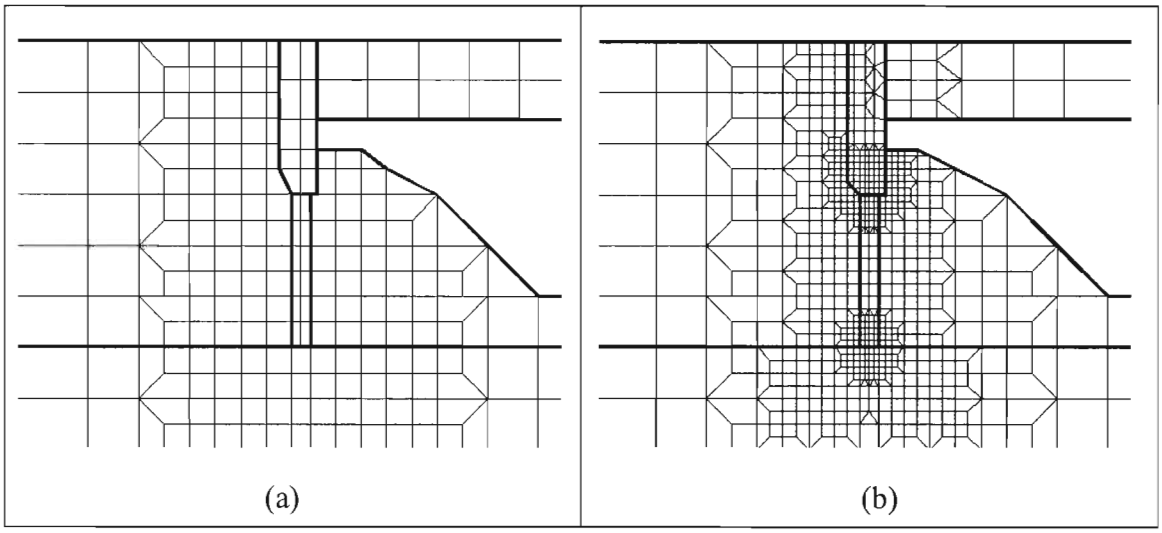

Figure 3.15. Comparison between (a) coarse and (b) refined mesh

3.6. Summary

The process of creating a two-dimensional finite element model for a parametric study of integral abutment bridges founded on short piles has been outlined in this chapter. Complex constitutive and surface interaction models were used in order to provide a more realistic depiction of the soil/structure interaction. Material properties were based on test data and theoretical values, and adjusted to more closely resemble the anticipated conditions at bridge sites in Maine. The elastic-plastic behavior and properties of the soil and piles were verified using simplified models to determine their accuracy. Several load cases to be used in the parametric study were created based on design recommendations from MDOT and AASHTO.

Preliminary finite element models were created and analyses were performed to resolve any abnormal model behavior. Factors such as the out-of-plane thickness of the two-dimensional elements, and varying the depth of the channel beneath the girder had unexpected influence on the behavior of the model. Once issues pertaining to these factors had been resolved or mitigated, critical model responses to be examined more closely in the parametric studies were selected. Accordingly, changes were made in the level of mesh refinement in order to provide a more accurate numerical solution for the selected model responses.

Chapter 4

PARAMETRIC STUDY

Chapter 3 of this thesis discusses the details of the development of material and geometric properties for a preliminary version of a finite element model incorporating advanced material behavior and interactions. Further discussion of the finite element model in this chapter involves the procedure used to analyze the structure. Parametric studies were carried out in order to quantify the effects of certain factors on the three critical pile responses determined in the previous chapter; movement at the tip and head of the pile, stresses in the pile, and forces at the pile/bedrock interface. A primary study was focused on the effect of significant changes in the geometry of the bridge and subsurface conditions. Secondary studies with limited scope were also performed in order to investigate the consequences of smaller changes in the loading and material properties of the model.

4.1. Analysis Procedure

Model data was output in two separate formats, a text file (*.dat) and a file that allows ABAQUS to display graphical data (*.odb). The graphic files were not used as the primary source of output data due to their large size. However, these files were very useful in some instances to obtain qualitative information on the displacements of the structure and locations of stresses. The text files allowed the data to be imported into a spreadsheet program, which simplified organization and display of the data. Output variables in these files included stresses and strains in the pile elements, normal and shear forces at contact surfaces between the structure and soil or rock, and nodal displacements

of the structure (piles, abutments, and girder) and the adjacent soil. An annotated example of ABAQUS script for a model used in the parametric study is given in Appendix A.

4.1.1. Simulation of Construction Sequence

An analysis procedure was written in order to mimic the construction process of an integral abutment bridge as closely as possible. This was accomplished by controlling the loads and displacements of certain areas of the model during increments of time. The detailed construction procedure used by the Maine Department of Transportation (MDOT) for each bridge was not known, so assumptions were made based on MDOT bridge plans and the procedures used by other agencies. Phase II of this research will examine the construction processes and may recommend changes.

At the start of the analysis, gravity forces were applied to all components of the modeled structure simultaneously. However, the nodes at the perimeter of the structural components were restrained such that no displacements occurred, and no stresses developed in these elements. The nodal restraints were then released in separate time increments, in the order that they would be placed in the field. The nodes of the piles were released, followed by the girder, and abutments. This is the general order of construction for a typical integral abutment bridge. In subsequent time increments, the supplemental dead loading of the approach pavement and girder were added. After all dead loads were added and all nodal restraints released, the system was allowed to come to equilibrium.

4.1.2. Composite vs. Non-Composite Girder Behavior

One aspect that is overlooked in this process is the changing moment of inertia of the composite girder at various stages of construction. This is discussed briefly in Chapter 3. For a short period in the life of an actual bridge, the steel girder supports the additional weight of the uncured deck, without being able to take advantage of the stiffness of the concrete deck. Similarly, after the deck has fully cured, the stiffness of the composite cross section decreases with time due to creep effects. These varied stiffnesses could possibly lead to larger displacements and stresses at different stages of the analysis. In effect, there are three different girder sections representing construction, early use, and later use of the bridge. Therefore, it would be more realistic to include the effects of these different section properties in the finite element analysis.

Calculations using the three separate section properties of the model girder were performed in order to quantify the differences in end rotations of a simply supported girder. A simply supported girder was studied, since the true support conditions provided by an integral abutment require the soil/structure interaction to be taken into account. The section properties considered were the short-term composite, long-term composite, and non-composite section properties. AASHTO (1996) defines the loadings appropriate for the given section properties. Non-composite sections only experience the dead load of the girder and uncured deck. Short-term composite sections experience these dead loads in addition to any dead loads from pavement, attachments, and barriers. Long-term composite sections experience only dead loads from pavement, attachments, and barriers. Live loading acts on the short-term composite section only.

Four rotations were calculated for all five of the girder lengths. θ_1 is the sum of the dead load rotations of the non-composite and long-term composite sections, while θ_2 is simply the dead load rotation of the short-term composite section. θ_3 and θ_4 were calculated by adding the live load rotation of the short-term composite section to θ_1 and θ_2 respectively. Comparisons of θ_1 to θ_2 for the five girder lengths show that the short-term section properties underestimate the end rotations by up to 78%, while comparisons of θ_3 and θ_4, which include live load effects, show that the short-term properties only underestimate the end rotations by approximately 50%.

While these comparisons may cause some to question the validity of the model results, there are additional factors that must be considered before any conclusions are made. The most important factor is the fact that all rotations (θ_1, θ_2, θ_3, θ_4) are calculated for a simply supported beam, which an integral abutment bridge is not. It is common practice (MDOT, 1999; Abendroth & Greimann, 1988) to assume that the end rotation of a simply supported girder is an upper bound on the rotation of the abutment and the pile head, since they are both rigidly connected to the girder. Data from the model shows that the interaction between pile, abutment, girder, and soil results in rotations under the same loading for the short-term section properties that are 67% less than θ_2 and 75% less than θ_4.

In addition to the effect of the actual support conditions, thermal effects help to compensate for the differences in end rotations. As will be discussed later in this chapter, and in Chapter 5, the controlling load cases always involve a negative temperature change, which works to increase the rotation of the abutments. Examination of the model

data shows that the rotational component of this temperature change is typically 1.5 to 2 times greater than the components of dead and live load rotation.

To the best of the writer's knowledge, only one researcher (Diceli, 2000) has tried to account for the effect of the changing moment of inertia of the girder at different stages. ABAQUS has provisions that allow the user to change the section properties of a beam element during an analysis, but not the material properties of the elements themselves. Since this model uses an equivalent Young's modulus and plane strain elements to define the section properties of the girder, there is no way that the changing moments of inertia can be accounted for explicitly. However, dead loads in future studies could be adjusted to compensate for the increased rotation of the non-composite and long-term properties.

Since the support conditions provided by an integral abutment reduce end rotations, and the change in end rotations due to thermal effects are much more significant than those caused by the changes in section properties, the difference in girder section properties was ignored in this parametric study. However, this is something that should be addressed in future research, in order to determine exactly what effect this phenomenon has on the bridge behavior.

4.2. Primary Parametric Study

The primary parametric study investigated how changes in the length of the piles and girders affected the critical pile responses. As mentioned in Chapter 3, the pile lengths varied in 1 m increments from 2 m (6.5 ft) to 6 m (20 ft), with 8 m and 10 m long piles also considered. The length of the girder was varied in 5 m (16.5 ft) increments

from 15 m (49 ft) to 35 m (115 ft), which resulted in 35 possible configurations of girder and pile geometries. From the 35 possible bridge configurations, models were created incorporating the six load cases presented in Table 3.9, and the three general soil categories: cohesive, granular, and till. A total of 630 combinations of bridge geometry, loading, and subsurface conditions were considered in this study. The effect of these combinations on pile stresses, pile kinematics, and the interaction between the pile and bedrock will be discussed separately in the following sections.

4.2.1. Pile Kinematics

There are several assumptions about the kinematics of laterally loaded piles with regards to integral abutment bridges that required investigation. Broms (1964a, 1964b) distinguishes between long and short piles based on comparisons between the stiffness of the pile section and the stiffness of the surrounding soil, with short piles having a much larger stiffness than the surrounding soil. The displacements of a laterally loaded pile depend on whether the pile is long or short, in addition to the manner in which the head of the pile is restrained. Figure 4.1 depicts the assumed deflections for short piles with heads that are allowed to rotate (free) and heads restrained against rotation (fixed), while Figure 4.2 depicts the same deflections for long piles.

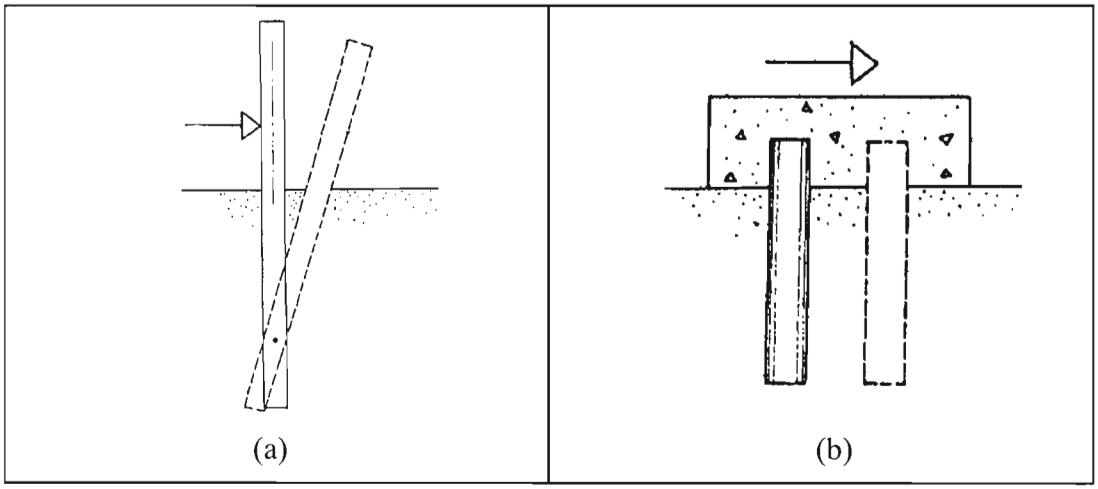

Figure 4.1. Deflections of short piles with (a) free head (b) fixed head (Broms, 1964a)

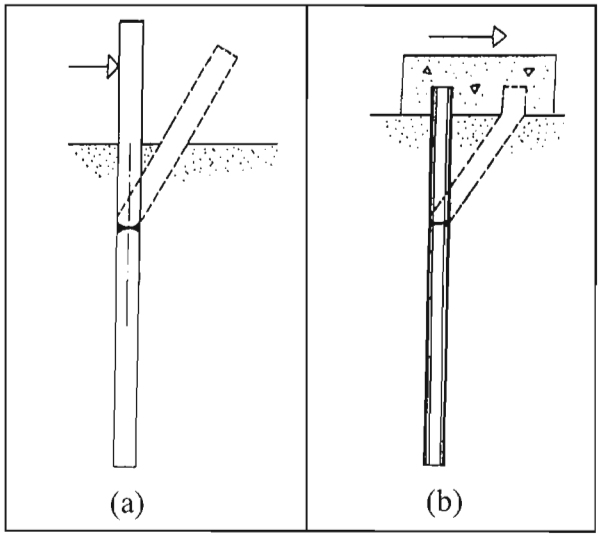

Figure 4.2. Deflections of long piles with (a) free head (b) fixed head (Broms, 1964a)

Piles supporting integral abutments have been shown to behave similarly to the pile shown in Figure 4.2(b). These piles are fixed at some depth, with inelastic rotation occurring somewhere between this point and the head of the pile. The equivalent cantilever method used in the design of these piles is based on the assumption that the bridge piles will behave in this manner. Therefore, it has been assumed by many that "short" piles supporting an integral abutment bridge would behave in the manner

depicted in Figure 4.1(b). If piles supporting a bridge abutment were to move en masse under lateral loading, the structure may not be able to handle the resulting forces and displacements. By confirming the pile kinematics through the finite element model, the validity of design assumptions to certain pile lengths can be determined.

The first aspect of pile kinematics examined was the behavior of the head of the pile. For both examples of fixed head piles shown in Figures 4.1 and 4.2, it is assumed that the concrete encasing the top of the pile only translates and does not undergo any rotation. In the case of integral abutment bridges, it is assumed that this translation of the abutment and pile head is caused only by thermal expansion and contraction of the girder. Examination of the graphic output from the model for all combinations of pile lengths, girder lengths, and soil types confirms that translation of the abutment and pile head occurs under thermal loading. As would be expected, longer girders resulted in larger displacements at the pile head. For a given girder length and temperature change, the length of pile had little effect on the displacements at the head. In general, piles longer than 4 m experienced slightly less deflection at the head of the pile than shorter piles.

However, under dead and live loading additional pile head deflection was observed. This is a result of the girder deflection inducing a rotation of the abutment. Because the stiffness of the abutment is much greater than that of the pile or the surrounding soil, there is relatively little resistance to this motion. Therefore, the length of the pile does not have any effect on the magnitude of this displacement. Figure 4.3 depicts the rotation of the abutment and resulting pile head displacement under live loading. Because the rotation of the abutment depends on dead and live loading, the magnitude of this deflection increases with girder length.

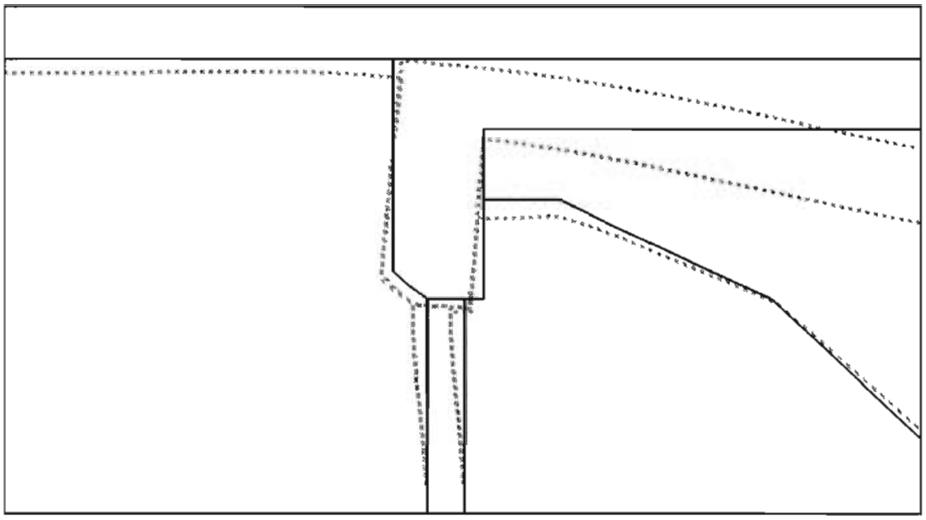

Figure 4.3. Pile deflection due to dead and live loads (deflections magnified 100x)

The second aspect of pile kinematics examined was the behavior of the pile at the tip, where it comes into contact with the bedrock. As can be seen in the figure above, lateral deflections along the length of the pile decrease with depth. For all load cases, and for all combinations of bridge geometry and soil conditions, there is no lateral deflection at the tip of the pile. This suggests that piles supporting integral abutment bridges do indeed behave as shown in Figure 4.2(b), for all pile lengths considered in this study. However, upon closer inspection of the pile response at the tip, it was shown that this is not accurate.

For piles shorter than 4 m (13 ft), the tip of the pile does not exhibit behavior consistent with a fixed support condition. Although there is no significant lateral or vertical deflection, the tips of the piles are not restrained against rotation, as evidenced in Figure 4.4. Under dead and live loading, the rotation of the pile tip is not substantial. For load cases 3-6, where the structure is subjected to thermal effects, the rotation of the pile tip becomes important. As pile length increases above 4 m, rotation at the pile tip decreases to a point where the assumption of fixed conditions is valid.

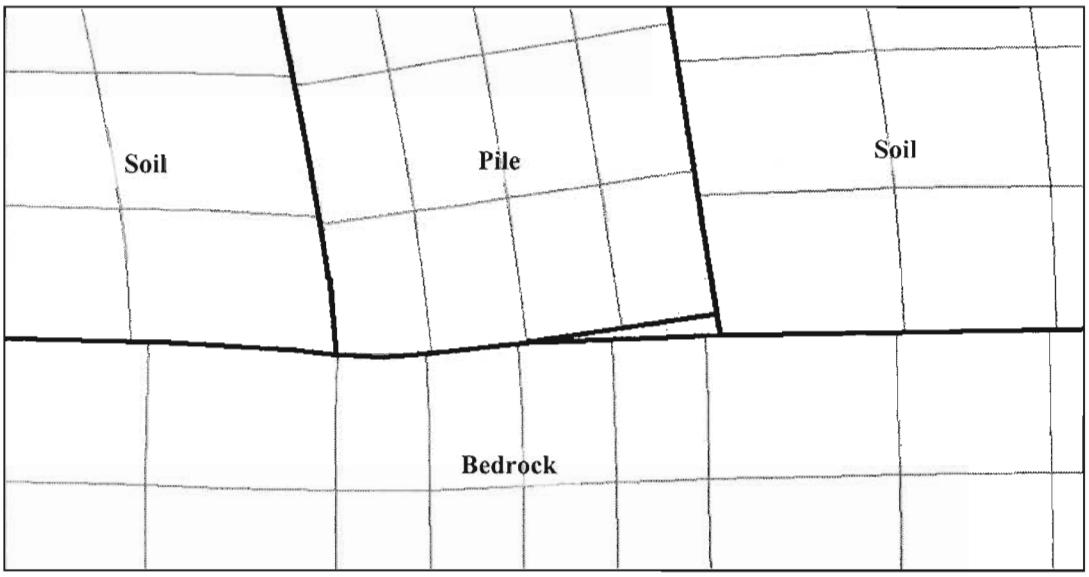

Figure 4.4. Rotation at tip of piles ≤ 4 m in length (deflections magnified 100x)

Initially, there was some concern about rotation occurring at the base of the pile, since this observation goes against the theoretical basis of how most integral abutment bridge piles are designed. However, in Broms' papers on laterally loaded piles (1964a), he presents a case for piles whose length falls in between the criteria for "short" and "long" piles. The deflection behavior of the piles in the finite element model compares well with the behavior that Broms proposed for laterally loaded piles of intermediate length. Figure 4.5(b) shows that Broms predicts a lateral translation of the pile head, with rotation occurring at the tip of the pile. The tips of the model piles do not rotate to the degree of Broms' intermediate pile, but this can be attributed to the interaction between the pile and the bedrock.

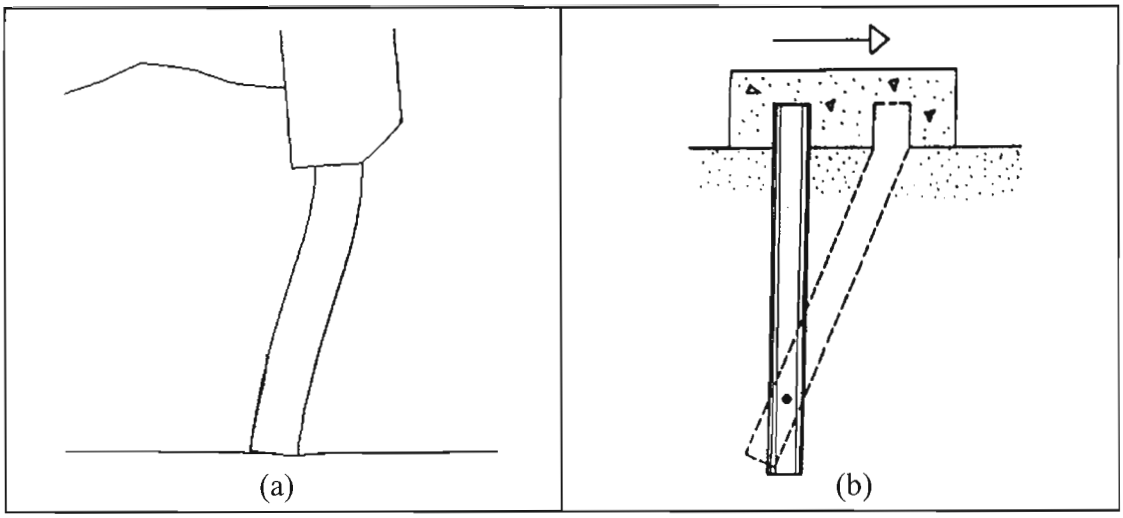

Figure 4.5. Comparison of deflections for (a) model pile (magnified 100x) and (b) intermediate pile with fixed head (Broms, 1964a)

4.2.2. Pile Stresses and Forces

Because almost all pile design criteria for integral abutment bridges utilize a limiting value of stress, a goal of the parametric study was to determine the effect of geometric and subsurface factors on the stresses in the pile. Specifically, it was important to determine the extent of yielding in the pile, and the locations where yielding occurs. Because the model utilizes a transformed cross section of the pile, as described in Chapter 3, the element stresses in the output files cannot be used directly. Therefore, element strains were used to calculate the stresses and moments in the actual pile cross-section, since they are unaffected by the section transformation. For all of the finite element models, strain data was taken at the integration points of the elements where it is the most accurate, and linearly extrapolated to the outer faces of the pile section.

The magnitude of the strains at the head of the pile is not greatly affected by the length of the pile. However, because longer piles have more rotational restraint at the tip,

the distribution of strains along the length of the pile is dependent on the length. Using the strains at the face of the pile, the axial load and moment along the pile was calculated. Figure 4.6a shows the distribution of moments from the finite element model along the length of a 3 m long pile, and Figure 4.6b shows the moment distribution proposed by Broms (1964a) for an intermediate length pile with a fixed head.

The distribution of moments along the model pile compares very well with the distribution proposed by Broms. It should be noted that the model pile has a small moment acting at the tip, while Broms' distribution has no moment acting at the tip. The moment at the tip of the model pile is a result of the interaction between the tip and the bedrock surface, which will be discussed in the next section. However, because the magnitude of this moment is relatively small, the observation that the pile is free to rotate can still be considered valid. Examination of the results for longer piles shows that this distribution does not apply when the length of the pile is greater than 4-5 m. Therefore, the tips of piles greater than this length will tend to behave as if they have rotational and translational restraint.

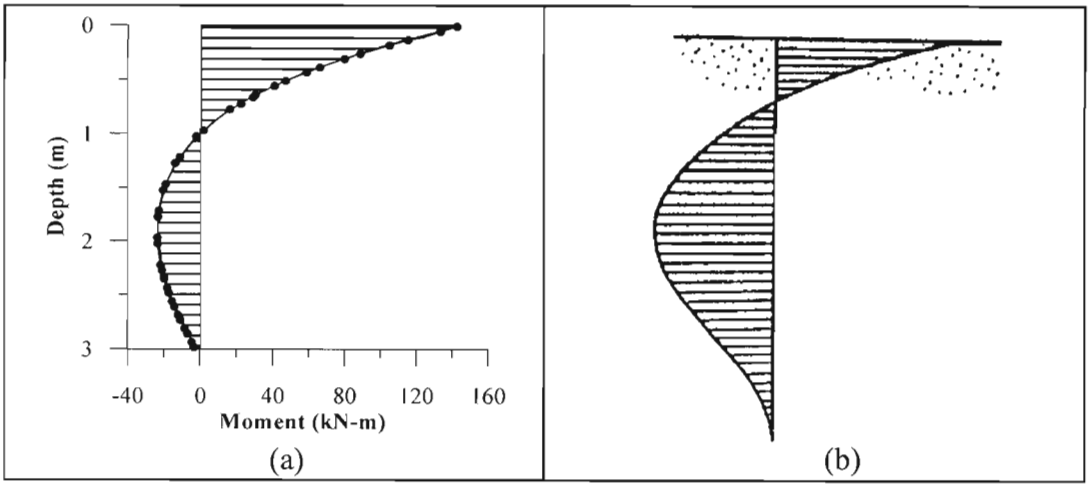

Figure 4.6. Comparison of moment distribution for (a) model pile and (b) intermediate pile with fixed head (Broms, 1964a)

Although the length of the pile did not greatly affect the magnitude of the strain at the head of the pile, the girder length and subsurface conditions were shown to have a significant effect on the magnitude of the strains. The discussion of pile kinematics showed that the displacements at the head of the pile for a given loading increase with girder length. Depending on the support provided by the surrounding soil, this displacement can cause large strains in the pile head. Piles in granular soil were shown to have the lowest strains at the pile head for a given combination of loading and geometry, while piles in cohesive soil were shown to have the highest strains. The strains at the head of piles in glacial till fell between the values for granular and cohesive soils.

Because the magnitude of pile head strains varies with the subsurface conditions, piles embedded in a weaker soil, such as clay, are more likely to experience yielding than piles embedded in granular soil. For example, when the length of the girder is 25m, piles in cohesive soil begin to yield in all load cases involving live load (cases 2, 5, and 6). In contrast, piles in granular soil and glacial till begin to yield only under Load Case #6, which causes the most severe rotation and translation of the pile head. For combinations of geometry and loading that cause yield in any soil type, the extent of yielding is greater for piles in weaker soil. Results of the finite element analysis show that for a 30 m (98 ft) long girder under dead and live load only, piles in cohesive soil experience yield strains at a greater depth than piles in granular soil or glacial till. Furthermore, a larger percentage of the depth (flange width) of the pile section had undergone yielding.

As would be expected, longer girders result in increased strains at the head of the pile. For girders 20 m (66 ft) in length and shorter, the strains at the pile head did not approach yield in any subsurface conditions. For girders 25 to 30 m (82 to 98 ft) long,

yielding occurred in only a few of the load cases. When the girder length reached 35 m (115 ft), yielding occurred in all load cases, with up to 55% of the depth of the cross-section experiencing yield in some cases. Because of the severity of yield that combinations of geometry and subsurface conditions can cause, girder length will be a limiting factor for most integral abutment bridges founded on short piles. Figure 4.7 illustrates the effect of soil type and girder length on the maximum compressive strains at the head of the piles.

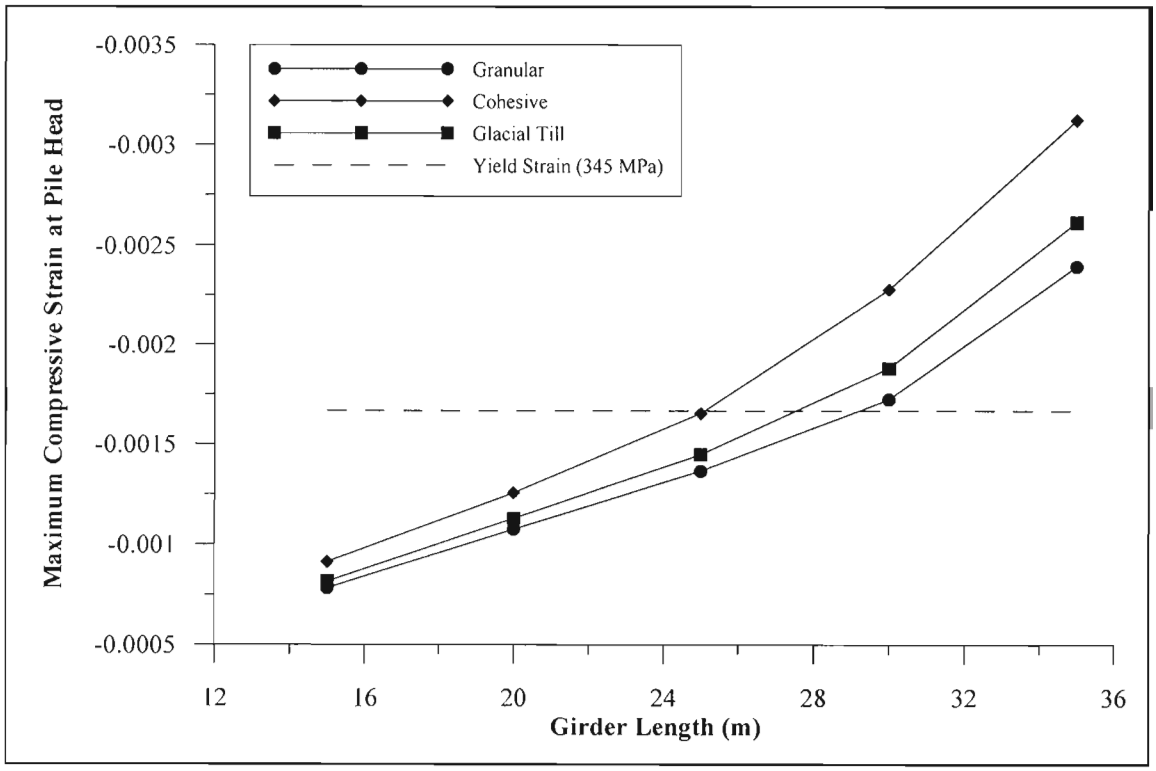

Figure 4.7. Effect of girder length and subsurface conditions on strains at head of pile under dead and live loading

4.2.3. Pile / Bedrock Interaction

As shown in Figure 4.4, the interaction between the tips of piles less than 4 m long and the bedrock is considerably different from the assumption of fixed conditions

that are typically associated with integral abutment bridge piles. The stiffness of a short pile is such that rotation will occur at the base, while lateral and vertical translations are resisted. The amount of rotation at the pile tip is generally governed by the support provided by the surrounding soil. Resistance to movement is dominated by the forces generated between the pile and bedrock.

Contact forces acting perpendicular (normal forces) and parallel (shear forces) to the surface of the bedrock were examined. The normal force in the pile was found to be controlled by the load case and the span length. As would be expected, larger spans result in higher axial loads, due to the increased dead and live loading. The subsurface conditions contribute to differences in the axial loads, primarily due to adhesion between the pile and soil. Soils with a larger cohesion intercept generate larger downdrag forces in the pile. However, the downdrag forces generated in the model were not a major component when compared to the forces generated due to dead and live load. Thermal loading does not generate any significant changes in the axial forces.

The shear forces acting parallel to the bedrock surface are controlled by the same factors that govern the normal forces. Subsurface conditions affect the shear force at the tip of the pile, in the same way that they change the strains in the head of the pile. Granular and glacial till will provide more lateral restraint to the pile than cohesive soils, thereby reducing the force that must be generated by the pile/rock interface in order to prevent translation of the pile tip. As in the case of the normal forces, girder length and load case again primarily dictate the shear forces generated between the bedrock and pile tip. This can be attributed to the amount of lateral deflection of the head of the pile caused by the rotation of the abutment under loading. Longer girders have an increased

dead and live load and therefore will have a larger deflection at the head of the pile. In addition, a negative temperature change in the girder will induce a large rotation in the abutment and cause a subsequent pile head deflection. Longer spans will undergo a larger amount of thermal contraction.

Unlike the normal force, shear force was affected by changes in the pile length. As pile length increased from 2 m to 4 m, the shear force at the tip of the pile also increased. In piles 5 m and longer, the shear force began to decrease with length. This behavior occurs because the 4 m models had the longest piles with the least amount of soil support provided under the bridge. Therefore, there is a tendency for the soil on the opposite side of the pile to push towards the centerline of the span. This effect is illustrated in Figure 3.14, where the largest pile deflections occur when the depth of channel is equal to the length of the pile. While an attempt to account for this phenomenon realistically is described in Chapter 3, the effects can be addressed better in a three-dimensional analysis. In order to quantify what the changes in shear force meant in terms of the stability of the structure, the ratio of shear to normal forces at the tip of the pile was calculated for each combination of geometry, soil, and load. This ratio was then compared to the friction factor (μ) used for the surface interaction between bedrock and the piles. As this ratio approaches μ, the likelihood of movement occurring between these two surfaces increases.

Typically, the highest shear to normal ratio was calculated for Load Case 3, where a negative temperature change was acting simultaneously with dead load. Load Case 6, where dead, live, and a negative temperature change act simultaneously, also produces large shear to normal ratios. These cases are the most severe because the strains in the

pile are the highest for the given axial load. The highest ratio of these forces that was obtained overall was approximately 0.45, for a 15 m long bridge with 4 m long piles in clay, under Load Case 3. As pile length increased past 5 m for all girder lengths and soil types, the shear-to-normal ratios approached a constant value of approximately 0.3, which further indicates that piles 4 m and shorter behave differently than longer piles.

4.3. Secondary Parametric Studies

Parametric studies of a much more focused nature were performed in order to answer questions on how changes in other aspects than the basic dimensions of the bridge components and the subsurface conditions affected behavior of the structure. A major portion of these studies concentrated on aspects related to the loading of the structure in an attempt to elicit certain structural responses. A small study was also performed to determine if having unequal length piles at either end of the bridge drastically changes the behavior observed in the primary study. Finally, models incorporating different pile sections were studied in order to better define parameters for the proposed design procedure discussed in Chapter 5.

4.3.1. Alternative Loadings

The six load cases discussed in previous chapters were created in an attempt to create the highest probable stress levels and displacements in the structure. However, after examining the preliminary data, questions arose as to whether or not there were additional loadings that may cause behavior that would lead to instability or unacceptable stresses and deflections. Since the shear and normal forces at the pile tip are important to the stability of the structure, a study was run where the design truck was placed such that

very large axial loads were developed in the pile. As mentioned in Chapter 3, MDOT uses a design truck with axle loads 125% greater than the AASHTO HL-93 truck. The effect of this loading on the behavior of the structure was also examined. Finally, since the bridge will presumably be loaded by a truck, or by seasonal temperature changes more than once in its design life, the consequences of applying cyclic live and thermal loadings were also investigated.

4.3.1.1. Live Loading for Maximum Shear in Girder

All of the load cases covered in the parametric study that incorporated live load (Load Cases 2, 5, and 6) had the AASHTO design truck placed on the girder in order to produce maximum bending moment. This in turn produced a rotation of the abutment, which caused strains and displacements in the pile head. Because the lateral restraint of the pile tip relies in part on the axial load in the pile, the effect of repositioning the location of the design truck along the length of the girder was investigated. The design truck was repositioned as shown in Figure 4.8, so that the rear axle was located at the interface between the girder and abutment.

As would be expected, the relocation of the live loads to the ends of the girder increases the axial load in the closest piles by 8-10%, while decreasing the axial load in the far piles by 17-20%. The difference between pile loads at opposite ends of the girder increases as the length of the girder increases. For piles in all soil types, the maximum compressive strains at the head under all load cases incorporating live load are approximately 85% of the strains developed when the girder is loaded for maximum bending moment. This is due to the reduced rotation of the abutments and smaller resulting pile head displacement. Overall, the deflected shape of the pile is not

significantly altered from the previous live load position; the magnitude of the deflections along the length of the pile is simply smaller. The observation of rotation occurring at the pile tip without translation is still valid for all the various positions of live load along the girder.

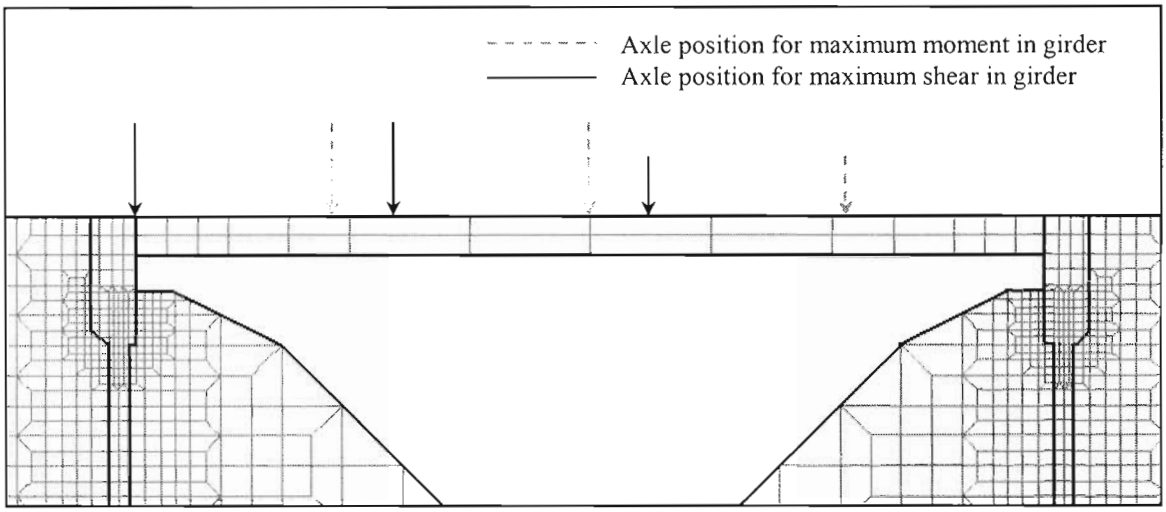

Figure 4.8. Placement of HL-93 truck on 15 m girder for maximum and minimum axial live load in piles

Repositioning of the live loading has the greatest effect on the contact forces at the tip of the pile. The larger axial load holds the pile tip against the bedrock more firmly, causing a larger portion of the resistance to deflection to be generated by the frictional interface between pile and rock. Data from the model shows that the shear forces generated at the tip of the pile are approximately 8% greater than when the girder is loaded for maximum live load moment. Coupled with increased axial forces in piles closer to the location of live loading, the shear to normal ratios for these piles decreases slightly. Shear to normal ratios increase for the piles at the opposite end of the girder, primarily due to the decrease in axial load but remain less than the values determined for the piles under the dead load cases.

The investigation into the effects of loading the girder for maximum shear shows some facts that are important considerations for the design procedure. Loading the girder for maximum shear produces smaller strains and deflections in the head of the pile. Axial loads in the piles are increased at one end of the girder, and decreased at the other end. These changes in axial loads affect the interaction between the pile tip and bedrock by increasing or reducing the shear-to-normal ratio, which has been used as an indicator of the stability of the structure. Shear-to-normal ratios in the piles with reduced axial loads are approximately equal to the values for piles under the load cases that do not include live load effects. As has been mentioned in this chapter, the load cases that do not include live loads produce higher shear-to-normal ratios than those that do. Repositioning the live load along the girder does not significantly affect the stability of the structure, since the shear-to-normal ratios for the controlling load cases are unchanged.

4.3.1.2. MDOT Live Load

Studies were conducted to show the effect of using the MDOT live load, which consists of the AASHTO HL-93 loading with a 25% increase in axle loads of the design truck. This loading is used in the Strength I limit state as defined by the AASHTO specifications. In these studies, the design truck was placed on the girder for maximum moment rather than for maximum shear. Maximum shear positioning was not considered because the axle loads in this study were simply increased, and it was assumed that results would be similar to the results of the study previously described.

Use of the increased axle loads resulted in increases to the magnitudes of the pile head strains and displacements. For piles in all soil types, the maximum compressive

strains at the head under all load cases incorporating live load are approximately 10% higher than the strains caused by the standard HL-93 axle loads. This fact is significant because for a given girder length, yielding is more likely to occur when the increased axle loads are used. The behavior of the tip of the pile was consistent with all of the other studies, in that the tip of the pile was able to rotate without any translations in the horizontal and vertical directions.

Increasing the magnitude of the axle loads did not have as large an effect on the contact forces at the tip of the pile as did repositioning them. Data from the model shows that the shear forces generated at the tip of the pile are reduced slightly when the magnitude of the axle loads is increased, possibly due to the decreased likelihood of movement at the pile tip. Combine this with an increase in the axial load in the pile of 5%, and the result is a decrease in the ratio of shear to normal forces at the pile/bedrock interface. As with the models run with the standard HL-93 loading placed for both maximum moment and shear, the load cases that do not include live load effects tend to have larger shear to normal ratios than the load cases that include live loading.

Based on the results of the study examining the effect of increased MDOT live loading over AASHTO HL-93 axle loads, it was determined that the change in pile strains is the most important consequence. Since the increased axle loads lower the shear to normal ratios at the pile tip, the MDOT live loading does not need to be considered in any design criteria regarding these forces. Further limits may have to be imposed on girder lengths in certain soil types in order to compensate for the increased likelihood of yielding at the pile head under the MDOT live loading.

4.3.1.3. Cyclic Loading

The goal of this short parametric study was to determine whether the application of additional thermal and live load cycles affected the behavior observed in the primary study, such as pile strains, deflections, and support conditions. In this portion of the study, the following cyclic loadings were considered:

- Annual temperature changes (ΔT = 0 °C, +20 °C, 0° C, - 55 °C, 0 °C)
- AASHTO HL-93 live load placed for maximum bending moment in girder
- Combination of -55 °C temperature change and HL-93 loading

The change in girder temperature was modulated between +20°C and –55°C, which comprised one annual temperature cycle. Because of increased computational constraints for these models, only five annual temperature cycles were applied to the model. For the case involving only live load, one million cycles were applied. As will be discussed later, it was determined that any additional load cycles past this value had no significant detrimental effect. A model was also studied where a million live load cycles were applied to a girder that had undergone a large negative temperature change. This was done in order to determine the behavior of the structure under the worst load case (Load Case #6) as determined from earlier studies.

As determined in the primary study, the deflections and stresses at the pile tip were more of a concern for thermal loading cycles than pile strains were. Under cyclic thermal loading, one of the concerns about having piles without fixed support conditions at the tip was "walking" or cumulative lateral deflection of the pile tips. Model data

showed that the pile tips did not translate under cyclic temperature loading, and behaved like all of the other models. Lateral deflection of the pile head increased slightly (less than 0.5 mm) over initial cycles, but then became constant. An explanation of the increasing deflection could lie in deformations exhibited in the approach backfill.

The soil elements in the areas of the approaches directly behind the abutment showed permanent deformation in the form of a "hump" which has been observed in actual bridges (Arsoy et al, 1999). This deformation of the approach soil due to thermal expansion of the girder is shown in Figure 4.9, the magnitude of which is 25 mm (1 in). In an actual bridge, this deformation is not permanent, and a depression typically forms behind the abutment. Ideally, modeling the approach backfill with smaller soil elements would allow for a more accurate representation of the soil deformation, in which the approach fill would settle as well as form a "hump". However, since the scope of this secondary study was limited, this sort of modification was not deemed necessary at this time. Whether modeled accurately or not, the occurrence of soil deformation behind the abutment helps to illustrate the necessity of approach slabs for integral abutment bridges to help maintain pavement integrity.

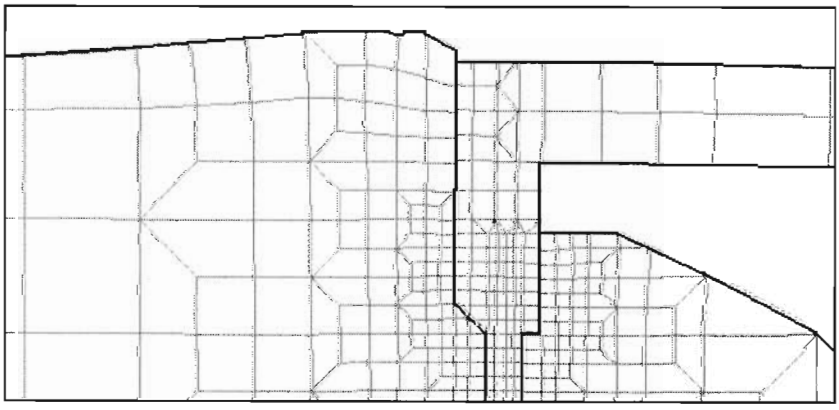

Figure 4.9. Deformation of approach backfill due to thermal expansion (deflections magnified 10x)

The forces at the pile tip were examined at the point in each cycle where the girder had experienced the maximum temperature change. As stated previously, the loading conditions where the bridge is simultaneously exposed to dead loads and negative temperature change produces the highest ratio of shear to normal forces. After the first cycle, the axial forces in the pile increase slightly and the shear force at the base of the pile decreases slightly. Over the subsequent cycles, these values remain constant. This results in a shear to normal ratio that drops below the value calculated for a single instance of negative temperature change, and remains constant in later cycles.

The models incorporating cyclic live loading only were analyzed for all three subsurface conditions. A major concern was the accumulation of plastic strains at the head of the pile, because pile stresses under live loading are often limited in integral abutment pile design procedures. Examination of the data shows that successive cycles of live load do not significantly increase the strains in the head of the pile. As shown in Figure 4.10, the flexural strains at the top of the pile increase slightly after initial live load cycles, and become constant for the remaining cycles. Deflections at the head of the pile also follow this trend, in that they increase initially and them remain constant for the remainder of the live load cycles. The largest increase in both pile strains and deflections over the initial cycles occurred for piles in cohesive soil and was approximately 1%.

Inspection of forces at the pile tip show that after initial cycles, the axial forces in the pile increase slightly. Conversely, the shear forces at the pile/rock interface decrease slightly. Over the subsequent cycles, these values reach a constant magnitude. The net effect of the changes in forces results in a shear to normal ratio that is equal to the values calculated in the models where a single live load is applied. Therefore, the live load

cycles that a bridge will experience over the design life will not affect the stability of the support conditions at the pile tip. As shown in the primary study, this loading rarely produces the highest values of shear to normal ratios.

Since neither of the analyses with cyclic loading resulted in significantly more yielding at the head of the pile than due to a single load application, a series of models were run where a cyclic live load was applied to a girder that had undergone a change in temperature of –55 °C. From the primary parametric studies, it was determined that the condition of live loading and negative temperature change produced the largest abutment rotations, and therefore the largest pile head strains. While the other two cyclic studies showed that pile head strains remained constant after repeated live and thermal loading, these strains were still in the range of elastic behavior.

The goal of these models was to determine whether the strains remained constant under cyclic loading once they had exceeded the yield strain. Data regarding displacements and forces at the tip of the pile were given a cursory examination, and were shown to mimic the behavior shown in the simple cyclic live load models. The only exception was that the magnitude of pile head displacement was larger, due to the additional abutment rotation caused by the temperature change.

Models were run in various soil types for all span lengths described in the parametric studies. Strains at the head of the pile began to exceed yield under combined thermal and cyclic live loading for girders longer than 25 m (82 ft). For girders 30 m (98 ft) long, the strains at the head of the pile reached a value 25% higher than the yield strain, ε_y, after the initial live load cycle. Further cycles of live load reduced the strain in the head of the pile to a value 20% higher than ε_y, where it remained constant. However,

analysis of models with girders longer than 30 m could not be completed under combined thermal and cyclic live loading for more than 3-5 load cycles. Results of the preliminary study show that the strains at the head of the pile in these cases exceed the yield strain by over 40%. A summary of all models involving cyclic live loading (including live loading and $-\Delta T$) is provided in Figure 4.10.

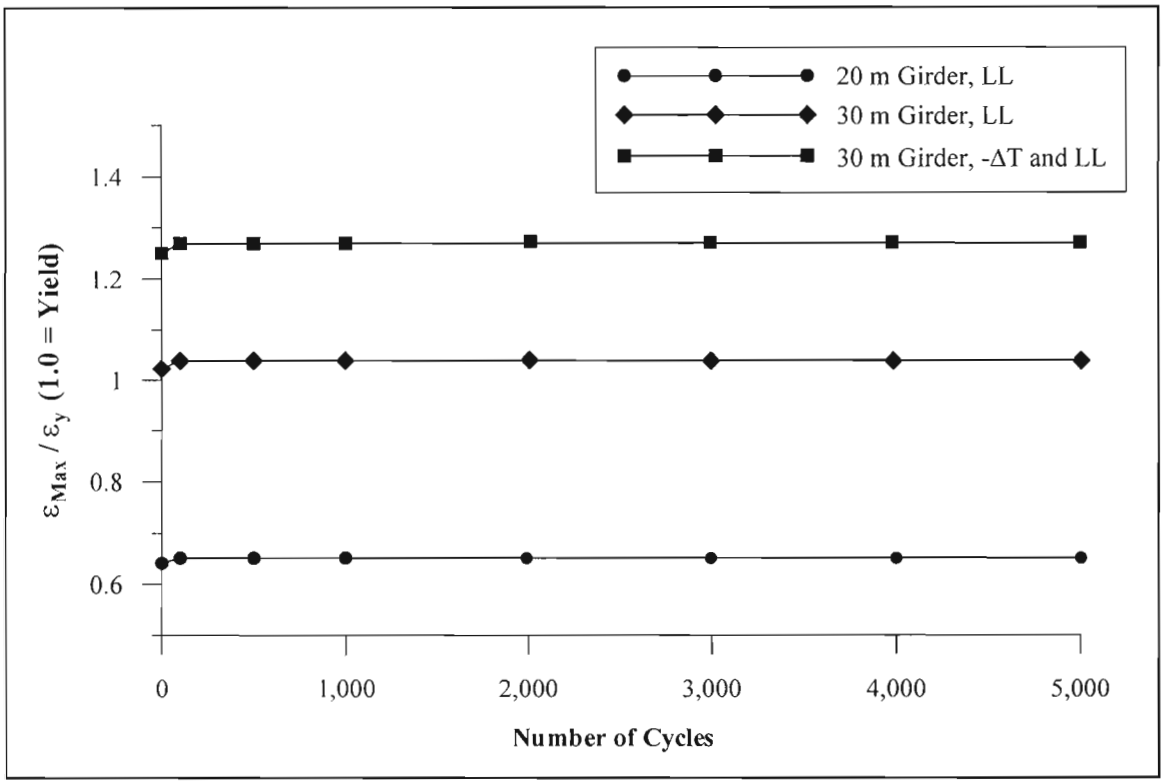

Figure 4.10. Change in pile head strains due to live load cycles

Based on these results, it was concluded that strains in the pile head do not accumulate under cyclic loading if they are below $1.25\varepsilon_y$ at the extreme fiber, after the initial load cycle. This criterion will allow pile sections to be used in cases where the predicted strains exceed yield, without fear of strains and deflections building up to a condition that would weaken the structure or cause instability. Based on this study, and the results of the primary study, limits can be imposed on girder lengths for piles in

certain soil conditions in order to reduce strains. It is possible that these limits are over conservative due to the inconclusive results for longer spans. However, this can only be resolved through further study involving finite element modeling and examination of data from field instrumentation.

4.3.2. Unequal Pile Lengths

All of the models analyzed in this study have had equal length piles at both ends of the girder. However, because of bedrock conditions at bridge sites, this rarely occurs in actual bridges. The proposed bridge over Nash Stream in Coplin Plantation, ME that will be instrumented in Phase II of this project has 3 m (10 ft) long piles at the north abutment, and 7 m (23 ft) piles at the south abutment. A finite element model was created to determine the effects of having unequal length piles on the response of the structure. Figure 4.11 shows the finite element mesh of a bridge with 3 m and 7m long piles, and a 25 m long girder. Although the vertical bedrock surface at the center of the model is unrealistic, this has little to no effect on the response of the piles.

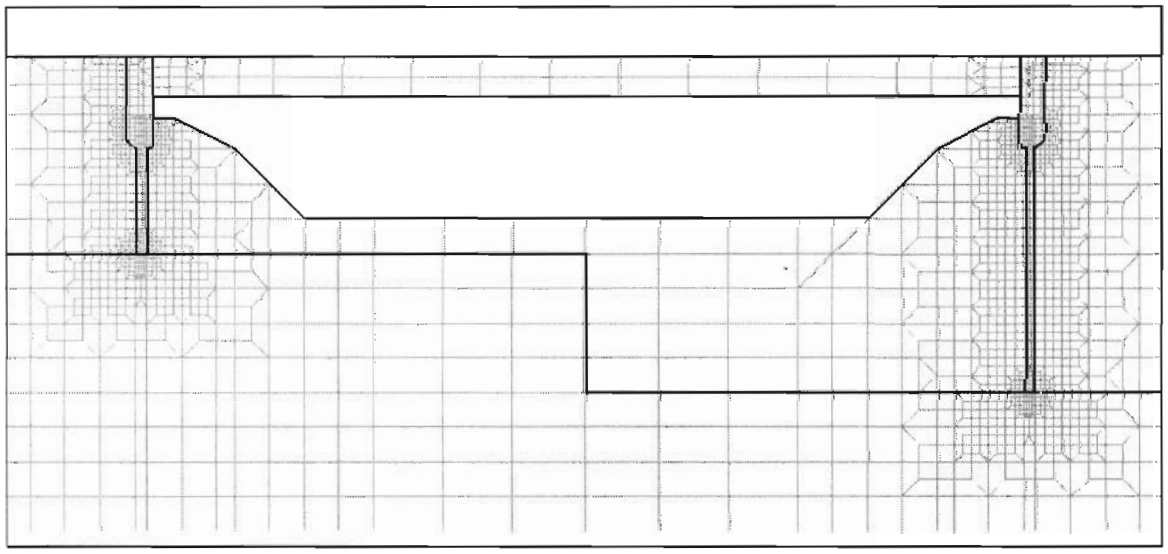

Figure 4.11. Finite element model of bridge with 3 m and 7 m long piles

The model bridge with unequal length piles was subjected to the same load cases used for the models in the primary parametric study. Granular soil conditions were the only conditions modeled initially, although the capability to analyze the other subsurface conditions existed if necessary. The live loading was at the center of the span, as shown in Figure 4.8, in order to induce maximum bending moment in the girder. Because the lengths of the piles were not symmetric about the centerline of the span, modifications were made to the cases incorporating live load. Live load cases with and without thermal effects were run with the design truck facing to the right (as shown in Figure 4.8) and with the truck facing towards the left.

Results of the unequal pile length analyses were compared to the results obtained from the primary parametric study. Since models with 7 m piles were not run in the primary study, the results from this study were compared with the results of 6 m and 8 m piles. Live load data for the 3 m piles was taken with the design truck facing left, while data for the 7 m piles was obtained with the truck facing right. This was because in each of the cases, the heavy rear axle of the truck was closer to the pile.

Pile head strains predicted by the unequal pile length model compared well to the data from the primary parametric study. For all of the load cases not involving live loads, the strains in the short pile were less than 1% smaller than the strains in a 3 m – 3 m bridge, and the data for the 7 m pile fell in between the values for the 6 m and 8 m piles. For the cases involving live load, the strains in the short pile were within 1% of the values from the 3 m – 3 m model, with Load Case #6 being higher, and the other two load cases (2 & 5) being less. The strains in the 7 m pile were 1% greater than the values given by the 6 m and 8 m models, for all load cases involving live load.

As with the cyclic temperature change model, there were concerns about the deflection behavior of an integral abutment bridge with one long pile and one short pile. Specifically, that the entire short pile would experience increased translation because of the fixed support conditions of the longer pile. Deflections along the entire lengths of both the 3 m and 7 m long piles were examined and shown to be consistent with the deflections from the models with equal length piles. There was no lateral deflection at the tips of either pile, and the support conditions at the tip of the shorter pile still allowed for rotation to occur. Displacements of the pile head under dead and live loading were identical to the values from the primary study, while values in load cases involving temperature change were within 1% agreement for both the short and long piles.

The contact forces at the tip of the 7 m long pile typically fell between the range of values for models with 6 m and 8 m piles from the primary study. However, since this length of pile can develop fixed support conditions under the current design guidelines, there was no real concern about behavior at the pile tip. Rather, the comparison was made simply to validate that both models behaved alike. The 3 m long pile showed decreased normal and increased shear forces for load cases 1, 2, 3, and 5. This resulted in shear-to-normal ratios that were up to 6% larger than those determined for a 3 m – 3 m bridge. However, in load cases 4 and 6, which typically produce the largest ratios of shear to normal forces, both the normal and shear forces decreased. The decrease in both forces resulted in shear to normal ratios that were less than 1% smaller than those calculated for a bridge with equal length piles. These shear to normal ratios were still the largest among all of the load cases, even with the 5% increase in the other four cases.

Since there were no major differences in any of the pile responses between bridges with equal and unequal length piles, no further studies were performed regarding girder length and soil type. It can be presumed that changes in girder length and soil type will affect the response of a bridge with unequal length piles in the same way that they would a bridge with equal pile lengths. Because of these observations, it was felt that instrumentation of the proposed bridge in Coplin Plantation would provide meaningful data, despite the fact that the lengths of the piles at each abutment were different.

4.3.3. Pile Cross-Sections

As discussed in Chapter 3, the section properties of the piles used in all of the models were based on an HP360x108 (HP14x73) pile, because that is what was used in the bridge design for the proposed Mill Pond Bridge. However, data about the behavior of other pile sections was necessary in order to give flexibility to the proposed design procedure. For integral abutments, in addition to the HP360x108 section, Maine commonly uses the following pile sections: HP 250x62 (10x42), HP 310x79 (12x53), and 360x123 (14x89). A parametric study was performed to determine the response of a pile with a higher moment of inertia (HP360x123) and a lower moment of inertia (HP310x79) than the piles used in all of the other studies. The HP250x62 section was not studied, because the current design provisions already allow for a minimum embedment length of 3 m (10 ft) for this pile section.

Equivalent section properties for each pile type were determined using the method described in Chapter 3 for the substructure elements. In addition, the mesh required slight modifications in order to accommodate the slightly different dimensions of each

pile section. Table 4.1 provides a comparison between the model section properties of the three different pile types. The effects of changing soil conditions, utilizing the three soil types discussed earlier, were considered in this parametric study

Table 4.1. Comparison of Model Section Properties for Different Pile Sections

	HP 310x79	HP 360x108	HP 360x123
Width	252 mm	308 mm	311 mm
Depth	299.7 mm	346 mm	351 mm
Moment of Intertia	399.7 x 10^6 mm^4	842.5 x 10^6 mm^4	879.8 x 10^6 mm^4
Area	75520 mm^2	106600 mm^2	109200 mm^2
Section Modulus	3.17 x 10^6 mm^3	5.47 x 10^6 mm^3	5.66 x 10^6 mm^3

Examination of the model results shows that the pile head strains vary with pile stiffness. For all subsurface conditions and girder lengths, the strains at the head of the pile were less for piles stiffer than the HP360x108 section, and greater for piles with less stiffness. This pattern holds true for all load cases. As was observed in the primary parametric studies, longer girders result in increased strains at the head of the pile. Therefore, for a given girder length, piles with a higher stiffness will be less likely to yield than piles with a lower stiffness. Figure 4.12 illustrates the effect of girder length on the stresses in the various pile sections for a given load case. The strains on the y-axis are given as a ratio of the pile head strain to the yield strain.

The deflection characteristics of the pile are also affected by the section properties. Because of the reduced stiffness of the HP310x79 section, it is able to achieve double curvature, which leads to an increase in pile head deflection over the HP360x108 section. Conversely, the stiffer HP360x123 section only exhibits bending in the upper portion of the pile. Because the soil cannot provide the necessary support for

the HP360x123 to achieve double curvature, the entire pile translates in the lateral direction. As a result, the deflections along the entire length of the HP360x123 section are greater than for the HP360x108 section.

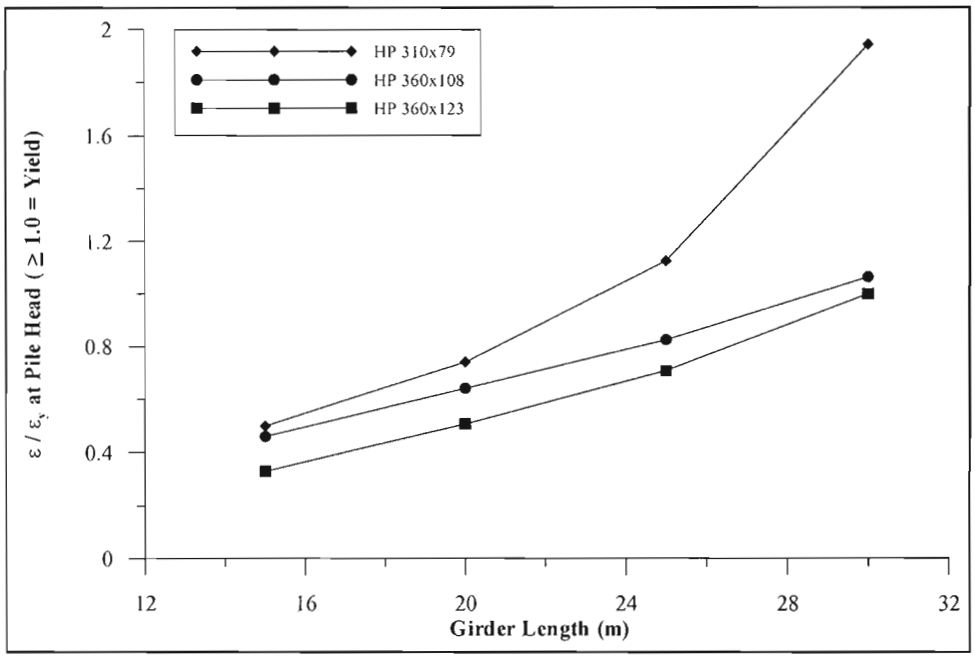

Figure 4.12. Effect pile stiffness on strains at pile head under dead and live loading in granular soil

Pile stiffness also alters the forces at the pile tip, in that stiffer pile sections generate larger shear forces. This allows the upper portions of stiff pile sections to translate laterally, but remain restrained at the tip. Because of the increase in shear forces, shear-to-normal ratios for the stiffer pile section are 5% greater than those calculated in the primary parametric study, while the shear-to-normal ratios for the HP310x79 section are 10-20% less.

These differences appear to be much less crucial to the design of a pile than the changes in strains and deflections are. The section moduli and stiffness of the various pile sections dictate the amount of axial load and moment that the pile can withstand

without yielding. The changes in the strains at the head of the pile for a given girder length, as shown in Figure 4.12, are much more drastic than the 5-20% change in the forces at the pile tip.

4.4. Summary

Parametric studies using the model described in Chapter 3 were performed in order to determine the effect of several variables on three major structural responses: pile stresses, pile kinematics, and pile/bedrock interaction. An analysis procedure was developed that approximated the construction sequence of an integral abutment bridge. However, one facet of this process that is neglected is the changing section properties of the girder at various stages of construction. Differences in the support conditions of the girder, as well as the degree to which girder behavior influences the critical load conditions allow for the effect of the section properties to be ignored. Nonetheless, the detailed consequences of these property changes should be addressed in future studies.

A primary parametric study was performed that investigated how changes in girder length, pile length, and subsurface conditions affected the pile responses. Inspection of the pile kinematics showed that piles less than 4 m in length behave similar to a laterally loaded, fixed-head pile of intermediate length, as defined by Broms (1964a, 1964b). The tip of the pile rotates, but does not translate horizontally or vertically, similar to a column with a pinned support. In addition to translation of the pile head due to thermal movement of the girder, dead and live loading of the girder induce a rotation of the abutments, causing additional pile head displacement, that is not typically accounted for.

The magnitudes of the pile strains were found to be independent of the pile length. Changes in the girder length (and therefore loading), as well as the subsurface conditions, cause the greatest differences in pile head strains. Therefore, piles embedded in clay soils are more likely to experience plastic deformation than those in granular soils are. Similarly, for piles in a given soil type, those supporting longer spans can be expected to experience some degree of plastic deformation. Because of the consequences of plastic deformation on the stability of the structure, limits on girder length may have to be imposed for various soil conditions in order to control this occurrence.

Forces at the tip of the pile were found to be an important factor in controlling the stability of the structure. A ratio of the shear force and the normal force acting at the bedrock was compared to the coefficient of friction determined for this interface, as a measure of the validity of the assumption of pinned support conditions. The normal force at this interface is dictated by loading and girder length, although downdrag resulting from certain soil conditions has some effect also. Subsurface conditions as well as pile length influence the magnitudes of shear forces at the tip. Inadequate soil support causes more of the force resisting translation of the tip to be developed between the bedrock and pile. Pile length indirectly influences the forces at the tip, mainly due to the effect of the depth of the channel under the bridge. The forces peak for a 4 m pile, because this is the longest pile with the least amount of soil supporting it on one face.

Smaller parametric studies were performed in order to investigate less significant changes in loading, geometry, and member properties. It was found that positioning the design truck at different locations along the girder had no adverse effect on the pile behavior. The larger live loading used by MDOT was found to increase strains at the

head of the pile, which may further reduce the allowable girder lengths used in design. The structure was shown to accommodate cyclic live and thermal loading without any major consequences. Under annual temperature cycles, the abutment backfill is shown to deform, illustrating the need for approach slabs behind integral abutments. Under combined cyclic live and thermal loading, plastic strains did not accumulate under progressive cycles, if the strains in the pile head were less than 1.25 ε_y.

Bridges constructed with unequal length piles at either end of the girder were examined. A major concern was that a bridge with a short pile, and a pile with adequate overburden would cause erratic behavior of the structure. In particular, the short pile would experience increased translations, since the other end of the structure had more lateral resistance. It was found that while deflections of the shorter pile were slightly different than for a structure with short piles on either end, there was no significant change in behavior for a bridge with unequal length piles.

The use of different pile sections was also considered in a smaller study. It was shown that stiffer piles experience smaller strains at the pile head. Therefore, the length of span and soil conditions may dictate the section of pile that can be used for a particular bridge, especially if the limiting strain at the pile head is considered to be a critical factor. Short, stiff pile sections cannot develop double curvature as readily as other pile sections, because of insufficient soil support. Because of this, stiffer piles experience more lateral translation along the entire length of the pile. Larger shear forces are generated at the tips of stiffer piles in order to compensate for the lack of lateral support provided by the soil. Therefore, there are some cases where simply specifying a larger pile section will not improve design.

Chapter 5

PRELIMINARY DESIGN GUIDELINES

Using data from the parametric studies described in the previous chapter, recommendations for a procedure to be used in the design of pile foundations for integral abutment bridges are made in this chapter. This procedure is intended to be utilized in instances where the depth to bedrock is less than the depth of embedment required to obtain fixity. This chapter discusses the underlying assumptions and principles of the proposed design procedure. The assumptions for design and construction of integral abutment bridges in the proposed procedure are essentially the same as in the current procedure. The only difference is the idealization of the support conditions at the pile tip.

5.1. Current Design Guidelines

Section 5.4.2 of the Maine Department of Transportation (MDOT) Bridge Design Guide (1999) addresses the use of piles to support integral abutments. Pile capacity is governed by axial and biaxial bending action of the pile. The axial stresses are a result of the dead loads of the piles, abutment, and superstructure, as well as the live loading on the superstructure. For single-span bridges, such as the ones considered in this study, shear forces in the pile induced by thermal displacement are not considered by MDOT. Research by Abendroth and Greimann (1988), discussed in Chapter 2, was used to evaluate maximum bridge length and design pile loads for four preferred pile sections used by MDOT.

Pile stresses are limited by two separate criteria. Axial stresses are limited to 0.25 F_y, as discussed in Section 5.7 of the MDOT Bridge Design Manual (MDOT, 1999),

while bending stresses in the pile are limited to 0.55 F_y. For this criterion, only the bending stresses in the pile induced by the superstructure live load reactions (W) are considered. Using these live loads, the end rotation of the girder (R_g) is calculated using a modified equation for the end rotation of a simply supported span:

$$R_g = \frac{2W L_S^2}{24 E_g I_g} \qquad \text{(Equation 5.1)}$$

where L_S is the length of the span, E_g is Young's modulus of the girder, and I_g is the moment of inertia of the girder. The stiffness of the abutments allows this rotation to be transferred directly to the pile head, inducing a moment (M) in the pile head, given by:

$$M = \frac{4 E_p I_p R_g}{L} \qquad \text{(Equation 5.2)}$$

where L is the length of pile below the ground surface, and E_p and I_p are Young's modulus and the moment of inertia of the pile, respectively. The bending stress in the pile (σ_p) caused by the applied end-rotation moment (M) is calculated with the following equation:

$$\sigma_p = \frac{M}{S_p} \qquad \text{(Equation 5.3)}$$

where S_p is the section modulus of the pile. If the value of σ_p exceeds 0.55 F_y, then a different pile section or a greater pile length must be used.

Based on the estimates of thermal movement from FHWA Technical Advisory T5140.13 (1980) and the stress criteria, the maximum bridge length and maximum allowable pile loads for integral abutments with fixed pile heads are given in Table 5.1 and Figure 5.1 respectively. Figure 5.1 follows the FHWA recommendation that the thermal movements for steel superstructures be calculated as 1¼ in/100 ft of length (1.04

mm/m), while thermal movements of concrete superstructures be calculated as ¾ in/100 ft (0.625 mm/m). The pile sections were evaluated as beam-columns without transverse loads between their ends, fixed at some depth and either pinned or fixed at their heads (MDOT, 1999). Because MDOT primarily uses fixed-head abutments, which were incorporated in the finite element model, discussion of the current and proposed design procedure is limited to this abutment configuration.

Table 5.1. Maximum Bridge Length for Steel Girders with Fixed-Head Abutments

Pile Section	0° - 19° Skew	20° - 25° Skew
HP 10x42 (HP 250x62)	200 ft (60 m)	140 ft (42 m)
HP 12x53 (HP 310x79)	130 ft (40 m)	75 ft (22 m)
HP 14x73 (HP 360x108)	120 ft (36 m)	70 ft (20 m)
HP 14x89 (HP 360x132)	200 ft (60 m)	200 ft (60 m)

After MDOT Bridge Design Guide (1999), Table 5-3

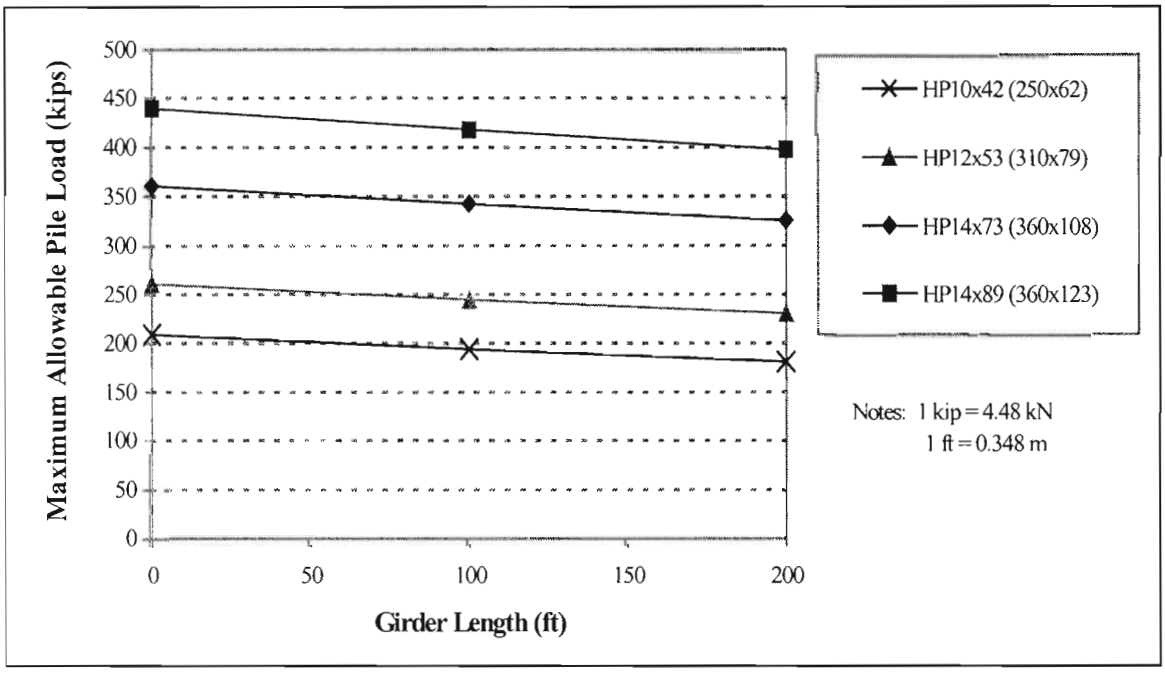

Figure 5.1. Maximum Allowable Pile Load for Steel Girders with Fixed-Head Abutments (MDOT, 1999)

The length of pile in Equation 5.2 for the purposes of design is generally taken as the minimum embedment length given in Table 5.2. However, soil and loading conditions may require additional pile embedment to achieve fixity at some point in the pile (MDOT, 1999). MDOT allows the minimum pile length to be evaluated using COM624P (Wang & Reese, 1993) or L-PILE (Ensoft, 2002), if site-specific loading and subsurface data exists. Both programs are widely used for the analysis of a single, laterally loaded pile.

Table 5.2. Minimum Embedment Lengths

Pile Section	Minimum Embedment Length
HP 10x42 (HP 250x62)	10 ft (3.0 m)
HP 12x53 (HP 310x79)	12 ft (3.6 m)
HP 14x73 (HP 360x108)	13 ft (3.9 m)
HP 14x89 (HP 360x132)	15 ft (4.5 m)

After MDOT Bridge Design Guide (1999), Table 5-5

5.2. Proposed Design Guidelines

The proposed design procedure outlined in this section is an extension of the current design procedure, to be used in cases where the depth of overburden, i.e. the distance from the bottom of the abutment to the bedrock surface, is less than the minimum embedment length. As determined from the parametric study presented in Chapter 4, short piles supporting integral abutments tend to behave similarly to columns with a pinned base rather than fixed, as is normally assumed for integral abutment bridge piles. Therefore, the same "long" pile capacity checks used in the current design procedure do not necessarily apply to short piles. In the proposed guidelines for short piles, two criteria are used to determine the suitability of a certain pile section for the

support of an integral abutment. The first criterion considers the moment capacity of the pile and resulting stress conditions at the pile head. The second criterion examines the interaction between the pile tip and the bedrock surface. In this criterion, the forces acting at the pile tip are used to assess the validity of the assumption that the piles behave similarly to a column with a pinned base. An example design problem illustrating the use of the design procedure is given in Appendix B.

5.2.1. Moment Capacity of the Pile

The proposed design guidelines limit the moment in the head of the pile to M_y under dead and live loading from the girder and abutments. Results of the parametric studies of Chapter 4 show that the moment at the head of the pile depends mainly on the length of the bridge girder. Table 5.3 can be used as a conservative estimation of an appropriate pile section for a given girder length and category of subsurface conditions, such that the moment induced in the pile under dead and live loading will not exceed M_y. Since the models used in the study were two-dimensional, effects of skew on the maximum girder length are not taken into account at this time. The effects of skewed bridge alignments on these guidelines will be considered in future studies, using data from an instrumented bridge with abutments that have a large skew angle (> 25°).

Table 5.3. Maximum Bridge Length for Fixed-Head Abutments on Piles < 4m

Pile Section	General Soil Category		
	Sand & Gravel	Clay	Glacial Till
HP 310x79 (HP 12x53)	25 m	25 m	25 m
HP 360x108 (HP 14x73)	30 m	25 m	30 m
HP 360x132 (HP 14x89)	35 m	30 m	30 m

Once the appropriate pile section is selected, the vertical pile loads P_{DL} and P_D are calculated. P_{DL} is calculated as the sum of the dead load superstructure reaction, the unfactored live load superstructure reaction, the abutment dead load, and the pile weight. MDOT includes an impact factor for live load in the current design guidelines. However, impact loading was not considered in the finite element model, since the focus of the design is on a buried component, not the superstructure or abutments, which is consistent with the AASHTO guidelines (AASHTO, 1996). P_D is calculated in a similar manner, except the contribution of the superstructure live load is neglected. The moments at the head of the pile are calculated using a relationship between pile head moment and vertical pile load, developed from the parametric study results. Although this relationship was based on the finite element models using the standard AASHTO HL-93 live load, it was shown to hold true for the increased MDOT live load case. For the appropriate subsurface conditions, P_D and P_{DL} are used in conjunction with Figures 5.2 – 5.7 to determine M_D and M_{DL}, respectively.

After determining M_D and M_{DL} from the appropriate figure, both moments must be adjusted to account for thermal forces on the structure. Since the integral abutment bridges in this study were all single-span, there are no additional axial forces due to thermal expansion/contraction. As shown in the results of the parametric study, the displacements caused by a negative temperature change tend to increase the pile head stresses, while a positive temperature change will have a tendency to reduce stresses in the pile head. The design negative temperature change is multiplied by the appropriate moment correction factor given in Table 5.4. This moment is added to M_D and M_{DL}, resulting in two additional moments M_{DT} and M_{DLT}, respectively.

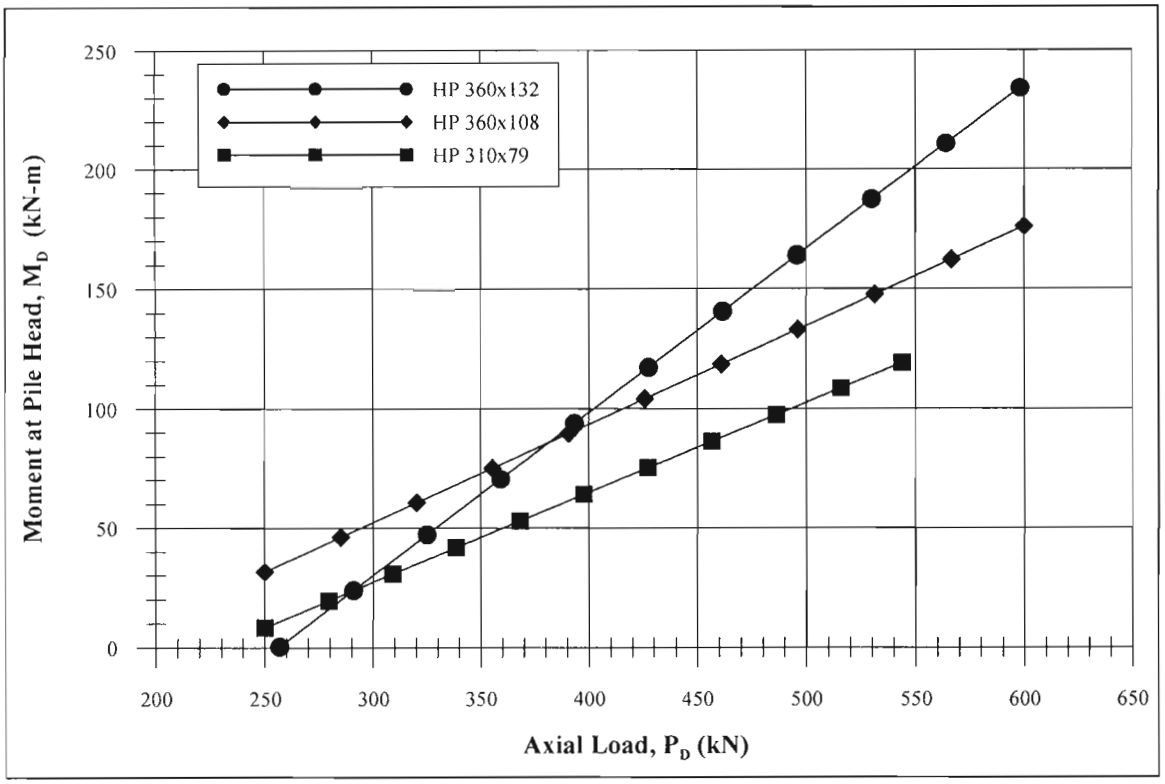

Figure 5.2. Dead load moment at top of piles in sand and gravel

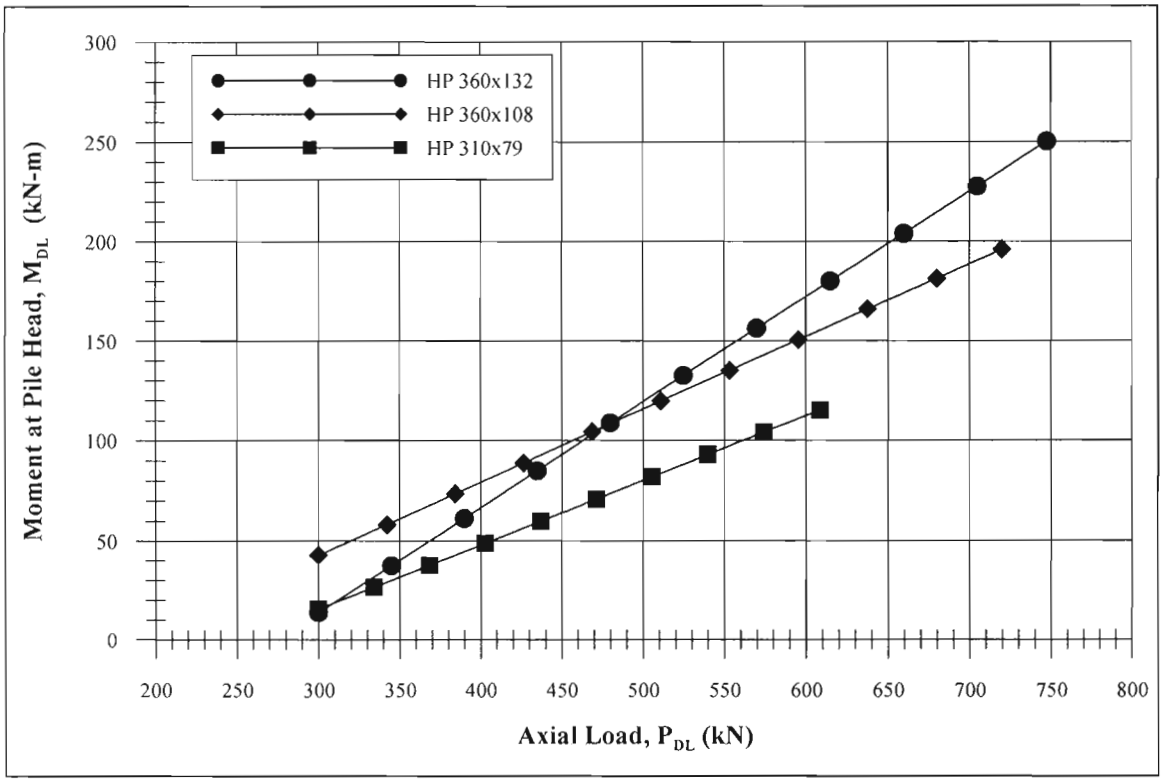

Figure 5.3. Dead and live load moment at top of piles in sand and gravel

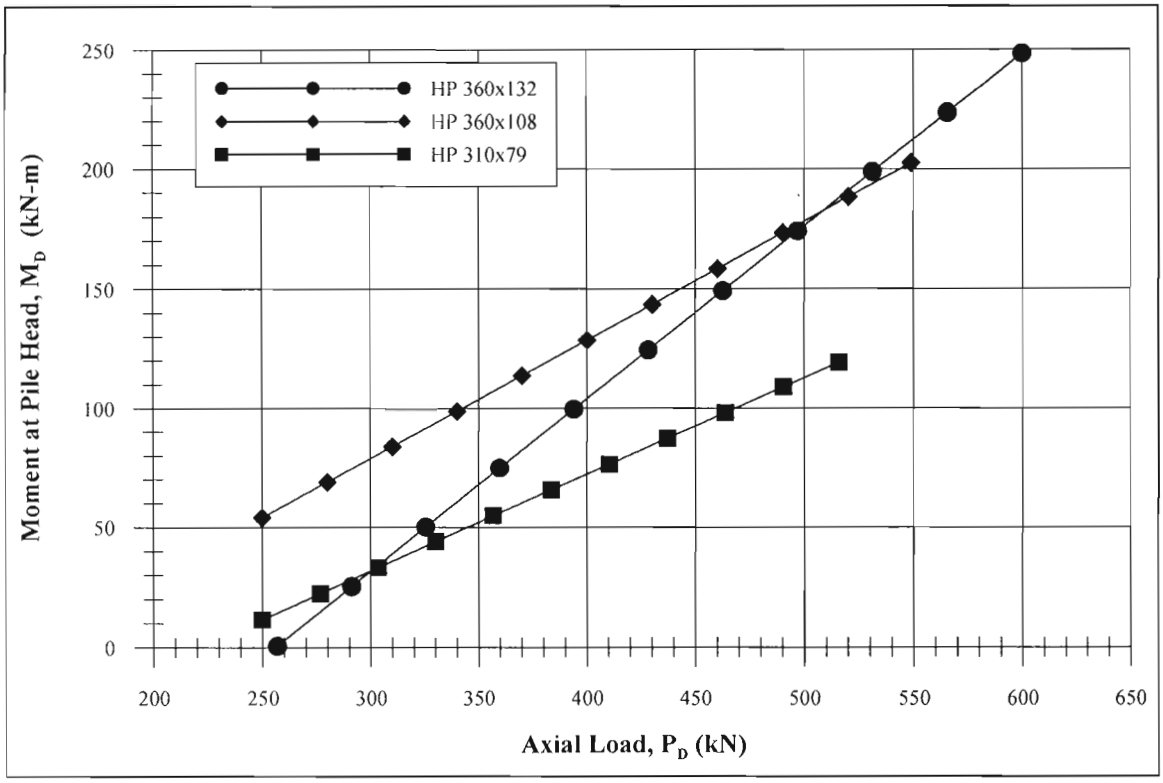

Figure 5.4. Dead load moment at top of piles in clay

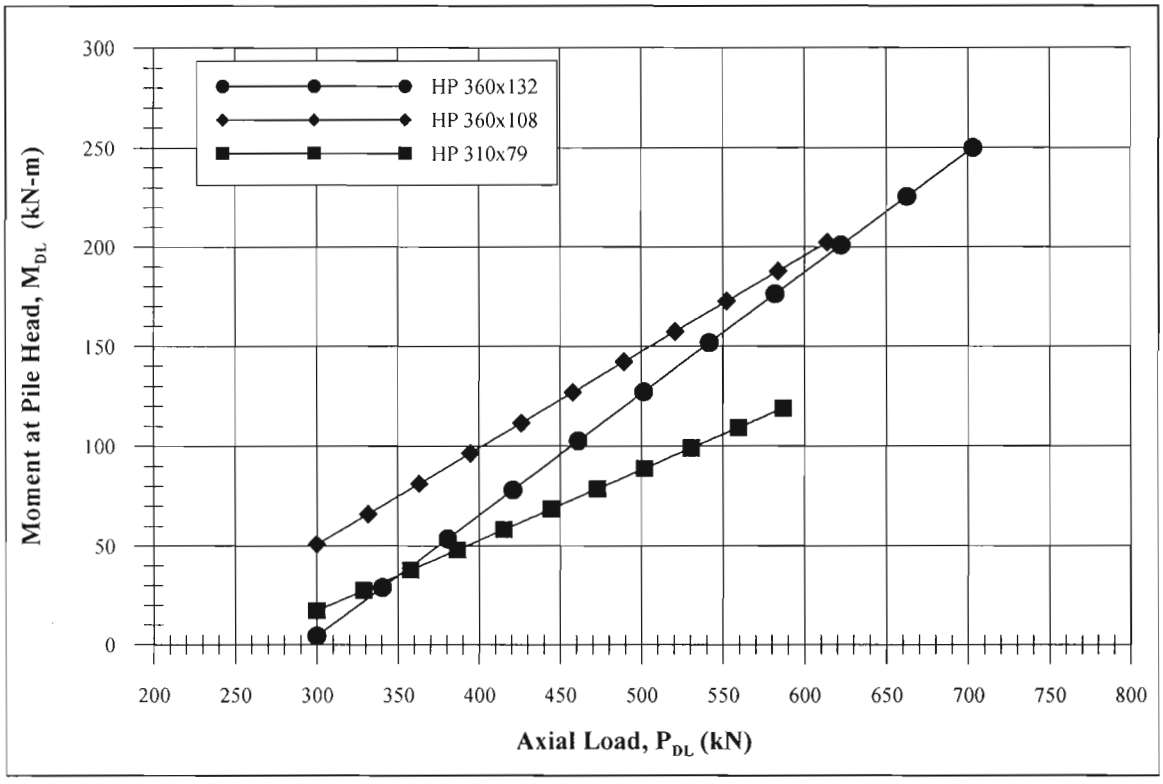

Figure 5.5. Dead and live load moment at top of piles in clay

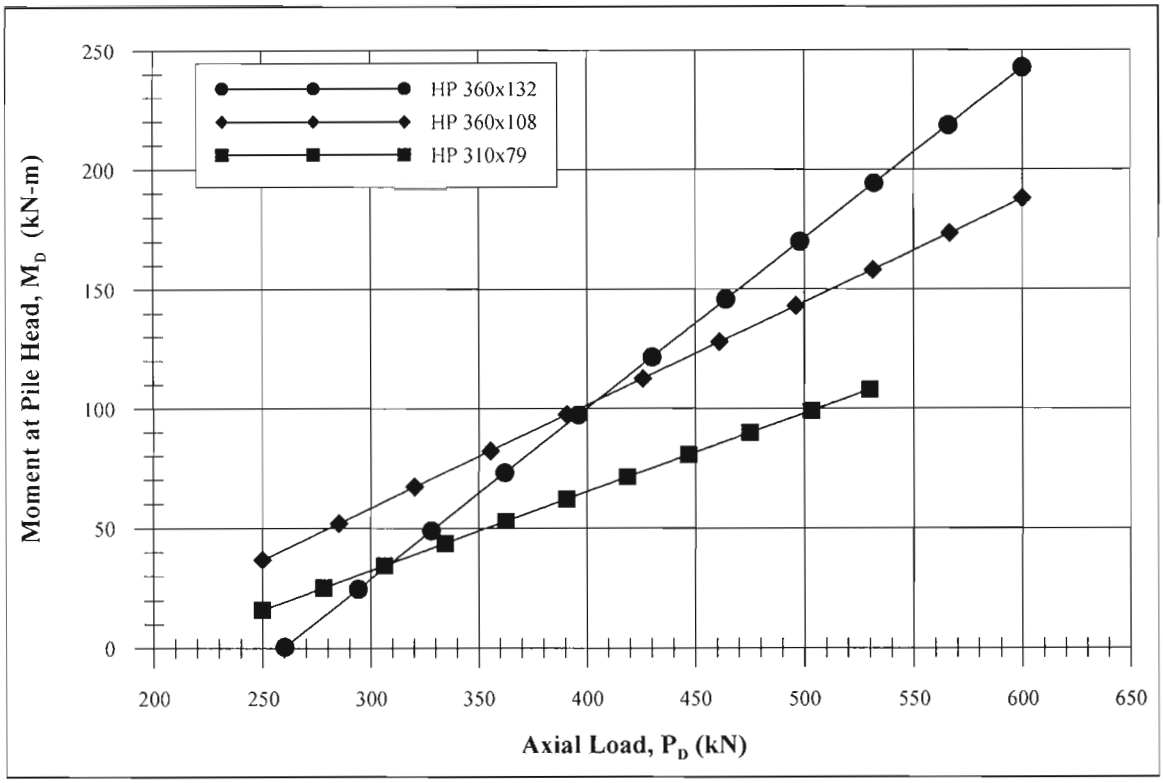

Figure 5.6. Dead load moment at top of piles in glacial till

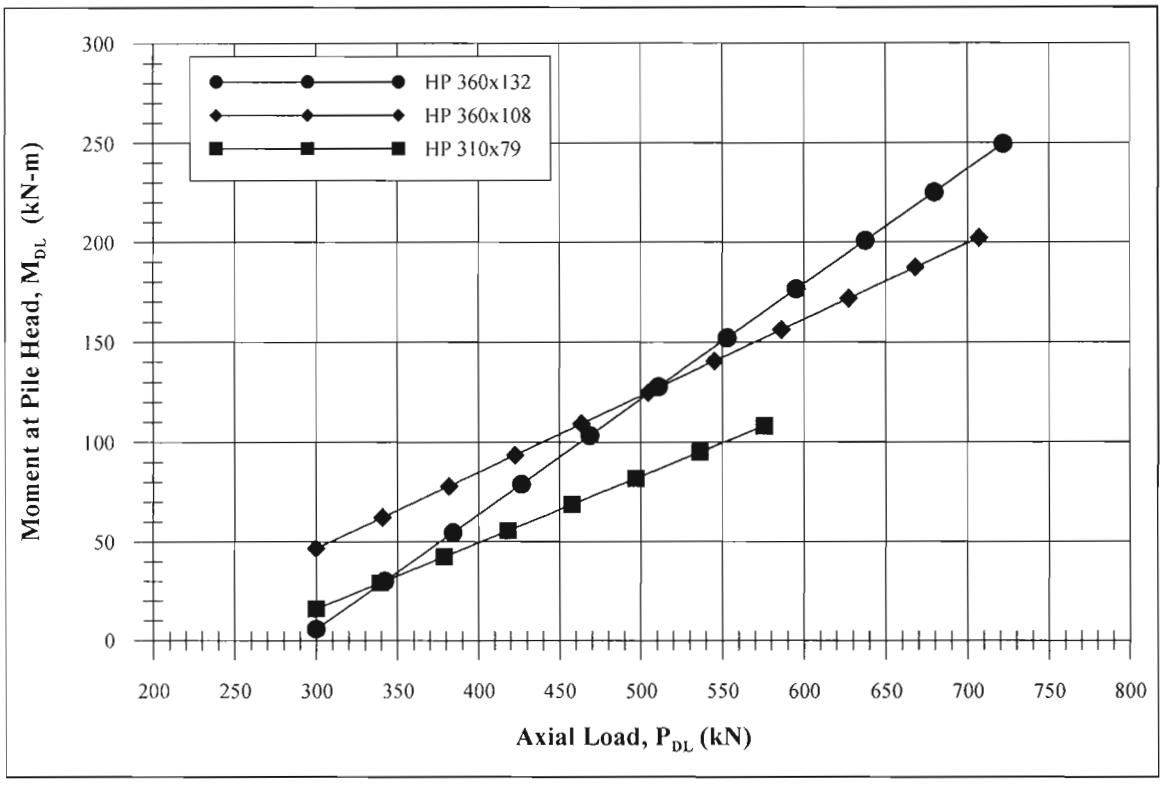

Figure 5.7. Dead and live load moment at top of piles in glacial till

Table 5.4. Negative Temperature Change Moment Correction Factors (kN-m/°C)

Pile Section	General Soil Category		
	Sand & Gravel	Clay	Glacial Till
HP 310x79 (HP 12x53)	0.45	0.19	0.40
HP 360x108 (HP 14x73)	0.61	0.23	0.54
HP 360x132 (HP 14x89)	0.67	0.29	0.61

For higher axial loads, this moment correction could result in M_{DLT} exceeding M_y, resulting in plastic deformation when subjected to dead, live, and thermal loading simultaneously. One of the cyclic live load studies discussed in Chapter 4 involved the application of live load cycles to a girder experiencing a negative temperature change. In all cases, the strains at the head of the pile exceeded ε_y, and portions of the pile yielded after one load cycle. However, for all cases with pile strains less than 1.25 ε_y, it was shown that there was no further plastic deformation with the application of additional live load cycles.

The strains in the three pile sections were studied in models incorporating the maximum allowable girder length for each type. The moments at the head of the pile under dead, live, and thermal loading were calculated with the maximum strain in the pile equal to 1.25 ε_y. The resulting moments at this strain were all approximately equal to 1.2 M_y, which is less than M_P in all cases. To ensure that the moment due to cyclic live load and thermal effects does not result in significant accumulation of plastic deformation, it is recommended that the values of M_{DT} and M_{DLT} do not exceed 1.15 M_y.

5.2.2. Forces Acting on Tip of the Pile

The moments M_D and M_{DL} are calculated primarily to verify that the piles do not reach M_y under dead and live loading. M_{DT} and M_{DLT} are used with a simplified approximation to determine the shear forces acting at the bottom of the pile. As stated earlier, piles less than 4 m long act more like a column with a pinned support at the tip, rather than the equivalent cantilever that is typically assumed. This approximation for short piles is shown in Figure 5.8. By applying M_{DT} and M_{DLT}, to the top of the column, the rotations and displacements of the pile head for the particular load cases are essentially defined.

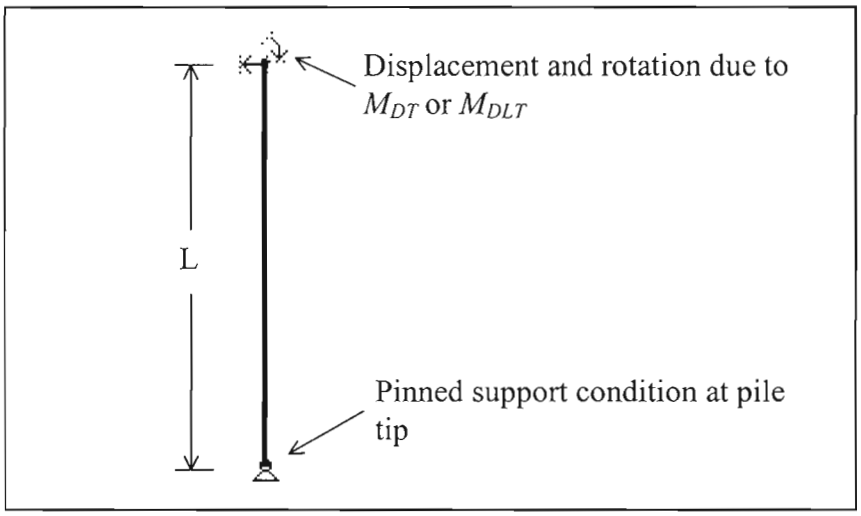

Figure 5.8. Idealization of pile with pinned support conditions at tip

The above simplification causes shear forces at the pile tip to decrease with length, which is to be expected. However, data from the parametric study shows that the shear forces increase for lengths up to 4 m and then decrease. This is due to the effect of the channel depth on the soil support provided to one face of the girder. Because this simplified model cannot possibly account for the interactions and behavior exhibited in the finite element model, factors (β_1 and β_2) were created for M_{DT} and M_{DLT} in order to

better approximate the shear values predicted by the model. Incorporating the β factors into the equation for shear at the support of the system shown in Figure 5.8 results in the following equations:

$$V_{DT} = \frac{\beta_1 * M_{DT}}{L} \qquad \text{(Equation 5.4)}$$

$$V_{DLT} = \frac{\beta_2 * M_{DLT}}{L} \qquad \text{(Equation 5.5)}$$

where V_{DT} and V_{DLT} are the shear forces at the pile tip due to M_{TD} and M_{DLT}, respectively. Values of β_1 and β_2 for various soil categories and pile lengths are given in Table 5.5. For pile lengths that fall between values on the table, the β factors for the greater pile length can be used conservatively. These factors along with Equations 5.4 and 5.5 apply for all pile sizes considered in the parametric study.

Table 5.5. Shear Coefficients for Short Piles

Pile Length (m)	Sand & Gravel		Clay		Glacial Till	
	β_1	β_2	β_1	β_2	β_1	β_2
2	0.91	0.14	2.55	1.13	1.66	0.67
3	3.12	1.95	5.03	3.42	4.1	2.72
4	4.69	3.23	6.79	5.04	5.83	4.17
5	5.9	4.23	8.15	6.3	7.17	5.29

The assumption of a pinned support at the base of the pile is verified by comparing the ratio of the shear and normal forces in the pile to the friction coefficient of the rock/pile interface (μ). This friction coefficient can be determined for specific bedrock conditions using Equation 3.9, if sufficient information exists to determine values for ϕ and *i*. The value of 0.7 used in the finite element models was determined

using a low value of ϕ for intact schist (26°) from Lama & Vutukuri (1978). Because this ϕ value compares well with published values of the residual friction angle (ϕ_r) for other types of rocks, $\mu = 0.7$ can be used conservatively for cases where site-specific bedrock data does not exist.

A factor of safety is applied to μ in order to account for the uncertainties in the condition of pile and bedrock profile. The ends of steel H-piles may become damaged or misaligned during driving, especially when driven to bedrock. Uncertainties in the bedrock surface include the extent and severity of weathering and the overall slope of the bedrock profile. A factor of safety of 1.75 should be considered appropriate in cases where there is insufficient data with regards to the surface of the bedrock. Based on work done by Rehnman & Broms (1971), the slope of the bedrock surface will have an effect on the capacity of piles driven to rock. If the overall slope of the bedrock in the vicinity of the pile can be determined with some degree of certainty from boring logs, adjustments to the factor of safety given in Table 5.6 can be applied.

Table 5.6. Recommended Factors of Safety if Slope of Bedrock Surface is Known

Slope of Bedrock	Factor of Safety (FS)
0° - 30°	1.5
30° - 45°	1.75
45° - 60°	2.0
> 60°	3.0

The following equations are used to compare the calculated shear and normal forces at the pile tip to μ, with the factor of safety (FS):

$$\frac{V_{DT}}{P_{DT}} = \frac{\mu}{FS} \qquad \text{(Equation 5.6)}$$

$$\frac{V_{DLT}}{P_{DLT}} = \frac{\mu}{FS} \qquad \text{(Equation 5.7)}$$

If Equations 5.6 and 5.7 are satisfied, than the chosen pile section can be considered suitable. However, if the shear/axial ratio is greater than μ divided by the factor of safety, it may be necessary to specify certain construction details. These details could include increasing the size of the abutments to increase dead load, or utilizing shallow rock sockets for the pile tip. The research performed by Rehnman and Broms (1971) indicate that if the pile penetrates into the rock by a depth equal to its diameter, the capacity of the rock/pile system is increased by approximately 25-50% over the capacity achieved when the pile does not penetrate the bedrock surface at all.

5.3. Summary

The current design procedure for piles supporting an integral abutment relies on the assumption of fixed conditions at the base of the pile. Maximum bridge lengths and pile loads were determined for certain pile sections, using the methods described by Abendroth & Greimann (1988). This method reduces the pile to an equivalent cantilever, based on loading and soil conditions. Therefore, sufficient pile length must be provided in order to achieve support conditions approximating a cantilever with a fixed end. However, there are often cases where the depth of soil to the bedrock is less than the minimum length required to achieve fixity.

Therefore, a design procedure is proposed as an addendum to the current procedure, when situations where the depth to bedrock results in pile lengths less than

currently allowed. Based on data from the parametric studies described in Chapter 4, a relationship between the moment at the head of the pile and the axial load was created for various soil conditions and loadings. The proposed guidelines inherently limit the strain in the pile to a maximum value of 1.25 ε_y, which was shown to be the point where plastic deformation accumulates under the most severe loading conditions (dead, live, and negative temperature change). This is different from the current guidelines, where stress in the piles (due to live load only), is limited to 0.55 F_y.

Unlike the current guidelines, the proposed guidelines idealize the support conditions at the pile tip as a pinned support, i.e. the pile tip cannot translate horizontally or vertically, but is free to rotate. Checks involving estimation of forces at the pile tip are used in order to determine if this idealization is valid for the proposed pile/soil/load combinations. The ratio of shear forces and normal forces are compared to the coefficient of friction between the pile and bedrock. A factor of safety is used to account for variations in the bedrock surface that may affect the amount of displacement restraint provided.

Shear forces are calculated from the moment at the head of the pile using a simplified structural model, as shown in Figure 5.8. Data from the parametric study shows that the effect of channel depth for piles less than 4 m long causes an increase in shear forces at the pile tip. Therefore, shear factors are necessary to obtain values from the simplified model that are similar to those provided by the finite element model. Figure 5.9 provides a comparison between pile head moments predicted by the finite element model, and moments determined using Figures 5.2-5.7. Figure 5.10 provides a similar comparison for the shear forces at the pile tip from the model and design method.

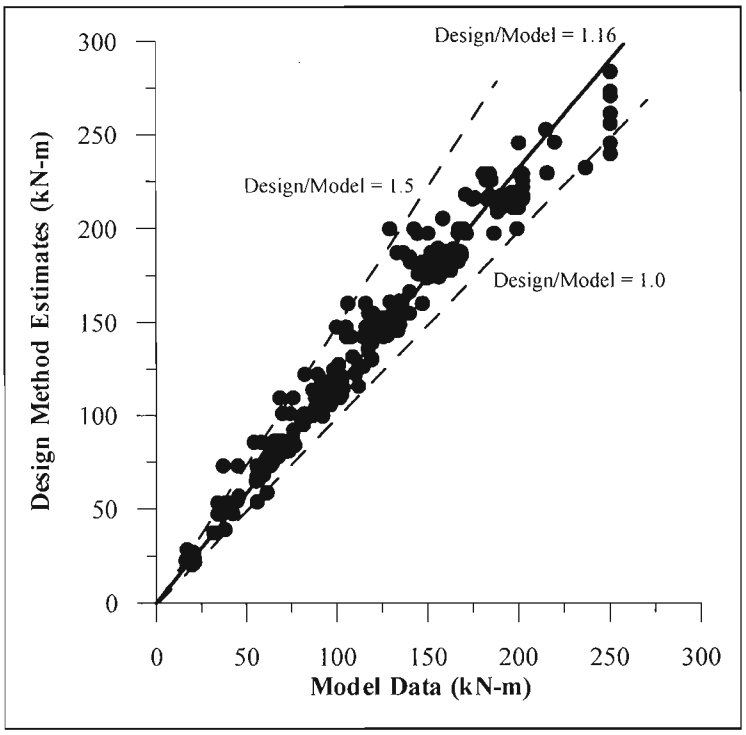

Figure 5.9. Comparison of moments predicted by model and design method

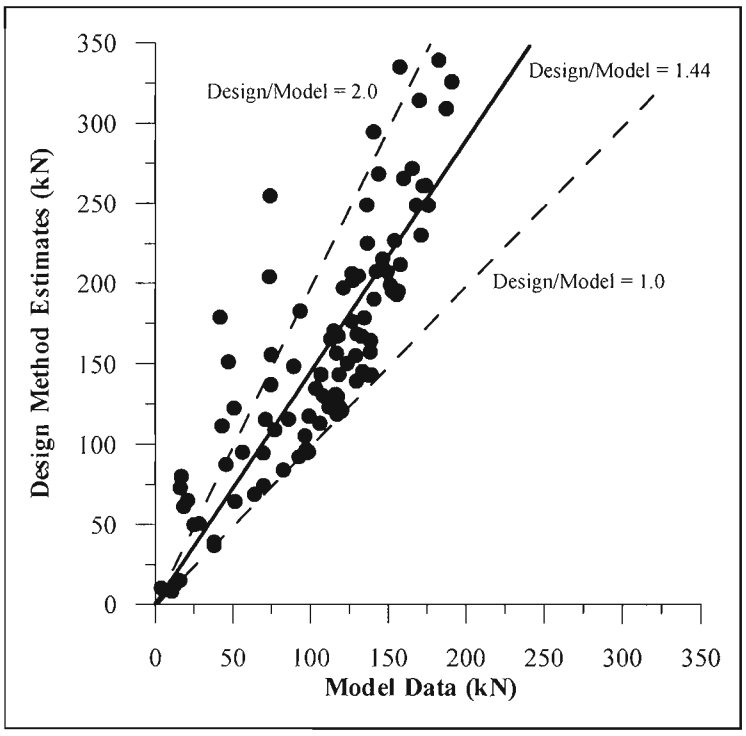

Figure 5.10. Comparison of shear forces predicted by model and design method

As shown in the previous figures, the values of moment at the pile head predicted by the design procedure compare very well with the values calculated using the finite element model. On average, the moments predicted using the proposed design method are 16% greater than those from the finite element data are, which is somewhat conservative. The values of the shear force at the tip of the pile obtained with the design procedure exceed the model data by 44% on average, which is conservative. The data points that overestimate shear are generally long spans supported by piles on the lower range of those considered "short". This is because the design procedure bases the shear force on the moment at the head of the pile, which increases proportionately with girder length.

Chapter 6

CONCLUSIONS AND RECOMMENDATIONS

This chapter provides a summary of the work done thus far in order to determine the feasibility of supporting integral abutment bridges on "short" piles. Conclusions drawn from the results of this research, as well as recommendations for areas of further study are also included.

6.1. Summary of Work Performed

The following sections provide a summary of the major components of this thesis. For a more detailed explanation of processes and results, please refer to the appropriate chapter.

6.1.1. Finite Element Model

The use of finite element analysis to study the performance of integral abutment bridges is widespread. Because of the large variety and limitations of modeling techniques, implementation of sophisticated and comprehensive methods of modeling may allow integral abutment bridges to be used in applications where simplified techniques have concluded they cannot. In view of this, a two-dimensional finite element model was created, based on a typical integral abutment bridge, incorporating complex constitutive and surface interaction models. The goal of using these more complex models was to provide a more realistic depiction of the soil/structure interaction, in the hopes of achieving an accurate representation of the structural response.

Material properties for the soil, bedrock, and structural elements were based on test data and theoretical values, and adjusted to more closely resemble the anticipated conditions at bridge sites in Maine. The soil elements incorporated Mohr-Coulomb failure criteria, while the piles were represented using elastic-plastic behavior. Simplified models were used to verify that the materials were behaving in the manner that one would expect for the parameters that were defined for each.

Preliminary models were developed and used to resolve any abnormal model behavior. It was shown that factors such as the out-of-plane thickness of the two-dimensional elements, and varying the depth of the channel beneath the girder had unexpected influence on the behavior of the model. While changes were made to the model in an attempt to mitigate these factors, they could not be eliminated because of the two-dimensional nature of the model. The preliminary models were also used to select critical model responses to be examined closer in the future parametric studies. As a result, refinements were made to the finite element mesh, in order to provide a more accurate numerical solution for the selected model responses.

Using the finite element mesh in its final form, an analysis procedure was written that approximated the construction sequence of an integral abutment bridge. While the general order of the construction stages was considered, the effect of the changing section properties of the girder at various stages of construction, e.g. uncured concrete during placement or creep under sustained dead loading, was neglected. It was determined that the differences in the support conditions of the girder, as well as the degree to which girder behavior influences the critical load conditions, allowed for the effect of the section properties to be ignored in this study.

6.1.2. Parametric Studies

Parametric studies were performed in order to determine the effect of several variables on three major structural responses determined using the preliminary models: pile stresses, pile kinematics, and pile/bedrock interaction. A main parametric study was performed to investigate how changes in girder length, pile length, and subsurface conditions influenced pile response. It was shown that piles on bedrock and less than 4 m in length behave similar to a laterally loaded, fixed-head pile that is pinned at the tip, in that the tip of the pile rotates, but does not translate horizontally or vertically. This is similar, in principle, to a column with a pinned support. Dead and live loading of the girder induces a rotation of the abutments, which causes pile head displacement. This displacement is not typically accounted for in current design procedures.

Changes in the girder length, loading, and subsurface conditions were found to cause the greatest differences in pile head strains. Piles embedded in weaker soils, such as clay, are more likely to experience plastic deformation than those embedded in stronger soils. Piles in a given soil type supporting longer spans can be expected to experience some degree of plastic deformation, while those supporting shorter spans (< 25 m) typically will not.

To validate the assumption of a pinned support at the base of the pile, a ratio of the shear force and the normal force acting at the bedrock/pile interface was compared to a coefficient of friction between these materials. The normal force at this interface is dictated by loading and girder length, while the shear forces depend on subsurface conditions, pile length, and loading.

Smaller parametric studies were performed in order to investigate less significant changes in loading, geometry, and member properties. It was found that the position of the live loading on the superstructure had no adverse effect on the pile behavior, while increasing the live loading was found to increase strains at the head of the pile. The model structure was shown to accommodate cyclic live and thermal loading without major consequence. Changes in geometry and member properties includes models incorporating unequal length piles at either end of the girder, and piles with section properties different from those in the primary study. It was shown that stiffer piles experience smaller strains at the pile head, but larger overall translations and shear forces at the pile tip.

6.1.3. Design Procedure

The current design procedure for piles supporting an integral abutment used by MDOT reduces the pile to an equivalent cantilever based on loading and soil conditions. Therefore, sufficient pile length must be used in order to provide fixed support conditions at some point along the pile length.

A design procedure was developed for situations where the depth to bedrock results in pile lengths less than currently allowed. Pile head moments are calculated from a relationship with the axial load, based on data from the parametric studies. These relationships were created for various soil conditions and loadings. The proposed guidelines do not have an explicit limitation on pile stresses/strains, as the current procedure does. Girder lengths for different pile sections and soil conditions are

implicitly limited by keeping the strain in the pile below a point where plastic strains start to increase under repeated applications of live and thermal loads.

The proposed guidelines idealize the support conditions at the pile tip as a pinned support, i.e. the pile cannot translate horizontally or vertically, but is free to rotate. This is drastically different from the assumption of fixed conditions commonly used for longer piles. Forces at the pile tip are calculated in order to determine if this idealization is valid for the proposed pile/soil/load combinations. The ratio of shear forces and normal forces are compared to the coefficient of friction between the pile and bedrock, along with a factor of safety.

6.2. Conclusions

Based on comparisons of the model behavior to the results of theoretical calculations and simplified models, it was felt that the finite element model in this research provided a reasonable approximation of the behavior of an actual structure. The phenomenon of the changing section properties of the girder at various stages of construction, caused by differences in concrete strength over time, is neglected in the analysis procedure. However, the degree to which girder stiffness influences the critical load conditions allow for the effect of the section properties to be ignored without major consequences.

Piles less than 4 m in length, for the cross-sections studied, behave differently than piles greater than this length. Because the tip of the pile rotates, but does not translate horizontally or vertically, support conditions at the base should be approximated as a pinned support. A ratio of the shear force and the normal force acting at the bedrock

can be compared to the coefficient of friction, as a measure of the validity of this approximation.

The structure was shown to accommodate cyclic live and thermal loading without any major consequences. Under annual temperature cycles, the abutment backfill is shown to deform, illustrating the need for approach slabs behind integral abutments. Under combined cyclic live and thermal loading, plastic strains did not accumulate under progressive cycles, if the strains in the pile head were less than 1.25 ε_y.

It was found that while deflections of the shorter pile were slightly different than for a structure with short piles on either end, there was no significant change in behavior for a bridge with unequal length piles. Stiffer piles experience increased lateral translation in addition to increased shear forces at the tip, due to the smaller relative stiffness of the surrounding soil. Therefore, there are some cases where simply specifying a larger pile section will not improve the performance of the structure.

The current MDOT procedure is sufficient for designing piles for integral abutment bridges. The proposed design procedure is an addendum to the current procedure, intended for use in cases where the depth to bedrock cannot provide fixed conditions along the pile. This design method results in values of moments and shear forces that are somewhat higher than those obtained from the finite element model. Inherent conservatism is built into the methods used to calculate both forces, presenting a worst-case design scenario. While this method certainly expands the application of integral abutments, there are cases where the support provided by the soil and bedrock will still be insufficient, and a pile-supported integral abutment bridge should not be used.

6.3. Recommendations

Based on the results of the finite element modeling and parametric study, it appears that it is indeed feasible to construct integral abutments in some areas with shallow bedrock. However, there are several areas that should be investigated before a final determination is made. The field study and additional finite element modeling proposed in Phase II of this research will deal with many of these issues.

The two-dimensional finite element model used in the parametric study adequately represented the behavior of an integral abutment bridge with no skew. However, a three-dimensional model is recommended in order to capture skew effects, as well as provide a better comparison to data obtained from the instrumented bridge. While the effects of the changing girder properties could not be accounted for in this study directly, it is recommended that modifications be made to dead loads in order to represent the deflections and stresses one would experience with different section properties.

Model data showed that the depth of the channel had an effect on the behavior of the piles that is not generally accounted for in conventional design. The two-dimensional model may not capture this phenomenon faithfully. Field data and results of three-dimensional studies should be used to verify the magnitude of this effect.

Pile behavior in the finite element model indicates that some methods of lateral analysis of piles, in the context of integral abutments, are lacking several important considerations. Rotation, in addition to translation, occurs at the pile head not only under thermal loading, but also under dead and live loading. Furthermore, programs such as COM624P (Wang & Reese, 1993) do not take any interaction between the pile tip and

bedrock, or effect of construction sequence into account. Finally, lateral pile analysis programs cannot model the effect of channel depth on the behavior of the pile. This could be important if the field data reveals that this effect is found to be as significant as shown in this study.

REFERENCES

AASHTO (1996). Standard Specifications for Highway Bridges. Washington, D.C. American Association of State Highway and Transportation Officials. 16th Edition.

Abendroth, R.E. and Greimann, L.F. (1988). Rational design approach for integral abutment piles. Transportation Research Record #1233. pp. 12-23.

Abendroth, R.E.; Greimann, L.F.; and Ebner, P.B. (1989). Abutment pile design for jointless bridges. Journal of Structural Engineering. Vol.115, No. 11. pp. 2914-2929.

AISC (1980). Manual of Steel Construction. Chicago, IL. American Institute of Steel Construction. 8th Edition.

Alberta Transportation (2003). Appendix C – Guidelines for Design of Integral Abutments. Alberta Transportation Bridge Design Manual.

ALGOR (1994). Reference Manual. Algor, Inc. Pittsburgh, PA.

Amde, A.M.; Chini, S.A.; and Mafi, M. (1997). Model study of H-piles subjected to combined loading. Geotechnical and Geological Engineering. Vol. 15. pp. 343-355.

Amos, J.A. (1987). The Geotechnical Characteristics of the Presumpscot Clay at Two Maine Landslide Sites. M.S. Thesis. Orono, ME. University of Maine.

Andrews, D.W. (1987). The engineering aspects of the Presumpscot formation. Geologic and Geotechnical Characteristics of the Presumpscot Formation Maine's Glaciomarine "Clay". D.W. Andrews, W.B. Thompson, T.C. Sandford, and I.D. Novak, eds. Orono, ME. University of Maine.

ANSYS (1987). Engineering Analysis System User's Manual. Swanson Analysis Systems, Inc. Houston, PA.

Army Corps of Engineers (1990). Engineering and Design – Settlement Analysis. United States Army Corps of Engineers publication No. EM1110-1-1904.

Army Corps of Engineers (1992). Engineering and Design – Bearing Capacity of Soils. United States Army Corps of Engineers publication No. EM1110-1-1905.

Arsoy, S.; Barker, R.M.; and Duncan, J.M. (1999). The behavior of integral abutment bridges. Virginia Transportation Research Council, Final Contract Report No. VTRC 00-CR3.

Arsoy, S.; Duncan, J.M.; and Barker, R.M. (2002). Performance of piles supporting integral bridges. Transportation Research Record #1808. pp. 162-167.

Bell, F.G. (1992). Engineering Properties of Soils and Rocks. Oxford, U.K. Butterworth-Heinemann Ltd. 3rd Edition.

Bentler, D.J.; Morrison, C.S.; Esterhuizen, J.J.B.; and Duncan, J.M. (1999). SAGE User's Guide. Center for Geotechnical Practice and Research, The Charles Via, Jr. Department of Civil Engineering, Virginia Tech.

Bishop, A.W. and Hight, D.W. (1977). The value of Poisson's ratio in saturated soils and rocks stressed under undrained conditions. Geotechnique. Vol. 27, No. 3, pp. 369–384.

Broms, B.B. (1964a). Lateral resistance of piles in cohesive soils. Journal for Soil Mechanics and Foundation Engineering. Vol. 90, SM2. pp. 27-63.

Broms, B.B. (1964b). Lateral resistance of piles in cohesionless soils. Journal for Soil Mechanics and Foundation Engineering. Vol. 90, SM3. pp. 123-156.

Burke, M.P. Jr. (1993). Integral bridges: attributes and limitations. Transportation Research Record #1393. pp. 1-8.

Chen, L. and Poulos, H.G. (1993). Analysis of pile-soil interaction under lateral loading using infinite and finite element analysis. Computers and Geotechnics. Vol. 15. pp. 189-220.

Cornforth, D.H. (1964). Some experiments on the influence of strain conditions on the strength of sand. Geotechnique. Vol. 14, No. 2. pp. 143–167.

Das, B.M. (1983). Advanced Soil Mechanics. New York, NY. McGraw-Hill Book Company.

Devin, S.C. (1990). Flowslide Potential of Natural Slopes in the Presumpscot Formation. M.S. Thesis. Orono, ME. University of Maine.

Diceli, M. (2000). Simplified model for computer-aided analysis of integral bridges. Journal of Bridge Engineering. Vol. 5, No. 3. pp. 240-248.

Diceli, M.; Eng, P.; and Albhaisi, S.M. (2003). Maximum length of integral bridges supported on steel H-piles driven in sand. Engineering Structures. Vol. 25. pp. 1491-1504.

Duncan, J.M. and Arsoy, S. (2003). Effect of bridge-soil interaction on behavior of piles supporting integral bridges. Transportation Research Record #1849. pp. 91-97.

Duncan, J.M. and Buchignani, A.L. (1976). An Engineering Manual for Slope Stability Studies. Department of Civil Engineering, University of California, Berkeley. 94 pp.

Duncan, J.M.; Byrne, P.; Wong, K.S.; and Mabry, P. (1980). Strength, stress-strain and bulk modulus parameters for finite element analyses of stresses and movements in soil masses. University of California, College of Engineering Report No. UCB/GT/80-01.

Berkeley, CA.

Ensoft, Inc. (2002). Computer program L-PILE Plus, Version 4.0M.

Faraji, S.; Ting, J.M; Crovo, D.S.; and Ernst, H. (2001). Nonlinear analysis of integral bridges: finite element model. Journal of Geotechnical and Geoenvironmental Engineering. Vol. 127, No. 5. pp. 454-461.

Fleming, W.G.K.; Weltman, A.J.; Randolph, M.F.; and Elson, W.K. (1992). Piling Engineering. London, U.K. 2nd Edition.

GangaRao, H.; Thippeswamy, H.; Dickson, B.; and Franco, J. (1996). Survey and design of integral abutment bridges. FHWA Workshop on Integral abutment Bridges, November 13-15, 1996. Pittsburgh, PA. pp. 129.

Gere, J.M. and Timoshenko, S.P. (1997). Mechanics of Materials. Boston, MA. PWS Publishing Co. 4th Edition.

Girton, D.D.; Hawkinson, T.R.; and Greimann, L.F. (1991). Validation of design recommendations for integral-abutment piles. Journal of Structural Engineering. Vol.117, No. 7. pp. 2117-2134.

Goodman, R.E. (1989). Introduction to Rock Mechanics. New York, NY. John Wiley & Sons, Inc. 2nd Edition.

Greimann, L.F.; Yang, P.; and Wolde-Tinsae, A.M. (1986). Nonlinear analysis of integral abutment bridges. Journal of Structural Engineering. Vol. 112, No. 10. pp. 2263-2280.

Greimann, L.F.; Abendroth, R.E.; Johnson, D.E.; and Ebner, P.B. (1987). Final report: Pile design and tests for integral abutment bridges. College of Engineering, Iowa State University.

Greimann, L. and Wolde-Tinsae, A.M. (1988). Design model for piles in jointless bridges. Journal of Structural Engineering. Vol. 114, No. 6. pp. 1355-1369.

GTSTRUDL (1991). GTSTRUDL User's Manual, Vol. 1, Rev. M. GTICES Sys. Lab., Georgia Institute of Technology, Atlanta.

Haberfield, C.M., and Johnston, I.W. (1994). A mechanistically-based model for rough rock joints. International Journal of Rock Mechanics, Mining Sciences, and Geomechanics Abstracts. Vol. 31, No. 4. pp. 279-292.

Head, K.H. (1986). Manual of Soil Laboratory Testing – Volume 3: Effective Stress Tests. New York, NY. John Wiley & Sons, Inc.

Highways Agency (1996). The design of integral bridges. Design Manual for Roads and Bridges. The Highways Agency. London, U.K. Vol. 1, Section 3, Part 12. BA 42/96, Amendment #1.

HKS, Inc. (2001). ABAQUS/Standard Version 6.2 User's Manual. Pawtucket, RI. Hibbitt, Karlsson & Sorensen, Inc. Volumes 1-3.

Holtz, R.D. and Kovacs, W.D. (1981). An Introduction to Geotechnical Engineering. Englewood Cliffs, NJ. Prentice-Hall, Inc.

Husain, I. and Bagnariol, D. (1996). Integral abutment bridges. Ministry of Transportation, Ontario, Canada. Structural Office Report No. SO-96-01.

Husain, I. and Bagnariol, D. (2000). Design and performance of jointless bridges in Ontario. Transportation Research Record #1696. pp. 109-121.

Ingram, E.E.; Burdette, E.G.; Goodpasture, D.W.; and Deatherage, J.H. (2003). Evaluation of applicability of typical column design equations to steel H-piles supporting integral abutments. AISC Engineering Journal. Q1, pp. 50-58.

Janbu, N. (1963). Soil compressibility as determined by oedometer and triaxial tests. European Conference on Soil Mechanics and Foundation Engineering, Wissbaden, Germany, Vol. 1, pp. 244-248.

Jorgenson, J.L. (1983). Behavior of abutment piles in an integral abutment in response to bridge movements. Transportation Research Record #903. pp. 72-79.

Krusinski, L. (2002). Project Research Progress Report: Design and Construction of Pile-Supported Integral Abutments at Bridge Sites with Shallow Bedrock. University of Maine, Department of Civil and Environmental Engineering. Unpublished, Volumes 1-3.

Kunin, J. and Alampalli, S. (2000). Integral abutment bridges: current practice in United States and Canada. Journal of Performance of Constructed Facilities. Vol. 14, No. 3. pp. 104-120.

Lama, R.D. and Vutukuri, V.S. (1978). Handbook on Mechanical Properties of Rocks – Testing Techniques and Results. Aedermannsdorf, Switzerland. Volumes 2 & 4.

Lambe, T.W. and Whitman, R.V. (1969). Soil Mechanics. New York, NY. John Wiley & Sons, Inc.

Lehane, B.M.; Keogh, D.M.; and O'Brien, E.J. (1999). Simplified elastic model for restraining effects of backfill soil on integral bridges. Computers and Structures. Vol. 73. pp. 303-313.

Linell, K.A. and Shea, H.F. (1961). Strength and deformation characteristics of various glacial tills in New England. Research Conference on Shear Strength of Cohesive Soils. American Society of Civil Engineers. pp. 275-314.

Lock, R.J. (2002). Integral bridge abutments. University of Cambridge Department of Engineering Technical Report CUED/D-SOILS/TR320. Cambridge, U.K.

Logan, D.L. (1993). A First Course in the Finite Element Method. Boston, MA. PWS Publishing Co.

Marsal, R.J., (1973). Mechanical properties of rockfill. Embankment Dam Engineering, Casagrande Memorial Volume. Hirschfield & Poulos, eds. New York, NY. John Wiley & Sons, Inc.

MDOT (1999). Bridge Design Guide. Augusta, ME. Maine Department of Transportation – Bridge Program.

Mistry, V.C. (2000). Integral abutment and jointless bridges. Retrieved October 1, 2002, from http://www.nabro.unl.edu/articles/20002012/download/vasant.pdf

Mitchell, J.K. (1993). Fundamentals of Soil Behavior. New York, NY. John Wiley & Sons, Inc. 2nd Edition.

Moulton, L.K.; GangaRao, H.V.S.; and Halvorsen, G.T. (1985). Tolerable movement criteria for highway bridges. Report FHWA/RD-85/107. FHWA Research Development Technology, McLean VA. pp. 1-109.

Mourad, S. and Tabsh, S.W. (1998). Pile forces in integral abutment bridges subjected to truck loads. Transportation Research Record #1633. pp. 77-83.

NAVFAC (1986). Design Manual 7.02 - Foundations and Earth Structures. United States Naval Facilities Engineering Command publication No. 0525-LP-300-7071.

Naylor, D.J. and Pande, G.N. (1981). Finite Elements in Geotechnical Engineering. Swansea, U.K. Pineridge Press.

Patton, F.D. (1966a). Multiple modes of shear failure in rock. Proceedings of the First International Conference of Rock Mechanics. Lisbon, Portugal. Volume 1. pp. 509-514.

Patton, F.D. (1966b). Multiple Modes of Shear failure in Rock and Related Materials. PhD. Thesis. University of Illinois.

Prakash, S. and Sharma, H.D. (1990). Pile Foundations in Engineering Practice. New York, NY. John Wiley & Sons, Inc.

Potts, D.M. and Zdravković, L. (1999). Finite Element Analysis in Geotechnical Engineering – Theory. London, U.K. Thomas Telford Ltd.

Potts, D.M. and Zdravković, L. (2001). Finite Element Analysis in Geotechnical Engineering – Application. London, U.K. Thomas Telford Ltd.

Poulos, H.G. and Davis, E.H. (1980). Pile Foundation Analysis and Design. New York, NY. John Wiley & Sons, Inc.

Rahim, A. (1998). The significance of non-associated plasticity – Part I. CRISP News. Issue #6, November 1998. Retrieved November 26, 2003 from http://www.crispconsortium.com/scnews/nov-98.pdf

Sandford, T.C. (1997). Freezing pressures in 'frost-free' materials caused by cyclic water levels. Proceedings of the Fourteenth International Conference on Soil Mechanics and Foundation Engineering. Hamburg, Germany. 6-12 September 1997. pp. 887-890.

SAP2000 (1998). Integrated finite element analysis and design of structures. Computers and Structures, Inc. Berkeley, CA.

Seidel, J.P. and Haberfield, C.M. (2002). Laboratory testing of concrete-rock joints in constant normal stiffness direct shear. Geotechnical Testing Journal. Vol. 25, No. 4. pp. 391-404.

Soltani, A.A. and Kukreti, A.R (1992). Performance evaluation of integral abutment bridges. Transportation Research Record #1371. pp. 17-25.

Taylor, H.P.J. (1999). Progress with integral bridges in the United Kingdom. Preprint CD-ROM, TRB 1999 Annual Meeting, January 11-14, Washington D.C.

Terzaghi, K.; Peck, R.B.; and Mesri, G. (1996). Soil Mechanics in Engineering Practice. New York, NY. John Wiley & Sons, Inc. 3rd Edition.

Thippeswamy, H.K.; Raju, P.R.; and GangaRao, H.V.S. (1994). Parametric study of single-span jointless steel bridges. Transportation Research Record #1460. pp. 25-36.

Thompson, W.B. (1987). The Presumpscot formation in Southwestern Maine. Geologic and Geotechnical Characteristics of the Presumpscot Formation Maine's Glaciomarine "Clay". D.W. Andrews, W.B. Thompson, T.C. Sandford, and I.D. Novak. eds. Orono, ME. University of Maine.

Wang, S.T. and Reese, L.C. (1993). COM624P – Laterally Loaded Pile Analysis Program for the Microcomputer, Version 2.0. Washington, D.C. United States Department of Transportation, Federal Highway Administration.

Wasserman, E.P. and Walker, J.H. (1996). Integral abutments for steel bridges. Highway Structures Design Handbook. Structures Division, Tennessee Department of Transportation. Vol. 2, Chapter 5.

APPENDICES

Appendix A

EXAMPLE ABAQUS INPUT FILE

This appendix provides a sample ABAQUS model input file used in the parametric study. Annotations have been added for clarification, and are preceded by multiple asterisks. ABAQUS commands and keywords are in all caps, and are preceded by a single asterisk. Required data lines for the various commands and keywords are preceded by a blank space.

For further information about ABAQUS commands or required data, please refer to the ABABQUS/Standard Version 6.2 User's Manual (HKS, 2001).

```
*HEADING
 25m span, 4m piles, Native soil: Sand & Gravel, OUTPUT: DL&+T, DL&LL&+T
**
** This model is an IAB with a 25m clear span and 4m long piles, The loading is a
** temperature increase of 20°C and an HL-93 truck placed for maximum bending
** moment in the girder.
**
** The native soil is granular glacial outwash (sand & gravel) modeled using Mohr-
** Coulomb plasticity.
**
** Dead & +T Output: Step 6, Dead/Live/+T Output: Step 8
**
**
*PREPRINT, ECHO=YES, MODEL=YES, HISTORY=YES, CONTACT=YES
** These commands provide information in the *.dat file useful for debugging
**
***------------------------------NODE & ELEMENT INPUT--------------------------------
**
** Nodal coordinates are read from comma delimited text files
*NODE, NSET=WSOIL,
INPUT=F:\TEMP\CURRENT\v3\MESH\25m_S\4m_P\ND_WSOIL_25_4.inp
*NODE, NSET=INSOIL,
INPUT=F:\TEMP\CURRENT\v3\MESH\25m_S\4m_P\ND_ISOIL_25_4.inp
*NODE, NSET=ESOIL,
INPUT=F:\TEMP\CURRENT\v3\MESH\25m_S\4m_P\ND_ESOIL_25_4.inp
*NODE, NSET=PILES,
INPUT=F:\TEMP\CURRENT\v3\MESH\25m_S\4m_P\ND_PILE_25_4.inp
*NODE, NSET=ABUTS,
INPUT=F:\TEMP\CURRENT\v3\MESH\25m_S\4m_P\ND_ABUT_25_4.inp
*NODE, NSET=ROCK,
INPUT=F:\TEMP\CURRENT\v3\MESH\25m_S\4m_P\ND_ROCK_25_4.inp
*NODE, NSET=GIRDER,
INPUT=F:\TEMP\CURRENT\v3\MESH\25m_S\4m_P\ND_GIRD_25_4.inp
**
** Element definitions are read from comma delimited text files.  The TYPE command
** specifies 6 noded or 8 noded plane stress/strain elements, or 5 noded infinite elements.
**
*ELEMENT, TYPE=CINPE5R, ELSET=WSOIL,
INPUT=F:\TEMP\CURRENT\v3\MESH\25m_S\4m_P\EL5_WSOIL_25_4.inp
*ELEMENT, TYPE=CPE8, ELSET=WSOIL,
INPUT=F:\TEMP\CURRENT\v3\MESH\25m_S\4m_P\EL8_WSOIL_25_4.inp
*ELEMENT, TYPE=CPE6, ELSET=WSOIL,
INPUT=F:\TEMP\CURRENT\v3\MESH\25m_S\4m_P\EL6_WSOIL_25_4.inp
*ELEMENT, TYPE=CPE8, ELSET=INSOIL,
INPUT=F:\TEMP\CURRENT\v3\MESH\25m_S\4m_P\EL8_ISOIL_25_4.inp
```

```
*ELEMENT, TYPE=CPE6, ELSET=INSOIL,
INPUT=F:\TEMP\CURRENT\v3\MESH\25m_S\4m_P\EL6_ISOIL_25_4.inp
*ELEMENT, TYPE=CINPE5R, ELSET=ESOIL,
INPUT=F:\TEMP\CURRENT\v3\MESH\25m_S\4m_P\EL5_ESOIL_25_4.inp
*ELEMENT, TYPE=CPE8, ELSET=ESOIL,
INPUT=F:\TEMP\CURRENT\v3\MESH\25m_S\4m_P\EL8_ESOIL_25_4.inp
*ELEMENT, TYPE=CPE6, ELSET=ESOIL,
INPUT=F:\TEMP\CURRENT\v3\MESH\25m_S\4m_P\EL6_ESOIL_25_4.inp
*ELEMENT, TYPE=CPS8, ELSET=PILE,
INPUT=F:\TEMP\CURRENT\v3\MESH\25m_S\4m_P\EL8_PILE_25_4.inp
*ELEMENT, TYPE=CPS6, ELSET=PILE,
INPUT=F:\TEMP\CURRENT\v3\MESH\25m_S\4m_P\EL6_PILE_25_4.inp
*ELEMENT, TYPE=CPS8, ELSET=ABUTMENT,
INPUT=F:\TEMP\CURRENT\v3\MESH\25m_S\4m_P\EL8_ABUT_25_4.inp
*ELEMENT, TYPE=CPS6, ELSET=ABUTMENT,
INPUT=F:\TEMP\CURRENT\v3\MESH\25m_S\4m_P\EL6_ABUT_25_4.inp
*ELEMENT, TYPE=CINPE5R, ELSET=BEDROCK,
INPUT=F:\TEMP\CURRENT\v3\MESH\25m_S\4m_P\EL5_ROCK_25_4.inp
*ELEMENT, TYPE=CPE8, ELSET=BEDROCK,
INPUT=F:\TEMP\CURRENT\v3\MESH\25m_S\4m_P\EL8_ROCK_25_4.inp
*ELEMENT, TYPE=CPE6, ELSET=BEDROCK,
INPUT=F:\TEMP\CURRENT\v3\MESH\25m_S\4m_P\EL6_ROCK_25_4.inp
*ELEMENT, TYPE=CPS8, ELSET=GIRDER,
INPUT=F:\TEMP\CURRENT\v3\MESH\25m_S\4m_P\EL8_GIRD_25_4.inp
*ELEMENT, TYPE=CPS6, ELSET=GIRDER,
INPUT=F:\TEMP\CURRENT\v3\MESH\25m_S\4m_P\EL6_GIRD_25_4.inp
**
**----------------------------------NODE SET GENERATION----------------------------------
**
** Sets of nodes are defined in order to apply boundary conditions or loads, or to obtain
** model output data, such as deflections.  The names of the node sets describe their
** locations.
*NSET, GENERATE, NSET=LEFT
 1, 5201, 400
 20500, 21300, 400
*NSET, GENERATE, NSET=BASE
 20000, 20094, 1
*NSET, GENERATE, NSET=RIGHT
 79, 5279, 400
 20570, 21370, 400
*NSET, NSET=CORNERS
 20000, 20094
*NSET, GENERATE, NSET=WSOILFACE
 5912, 12712, 100
 5360, 7660, 100
 8056, 9456, 100
```

```
 14310, 15710, 100
*NSET, NSET=WFACE_ANGLE
 7759, 7858, 7957
*NSET, GENERATE, NSET=W_APPROACH
 15701, 15710, 1
*NSET, GENERATE, NSET=INSOILFACES
 5913, 12713, 100
 5361, 7661, 100
 7663, 9063, 100
 5936, 12736, 100
 5384, 7684, 100
 7682, 9082, 100
*NSET, NSET=INSOILFACES
 7662, 7683
*NSET, GENERATE, NSET=ESOILFACE
 5937, 12737, 100
 5385, 7685, 100
 8089, 9489, 100
 14339, 15739, 100
*NSET, NSET=EFACE_ANGLE
 7786, 7887, 7988
*NSET, GENERATE, NSET=E_APPROACH
 15739, 15748, 1
*NSET, NSET=SOILFACES
 WSOILFACE, INSOILFACES, ESOILFACE
*NSET, NSET=APPROACHES
 W_APPROACH, E_APPROACH
*NSET, GENERATE, NSET=PILEBASES
 80, 97, 1
*NSET, GENERATE, NSET=PILETOPS
 13580, 13597, 1
*NSET, GENERATE, NSET=PILE_CL
 84, 5284, 100
 9684, 13584, 100
 93, 5293, 100
 9693, 13593, 100
*NSET, GENERATE, NSET=ABUTBASES
 13654, 13662, 1
 13667, 13675, 1
*NSET, GENERATE, NSET=ABUTTOPS
 16850, 16858, 1
 16865, 16875, 1
*NSET, GENERATE, NSET=ABUTFACES
 15164, 15264, 100
 15358, 16858, 100
 15165, 15265, 100
```

```
 15365, 16865, 100
*NSET, GENERATE, NSET=BACKWALLS
 14050, 16850, 100
 14079, 15279, 100
 15375, 16875, 100
*NSET, GENERATE, NSET=GIRDER_TOP
 17801, 17853
**
**----------------------------------ELEMENT SET GENERATION-----------------------------
**
** Sets of elements are created in order to apply certain material properties to elements,
** define contact surfaces,  or to obtain model output data, such as strains.  The names of
** the sets describe their locations and material.
**
****MATERIAL PROPERTY SETS (Used with *SOLID SECTION command)
**
*ELSET, GENERATE, ELSET=WNATIVE_ELASTIC
 1, 10, 1
 14, 23, 1
 27, 36, 1
 40, 49, 1
 53, 82, 1
 92, 111, 1
 118, 177, 1
 196, 235, 1
*ELSET, GENERATE, ELSET=WNATIVE_MC
 248, 286, 1
 294, 329, 1
 337, 370, 1
 1471, 1490, 1
 1506, 1510, 1
 1532, 1540, 1
*ELSET, GENERATE, ELSET=INNATIVE_ELASTIC
 480, 991, 1
*ELSET, GENERATE, ELSET=INNATIVE_MC
 371, 479, 1
 992, 1100, 1
 1546, 1571, 1
 1574, 1578, 1
 1581, 1608, 1
 1611, 1619, 1
*ELSET, GENERATE, ELSET=ENATIVE_ELASTIC
 1224, 1263, 1
 1276, 1335, 1
 1354, 1373, 1
 1380, 1409, 1
```

1419, 1428, 1
1432, 1441, 1
1445, 1454, 1
1458, 1467, 1
*ELSET, GENERATE, ELSET=ENATIVE_MC
1101, 1170, 1
1178, 1216, 1
1622, 1647, 1
1653, 1657, 1
1679, 1681, 1
*ELSET, GENERATE, ELSET=WFILL_ELASTIC
1543, 1545, 1
*ELSET, GENERATE, ELSET=WFILL_MC
11, 13, 1
24, 26, 1
37, 39, 1
50, 52, 1
83, 91, 1
112, 117, 1
178, 195, 1
236, 247, 1
287, 293, 1
330, 336, 1
1491, 1505, 1
1511, 1531, 1
1541, 1542, 1
*ELSET, GENERATE, ELSET=INFILL_MC
1572, 1573, 1
1579, 1580, 1
1609, 1610, 1
1620, 1621, 1
1800, 1879, 1
*ELSET, GENERATE, ELSET=EFILL_ELASTIC
1650, 1652, 1
*ELSET, GENERATE, ELSET=EFILL_MC
1264, 1275, 1
1336, 1353, 1
1374, 1379, 1
1410, 1418, 1
1429, 1431, 1
1442, 1444, 1
1455, 1457, 1
1468, 1470, 1
1171, 1177, 1
1217, 1223, 1
1648, 1649, 1

```
 1658, 1678, 1
 1682, 1696, 1
*ELSET, GENERATE, ELSET=ROCK_ELASTIC
 4000, 4144, 1
 4200, 4244, 1
*ELSET, GENERATE, ELSET=ROCK_MC
 4300, 4643, 1
**
****SURFACE SETS (Used with *SURFACE command)
**
*ELSET, GENERATE, ELSET=WESTSOIL_PILE
 362, 370, 1
 1478, 1486, 2
 1534, 1542, 2
*ELSET, ELSET=WESTSOIL_PILE
 1487, 1533, 337
*ELSET, GENERATE, ELSET=WESTSOIL_ABUT
 330, 336, 1
 1518, 1528, 2
*ELSET, ELSET=WESTSOIL_ABUT
 1531
*ELSET, ELSET=WSOIL_ONROCK
 14, 27, 40, 53, 54, 92, 118,
 119, 196, 248, 1472, 1477, 1478
*ELSET, ELSET=WSOIL_SURF
 26, 39, 52, 91, 117, 193, 195, 247, 293, 336
*ELSET, GENERATE, ELSET=INSOIL_WPILE
 396, 404, 1
 1546, 1554, 2
 1564, 1572, 2
*ELSET, ELSET=INSOIL_WPILE
 1555, 1563, 371
*ELSET, GENERATE, ELSET=INSOIL_WABUT
 1800, 1806, 1
*ELSET, GENERATE, ELSET=INSOIL_EPILE
 1092, 1100, 1
 1591, 1599, 2
 1613, 1621, 2
*ELSET, ELSET=INSOIL_EPILE
 1600, 1612, 1067
*ELSET, GENERATE, ELSET=INSOIL_EABUT
 1873, 1879, 1
*ELSET, ELSET=INSOIL_ONROCK
 1546, 1547, 1557, 441, 480, 520, 522, 580, 581, 619, 621, 648,
 659, 670, 681, 691, 701, 761, 771, 781, 791, 802, 813, 824, 825,
 853, 854, 892, 893, 952, 992, 1585, 1590, 1591
```

```
*ELSET, GENERATE, ELSET=EASTSOIL_PILE
 1126, 1134, 1
 1622, 1630, 2
 1640, 1648, 2
*ELSET, ELSET=EASTSOIL_PILE
 1631, 1639, 1101
*ELSET, GENERATE, ELSET=EASTSOIL_ABUT
 1664, 1676, 2
 1171, 1177, 1
*ELSET, ELSET=ESOIL_ONROCK
 1622, 1623, 1633, 1178, 1224, 1276,
 1278, 1354, 1380, 1382, 1419, 1432, 1445
*ELSET, ELSET=ESOIL_SURF
 1177, 1223, 1275, 1352, 1353, 1379, 1417, 1431, 1444, 1457
*ELSET, ELSET=SOIL_UP
 24, 37, 50, 83, 84, 112, 178, 179, 236, 1491, 1492, 1513,
 1514, 1543, 1544, 1650, 1651, 1660, 1661, 1682, 1684, 1264, 1336,
 1338, 1374, 1410, 1412, 1429, 1442, 1455
**
*ELSET, GENERATE, ELSET=WPILE_LEFT
 2076, 2092, 2
 2000, 2016, 4
 2100, 2116, 4
*ELSET, ELSET=WPILE_LEFT
 2026
*ELSET, GENERATE, ELSET=WPILE_RIGHT
 2077, 2093, 2
 2003, 2019, 4
 2103, 2119, 4
*ELSET, ELSET=WPILE_RIGHT
 2027
*ELSET, GENERATE, ELSET=EPILE_LEFT
 2196, 2212, 2
 2120, 2136, 4
 2220, 2236, 4
*ELSET, ELSET=EPILE_LEFT
 2146
*ELSET, GENERATE, ELSET=EPILE_RIGHT
 2197, 2213, 2
 2123, 2139, 4
 2223, 2239, 4
*ELSET, ELSET=EPILE_RIGHT
 2147
*ELSET, GENERATE, ELSET=WPILE_TOP
 2116, 2119, 1
*ELSET, GENERATE, ELSET=WPILE_TIP
```

```
 2000, 2003, 1
*ELSET, GENERATE, ELSET=EPILE_TOP
 2236, 2239, 1
*ELSET, GENERATE, ELSET=EPILE_TIP
 2120, 2123, 1
**
*ELSET, GENERATE, ELSET=WABUT_LEFT
 3013, 3048, 7
 3058, 3062, 4
 3066, 3076, 2
*ELSET, GENERATE, ELSET=WABUT_RIGHT
 3005, 3047, 7
*ELSET, GENERATE, ELSET=WABUT_BASE
 3001, 3004, 1
*ELSET, GENERATE, ELSET=EABUT_LEFT
 3092, 3134, 7
*ELSET, GENERATE, ELSET=EABUT_RIGHT
 3112, 3140, 7
 3150, 3158, 4
 3174, 3184, 2
*ELSET, GENERATE, ELSET=EABUT_BASE
 3093, 3096, 1
**
*ELSET, GENERATE, ELSET=TOP_GIRDER
 5016, 5028, 2
 5046, 5056, 2
*ELSET, ELSET=TOP_GIRDER
 5006, 5007, 5069, 5070
**
*ELSET, ELSET=WROCK_SURF
 4002, 4005, 4008, 4015, 4017, 4311, 4361,
 4362, 4363, 4364, 4529, 4576, 4577, 4578
*ELSET, GENERATE, ELSET=WPILE_ROCK
 4578, 4581, 1
**
*ELSET, ELSET=INTROCK_SURF
 4581, 4582, 4583, 4550, 4399, 4400, 4401, 4402, 4410, 4037, 4045,
 4046, 4049, 4052, 4055, 4058, 4061, 4064, 4082, 4085, 4088, 4091,
 4094, 4097, 4104, 4106, 4112, 4423, 4473, 4474, 4475, 4476, 4589,
 4636, 4637, 4638
**
*ELSET, GENERATE, ELSET=EPILE_ROCK
 4638, 4641, 1
*ELSET, ELSET=EROCK_SURF
 4641, 4642, 4643, 4610, 4511, 4512, 4513,
 4514, 4522, 4134, 4135, 4138, 4141, 4144
```

```
**
**----------------------------------SURFACE DEFINITIONS----------------------------------
**
** Element-based surfaces are created using the element sets defined above, to be used
** with the *CONTACT PAIR command.
**
*SURFACE, NAME=WSOIL_BOT
 WSOIL_ONROCK, S1
*SURFACE, NAME=WSOIL_TOP
 WSOIL_SURF, S3
*SURFACE, NAME=WSOIL_PILE
 WESTSOIL_PILE, S2
*SURFACE, NAME=WSOIL_ABUT
 WESTSOIL_ABUT, S2
 1544, S2
 1545, S2
**
*SURFACE, NAME=INSOIL_BOT
 INSOIL_ONROCK, S1
*SURFACE, NAME=INSOIL_W_PILE
 INSOIL_WPILE, S4
 1572, S3
*SURFACE, NAME=INSOIL_W_ABUT
 INSOIL_WABUT, S4
*SURFACE, NAME=INSOIL_E_PILE
 INSOIL_EPILE, S2
 1621, S3
*SURFACE, NAME=INSOIL_E_ABUT
 INSOIL_EABUT, S2
*SURFACE, NAME=INSOIL_WTOP
 1572, S3
 1572, S4
*SURFACE, NAME=INSOIL_ETOP
 1621, S2
 1621, S3
**
*SURFACE, NAME=ESOIL_BOT
 ESOIL_ONROCK, S1
*SURFACE, NAME=ESOIL_TOP
 ESOIL_SURF, S3
*SURFACE, NAME=ESOIL_PILE
 EASTSOIL_PILE, S4
*SURFACE, NAME=ESOIL_ABUT
 EASTSOIL_ABUT, S4
 1650, S3
 1652, S3
```

```
**
*SURFACE, NAME=SOIL_REACTION
 SOIL_UP, S1
**
*SURFACE, NAME=WROCK_TOP
 WROCK_SURF, S3
*SURFACE, NAME=WPILEROCK
 WPILE_ROCK, S3
*SURFACE, NAME=INROCK_TOP
 INTROCK_SURF, S3
*SURFACE, NAME=EPILEROCK
 EPILE_ROCK, S3
*SURFACE, NAME=EROCK_TOP
 EROCK_SURF, S3
**
*SURFACE, NAME=WPILE_LH
 WPILE_LEFT, S4
 2020, S3
 2094, S3
*SURFACE, NAME=WPILE_RH
 WPILE_RIGHT, S2
 2099, S2
 2025, S2
*SURFACE, NAME=EPILE_LH
 EPILE_LEFT, S4
 2214, S3
 2140, S3
*SURFACE, NAME=EPILE_RH
 EPILE_RIGHT, S2
 2219, S2
 2145, S2
*SURFACE, NAME=WPILE_BASE
 WPILE_TIP, S1
*SURFACE, NAME=WPILE_ABUT
 WPILE_TOP, S3
*SURFACE, NAME=EPILE_BASE
 EPILE_TIP, S1
*SURFACE, NAME=EPILE_ABUT
 EPILE_TOP, S3
**
*SURFACE, NAME=WABUT_LH
 WABUT_LEFT, S4
 3000, S1
 3006, S1
*SURFACE, NAME=WABUT_RH
 WABUT_RIGHT, S2
```

```
 3057, S2
*SURFACE, NAME=WABUT_PILE
 WABUT_BASE, S1
*SURFACE, NAME=WABUT_TIP
 3005, S1
*SURFACE, NAME=EABUT_LH
 EABUT_LEFT, S4
 3141, S3
*SURFACE, NAME=EABUT_RH
 EABUT_RIGHT, S2
 3097, S1
 3105, S1
*SURFACE, NAME=EABUT_PILE
 EABUT_BASE, S1
*SURFACE, NAME=EABUT_TIP
 3092, S1
**
*SURFACE, NAME=TOPGIRDER
 TOP_GIRDER, S3
 5014, S2
 5062, S3
**
**----------------------------------------CONTACT PAIRS----------------------------------------
**
** The *SURFACE INTERACTION command specifies the z-dimension of the contact
** between two elements.  The coefficient of friction between the two surfaces is defined
** using the *FRICTION command
**
*SURFACE INTERACTION, NAME=SOIL_ROCK
 2.7
*FRICTION
 0.5
**
*SURFACE INTERACTION, NAME=SOIL_PILE
 0.346
*FRICTION
 0.0
**
*SURFACE INTERACTION, NAME=SOIL_ABUT
 2.7
*FRICTION
 0.0
** The coefficients of friction between soil/abutments and soil/piles are set to zero
** initially, to prevent excessive downdrag forces that occur during the construction steps
** (1 & 2)
**
```

```
*SURFACE INTERACTION, NAME=PILE_ROCK
 0.346
*FRICTION
 0.7
**
*SURFACE INTERACTION, NAME=PILE_ABUT
 0.346
*FRICTION, ROUGH
** The rough parameter results in no tangential motion between surfaces, or a coefficient
** of friction equal to 1.0
**
** The *CONTACT PAIR command groups the surfaces defined earlier, and assigns a
** surface interaction
**
*CONTACT PAIR, INTERACTION=PILE_ABUT, ADJUST=1.78E-15, TIED
 WABUT_PILE, WPILE_ABUT
*CONTACT PAIR, INTERACTION=PILE_ABUT, ADJUST=1.78E-15, TIED
 EABUT_PILE, EPILE_ABUT
** The TIED parameter keeps the surfaces of two element sets from separating, and
** allows them to carry tension.  The ADJUST parameter corrects initial overlapping or
** separation of the surfaces
**
*CONTACT PAIR, INTERACTION=SOIL_ROCK, ADJUST=0.0
 WSOIL_BOT, WROCK_TOP
*CONTACT PAIR, INTERACTION=SOIL_ROCK, ADJUST=0.0
 INSOIL_BOT, INROCK_TOP
*CONTACT PAIR, INTERACTION=SOIL_ROCK, ADJUST=0.0
 ESOIL_BOT, EROCK_TOP
**
*CONTACT PAIR, INTERACTION=SOIL_PILE, ADJUST=1.78E-15
 WSOIL_PILE, WPILE_LH
*CONTACT PAIR, INTERACTION=SOIL_PILE, ADJUST=0.0
 INSOIL_W_PILE, WPILE_RH
*CONTACT PAIR, INTERACTION=SOIL_PILE, ADJUST=0.0
 INSOIL_E_PILE, EPILE_LH
*CONTACT PAIR, INTERACTION=SOIL_PILE, ADJUST=7.11E-15
 ESOIL_PILE, EPILE_RH
**
*CONTACT PAIR, INTERACTION=SOIL_ABUT, ADJUST=0.0
 WSOIL_ABUT, WABUT_LH
*CONTACT PAIR, INTERACTION=SOIL_ABUT, ADJUST=0.0
 INSOIL_W_ABUT, WABUT_RH
*CONTACT PAIR, INTERACTION=SOIL_ABUT, ADJUST=0.0
 INSOIL_E_ABUT, EABUT_LH
*CONTACT PAIR, INTERACTION=SOIL_ABUT, ADJUST=7.11E-15
 ESOIL_ABUT, EABUT_RH
```

```
*CONTACT PAIR, INTERACTION=SOIL_ABUT, ADJUST=0.0
 INSOIL_WTOP, WABUT_TIP
*CONTACT PAIR, INTERACTION=SOIL_ABUT, ADJUST=0.0
 INSOIL_ETOP, EABUT_TIP
**
*CONTACT PAIR, INTERACTION=PILE_ROCK, ADJUST=0.0
 WPILEROCK, WPILE_BASE
*CONTACT PAIR, INTERACTION=PILE_ROCK, ADJUST=0.0
 EPILEROCK, EPILE_BASE
**
**----------------------------------MATERIAL DEFINITION----------------------------------
**
******LINEARLY ELASTIC MATERIALS
** Materials incorporating linearly elastic behavior are defined with Young's modulus,
** Poisson's ratio, and a mass density.  Stresses are in Pa, densities are kg/m^3
**
*MATERIAL, NAME=EL_GRAVEL
*ELASTIC
 1.2E+08, 0.4
*DENSITY
 2000.0
**
*MATERIAL, NAME=EL_TILL
*ELASTIC
 8.0E+07, 0.45
*DENSITY
 2200.0
**
*MATERIAL, NAME=EL_CLAY
*ELASTIC
 3.0E+07, 0.499
*DENSITY
 1800.0
**
*MATERIAL, NAME=EL_ROCK
*ELASTIC
 3.5E+09, 0.25
*DENSITY
 2660.0
**
*MATERIAL, NAME=ABUTMENTS
*ELASTIC
 2.8398E+10, 0.11
*DENSITY
 2400.0
**
```

```
*MATERIAL, NAME=GIRDER
*ELASTIC
 2.1214E+10, 0.28
*DENSITY
 1517.4
*EXPANSION
 11.0E-6,
** The *EXPANSION command defines the coefficient of thermal expansion to be used
** in thermal loading of the girder.
**
******NONLINEAR MATERIALS
** Nonlinear materials are defined exactly like elastic materials, but with additional
** parameters.  f and y are defined under the *MOHR COULOMB command in degrees,
** while c is defined with the first parameter in the *MOHR COULOMB HARDENING
** command in Pa.  The second value is always zero.
**
*MATERIAL, NAME=MC_GRAVEL
*ELASTIC
 1.2E+08, 0.4
*DENSITY
 2000.0
*MOHR COULOMB
 45.0, 40.0
*MOHR COULOMB HARDENING
 0.3E+03, 0.0
**
*MATERIAL, NAME=MC_TILL
*ELASTIC
 8.0E+07, 0.45
*DENSITY
 2200.0
*MOHR COULOMB
 35.0, 30.0
*MOHR COULOMB HARDENING
 9.0E+03, 0.0
**
*MATERIAL, NAME=MC_CLAY
*ELASTIC
 3.0E+07, 0.499
*DENSITY
 1800.0
*MOHR COULOMB
 0.001, 0.0
*MOHR COULOMB HARDENING
 35.0E+03, 0.0
**
```

```
*MATERIAL, NAME=MC_ROCK
*ELASTIC
 3.5E+09, 0.25
*DENSITY
 2660.0
*MOHR COULOMB
 26.0, 21.0
*MOHR COULOMB HARDENING
 82.7E+06, 0.0
**
*MATERIAL, NAME=HPILES
*ELASTIC
 2.6782E+10, 0.28
*PLASTIC
 36.998E+06, 0.0
 36.9981E+06, 0.001
 36.9982E+06, 1.0
*DENSITY
 3172.0
** The *PLASTIC command defines the yield stress in Pa.  As it is defined here, the
** yield plateau has a small positive slope, rather than being perfectly horizontal.
**
**--------------------------------------SECTION DEFINITION----------------------------------
**
** The *SOLID SECTION command is used to assign material properties to various
** element sets.
**
*ELSET, ELSET=EL_NATIVE
 WNATIVE_ELASTIC, INNATIVE_ELASTIC, ENATIVE_ELASTIC
*SOLID SECTION, MATERIAL=EL_GRAVEL, ELSET=EL_NATIVE
 1.0
**
*ELSET, ELSET=EL_FILL
 WFILL_ELASTIC, EFILL_ELASTIC
*SOLID SECTION, MATERIAL=EL_GRAVEL, ELSET=EL_FILL
 2.7
**
*ELSET, ELSET=MC_NATIVE
 WNATIVE_MC, INNATIVE_MC, ENATIVE_MC
*SOLID SECTION, MATERIAL=MC_GRAVEL, ELSET=MC_NATIVE
 1.0
**
*ELSET, ELSET=MC_FILL
 WFILL_MC, INFILL_MC, EFILL_MC
*SOLID SECTION, MATERIAL=MC_GRAVEL, ELSET=MC_FILL
 2.7
```

```
**
*SOLID SECTION, MATERIAL=EL_ROCK, ELSET=ROCK_ELASTIC
 1.0
**
*SOLID SECTION, MATERIAL=MC_ROCK, ELSET=ROCK_MC
 1.0
**
*SOLID SECTION, MATERIAL=ABUTMENTS, ELSET=ABUTMENT
 2.7
*SOLID SECTION, MATERIAL=HPILES, ELSET=PILE
 0.346
*SOLID SECTION, MATERIAL=GIRDER, ELSET=GIRDER
 1.0
**
**-------------------------------------INITIAL CONDITIONS---------------------------------
**
** Initial states (displacement, stress, temperature) and amplitude curves are defined
**
*BOUNDARY, FIXED
 LEFT, 1
 RIGHT, 1
 CORNERS, 1
 BASE, 2
** Perimeter nodes of the finite element model are fixed
**
*INITIAL CONDITIONS, TYPE=STRESS, GEOSTATIC
 BEDROCK, 0.0,      0.0,    -104378.4,    -4.0,     0.3333
** Geostatic stress state is applied to bedrock
**
*INITIAL CONDITIONS, TYPE=TEMPERATURE
 GIRDER, 20.0
** Initial (construction) temperature of the girder is set to 20°C
**
*AMPLITUDE, NAME=TEMP_POS, TIME=TOTAL TIME
 4., 1.0, 5., 1.0, 6., 1.2, 7., 1.4,
 8., 1.6, 9., 1.8, 10., 2.0
** This amplitude curve is defined to vary the temperature in the girder with step time
**
*AMPLITUDE, NAME=GRAVITY_EXP, DEFINITION=EQUALLY SPACED,
FIXED INTERVAL=0.05
 0.0, 0.01, 0.01274275, 0.016237767, 0.020691381, 0.026366509, 0.033598183,
0.042813324, 0.054555948, 0.06951928, 0.088586679, 0.112883789, 0.143844989,
0.183298071, 0.233572147, 0.297635144, 0.379269019, 0.483293024, 0.615848211,
0.78475997, 1.0
** This amplitude curve ramps the gravitational forces from zero to the full magnitude
** gradually, instead of all at once.
```

```
**
**----------------------------------------LOAD STEPS----------------------------------------
**
**
*STEP, NLGEOM=YES, EXTRAPOLATION=NO
 STEP 1
** Geometric nonlinearity is accounted for, extrapolation from previous incremental
** solution is not used
**
*STATIC
 0.5
** Static load step, with an initial time increment of 0.5
**
*CONTROLS, PARAMETERS=TIME INCREMENTATION
 8, 10, 9, 16, 10, 6, 20, 8, 8,
 0.5, , , , 0.5, 0.5, 1.5,
*CONTROLS, PARAMETERS=FIELD
 .01, 1
** These parameters are used to improve solution convergence.  They adjust ABAQUS'
** automatic time incrementation, as well as set parameters for satisfying field equations.
**
*BOUNDARY, FIXED, OP=MOD
 WFACE_ANGLE, 1
 EFACE_ANGLE, 1
 ABUTFACES, 1
 ABUTTOPS, 2
 PILEBASES, 2
 PILE_CL, 1
** OP=MOD allows boundary conditions defined in initial conditions section to remain,
** while new boundary conditions are defined.  All structural elements restrained.
**
*DLOAD, AMPLITUDE=GRAVITY_EXP
 ESOIL, GRAV, 9.81, 0., -1., 0.
 WSOIL, GRAV, 9.81, 0., -1., 0.
 INSOIL, GRAV, 9.81, 0., -1., 0.
 BEDROCK, GRAV, 9.81, 0., -1., 0.
** Gravity is applied to soil and bedrock elements.
**
*DSLOAD, AMPLITUDE=GRAVITY_EXP
 SOIL_REACTION, P, 32416.4
** Load to counteract difference in 2.7m and 0.346m wide soil elements in contact with
** each other.
**
*PRINT, PLASTICITY=YES
*END STEP
**
```

```
***
**
*STEP, NLGEOM=YES, EXTRAPOLATION=NO
 STEP 2
*STATIC
*CONTROLS, PARAMETERS=CONSTRAINTS
 0.001
** Adjusts tolerances on constraint equations
**
*BOUNDARY, FIXED, OP=NEW
 WFACE_ANGLE, 1
 EFACE_ANGLE, 1
 LEFT, 1
 RIGHT, 1
 CORNERS, 1
 BASE, 2
 PILE_CL, 1
 ABUTFACES, 1
** OP=NEW clears all existing boundary conditions and redefines them.  Piles and
** abutments allowed to move vertically
**
*CHANGE FRICTION, INTERACTION=SOIL_PILE
*FRICTION
 0.45
*CHANGE FRICTION, INTERACTION=SOIL_ABUT
*FRICTION
 0.45
** Coefficient of friction between soil/piles and soil/abutments is changed from 0.0
**
*DLOAD, AMPLITUDE=GRAVITY_EXP
 PILE, GRAV, 9.81, 0., -1., 0.
 ABUTMENT, GRAV, 9.81, 0., -1., 0.
** Gravity loading applied to piles and abutments
**
*PRINT, PLASTICITY=YES
*END STEP
**
***
**
*STEP, NLGEOM=YES, EXTRAPOLATION=NO
 STEP 3
*STATIC
**
*DLOAD, AMPLITUDE=GRAVITY_EXP
 GIRDER, GRAV, 9.81, 0., -1., 0.
** Gravity loading applied to girder elements
```

```
**
*DSLOAD, AMPLITUDE=GRAVITY_EXP
 TOPGIRDER, P, 6965.0
** Supplemental dead load applied to girder surface
 WSOIL_TOP, P, 3438.6
 ESOIL_TOP, P, 3438.6
** Dead load of pavement applied to approach fill surface
**
*DSLOAD, AMPLITUDE=GRAVITY_EXP
 SOIL_REACTION, P, 2165.04
** Additional reaction force to account for pavement on 2.7m wide soil elements.
**
*PRINT, PLASTICITY=YES
*END STEP
**
***
**
*STEP, NLGEOM=YES, EXTRAPOLATION=NO
 STEP 4
*STATIC
**
*BOUNDARY, FIXED, OP=NEW
 LEFT, 1
 RIGHT, 1
 CORNERS, 1
 BASE, 2
** All structural elements released and allowed to come to equilibrium
**
*PRINT, PLASTICITY=YES
**
*END STEP
**
***
**
*STEP, NLGEOM=YES, EXTRAPOLATION=NO
 STEP 5
*STATIC
 1.0, 6.0, , 1.0
** Static load step, with an initial time increment of 1.0, lasting for 6 increments.
**
*CONTROLS, PARAMETERS=TIME INCREMENTATION
 8, 10, 9, 16, 10, 6, 20, 5, 5,
 0.5, , , , 0.5, 0.5, 1.5,
*TEMPERATURE, AMPLITUDE=TEMP_POS
 GIRDER, 20.0
** Temperature is varied with time increment, according to amplitude curve
```

```
*PRINT, PLASTICITY=YES
*END STEP
**
***
**
*STEP, NLGEOM=YES, EXTRAPOLATION=NO
 STEP 6
*STATIC
**
** This step provides data for the DL+T load case (Load Case #3)
** No loading takes place in this step.  Requests for nodal, element, and contact surface
** data are made
**
*PRINT, PLASTICITY=YES
**
*CONTACT PRINT, SUMMARY=YES, FREQUENCY=1
 CSTRESS, CDISP
** Shear and normal stresses, surface openings, and relative tangential displacements.
*CONTACT PRINT, SUMMARY=YES, FREQUENCY=1
 CFN, CFS
** Total normal and shear forces on surface
*CONTACT PRINT, SUMMARY=YES, FREQUENCY=1
 XN, XS, CAREA
** Centers of total normal and shear forces, total area of surface in contact.
**
*NODE PRINT, NSET=PILE_CL, FREQUENCY=1
 U1, U2, COOR1, COOR2
** Displacements in horizontal and vertical directions, X & Y coordinates of nodes
*NODE PRINT, NSET=PILETOPS, FREQUENCY=1
 U1, U2, COOR1, COOR2
*NODE PRINT, NSET=PILEBASES, FREQUENCY=1
 U1, U2, COOR1, COOR2
*NODE PRINT, NSET=GIRDER_TOP, FREQUENCY=1
 U1, U2, COOR1, COOR2
*NODE PRINT, NSET=APPROACHES, FREQUENCY=1
 U1, U2, COOR1, COOR2
*NODE PRINT, NSET=ABUTFACES, FREQUENCY=1
 U1, U2, COOR1, COOR2
*NODE PRINT, NSET=BACKWALLS, FREQUENCY=1
 U1, U2, COOR1, COOR2
**
*EL PRINT, ELSET=PILE, POSITION=AVERAGED AT NODES, FREQUENCY=1
 S, SP
** All stress and principle stress components, extrapolated to nodes of the elements
*EL PRINT, ELSET=PILE, POSITION=INTEGRATION POINTS, FREQUENCY=1
 S, SP
```

```
** All stress and principle stress components, at integration points of the elements
*EL PRINT, ELSET=PILE, POSITION=AVERAGED AT NODES, FREQUENCY=1
 E, EP
** All strain and principle strain components, extrapolated to nodes of the elements
*EL PRINT, ELSET=PILE, POSITION=INTEGRATION POINTS, FREQUENCY=1
 E, EP
** All strain and principle strain components, at integration points of the elements
*EL PRINT, ELSET=PILE, POSITION=AVERAGED AT NODES, FREQUENCY=1
 PE
** All plastic strain components, extrapolated to nodes of the elements
*EL PRINT, ELSET=PILE, POSITION=INTEGRATION POINTS, FREQUENCY=1
 PE
** All plastic strain components, at integration points of the elements
**
*END STEP
**
***
**
*STEP, NLGEOM=YES, EXTRAPOLATION=NO
 STEP 7
*STATIC
 0.25
** Static load step, with an initial time increment of 0.25
**
*CLOAD
 17814, 2, -21750.0
 17815, 2, -50750.0
 17819, 2, -72500.0
 17839, 2, -12250.0
 17840, 2, -5250.0
** HL-93 axle loads applied at nodes of the girder with 0.5 DF.  Where axles fell
** between nodes, equivalent loading was placed on adjacent nodes.
**
*DSLOAD
 TOPGIRDER, P, 4650.0
** HL-93 LANE LOAD WITH 0.5 DISTRIBUTION FACTOR
**
*PRINT, PLASTICITY=YES
**
** Output from last step is suppressed for this step in order to reduce memory demand
*CONTACT PRINT, SUMMARY=YES, FREQUENCY=0
 CSTRESS, CDISP
*CONTACT PRINT, SUMMARY=YES, FREQUENCY=0
 CFN, CFS
*CONTACT PRINT, SUMMARY=YES, FREQUENCY=0
 XN, XS, CAREA
```

```
**
*NODE PRINT, NSET=PILE_CL, FREQUENCY=0
 U1, U2, COOR1, COOR2
*NODE PRINT, NSET=PILETOPS, FREQUENCY=0
 U1, U2, COOR1, COOR2
*NODE PRINT, NSET=PILEBASES, FREQUENCY=0
 U1, U2, COOR1, COOR2
*NODE PRINT, NSET=GIRDER_TOP, FREQUENCY=0
 U1, U2, COOR1, COOR2
*NODE PRINT, NSET=APPROACHES, FREQUENCY=0
 U1, U2, COOR1, COOR2
*NODE PRINT, NSET=ABUTFACES, FREQUENCY=0
 U1, U2, COOR1, COOR2
*NODE PRINT, NSET=BACKWALLS, FREQUENCY=0
 U1, U2, COOR1, COOR2
**
*EL PRINT, ELSET=PILE, POSITION=AVERAGED AT NODES, FREQUENCY=0
 S, SP
*EL PRINT, ELSET=PILE, POSITION=INTEGRATION POINTS, FREQUENCY=0
 S, SP
*EL PRINT, ELSET=PILE, POSITION=AVERAGED AT NODES, FREQUENCY=0
 E, EP
*EL PRINT, ELSET=PILE, POSITION=INTEGRATION POINTS, FREQUENCY=0
 E, EP
*EL PRINT, ELSET=PILE, POSITION=AVERAGED AT NODES, FREQUENCY=0
 PE
*EL PRINT, ELSET=PILE, POSITION=INTEGRATION POINTS, FREQUENCY=0
 PE
**
*END STEP
**
***
**
*STEP, NLGEOM=YES, EXTRAPOLATION=NO
 STEP 8
*STATIC
**
** This step provides data for the DL, LL,+T load case (Load Case #5)
** No loading takes place in this step.  Requests for nodal, element, and contact surface
** data are made
**
*PRINT, PLASTICITY=YES
**
*CONTACT PRINT, SUMMARY=YES, FREQUENCY=1
 CSTRESS, CDISP
*CONTACT PRINT, SUMMARY=YES, FREQUENCY=1
```

```
 CFN, CFS
*CONTACT PRINT, SUMMARY=YES, FREQUENCY=1
 XN, XS, CAREA
**
*NODE PRINT, NSET=PILE_CL, FREQUENCY=1
 U1, U2, COOR1, COOR2
*NODE PRINT, NSET=PILETOPS, FREQUENCY=1
 U1, U2, COOR1, COOR2
*NODE PRINT, NSET=PILEBASES, FREQUENCY=1
 U1, U2, COOR1, COOR2
*NODE PRINT, NSET=GIRDER_TOP, FREQUENCY=1
 U1, U2, COOR1, COOR2
*NODE PRINT, NSET=APPROACHES, FREQUENCY=1
 U1, U2, COOR1, COOR2
*NODE PRINT, NSET=ABUTFACES, FREQUENCY=1
 U1, U2, COOR1, COOR2
*NODE PRINT, NSET=BACKWALLS, FREQUENCY=1
 U1, U2, COOR1, COOR2
**
*EL PRINT, ELSET=PILE, POSITION=AVERAGED AT NODES, FREQUENCY=1
 S, SP
*EL PRINT, ELSET=PILE, POSITION=INTEGRATION POINTS, FREQUENCY=1
 S, SP
*EL PRINT, ELSET=PILE, POSITION=AVERAGED AT NODES, FREQUENCY=1
 E, EP
*EL PRINT, ELSET=PILE, POSITION=INTEGRATION POINTS, FREQUENCY=1
 E, EP
*EL PRINT, ELSET=PILE, POSITION=AVERAGED AT NODES, FREQUENCY=1
 PE
*EL PRINT, ELSET=PILE, POSITION=INTEGRATION POINTS, FREQUENCY=1
 PE
**
*END STEP
**
**Analysis complete
```

Appendix B

DESIGN EXAMPLE

Given: Single span, steel girder bridge with fixed-head integral abutment

Span length: 32 m (105 ft)

Skew: 0°

Girder and pile spacing: 2.5 m (8 ft)

Abutment height: 3 m (10 ft)

Abutment wall thickness: 750 mm (2.5 ft)

Depth to bedrock (pile length): 2.5 m (8 ft)

General subsurface category: Sand & Gravel

Step 1: Check adequacy of pile using Procedure 5-4 from the MDOT Bridge Design Guide (1999).

If the conditions of Procedure 5-4 are not satisfied, continue to Step 2. If the conditions of Procedure 5-4 are met, then no further steps are required. For the given parameters, Procedure 5-4 determines whether the proposed integral abutment bridge can be supported on H-piles, or whether the pile length is less than the minimum embedment length required for any of the "preferred" pile sections.

Step 2: Determine M_D and M_{DL} from values of P_D and P_{DL}.

The vertical pile loads from Procedure 5-4 are:

Dead load superstructure reaction: 295 kN

Live load superstructure reaction (including impact): 205 kN

Abutment dead load: 0.75 m * 3.0 m * 2.5 m * 23.5 kN/m^3 = 132 kN

Pile dead load (assume HP 360x132) 1.3 kN/m * 2 m = 3 kN

P_D = 295 kN + 132 kN + 3 kN = 430 kN

P_{DL} = 295 kN + 205 kN + 132 kN + 3 kN = 635 kN

Using Figures 5.2 and 5.3 in Chapter 5, the following pile head moment are determined for various pile sections as shown in Table B.1.

Table B.1. Calculated Pile Head Moments for Example Problem

Pile Section	M_D (kN-m)	M_{DL} (kN-m)
HP 310x79 (HP 12x53)	75	-
HP 360x108 (HP 14x73)	105	165
HP 360x132 (HP 14x89)	120	190

A value of M_{DL} was not able to be determined for the HP 310x79 section, because the yield moment is exceeded. Therefore, either the HP 360x108 or 360x132 sections are suitable for support of the bridge.

Step 3: Determine the additional pile head moment due to negative temperature change.

From Table 5.4, the moment correction factors for HP 360x108 and 360x132 piles in sand and gravel are 0.61 and 0.67 kN-m/°C, respectively. The resulting pile head moments in each pile section due to a 55 °C negative temperature change are given below.

For HP 360x108:

M_{DT} = 105 kN-m + (0.61 kN-m/°C) * 55 °C = 138 kN-m

M_{DLT} = 165 kN-m + (0.61 kN-m/°C) * 55 °C = 198 kN-m

For HP 360x132:

M_{DT} = 120 kN-m + (0.67 kN-m/°C) * 55 °C = 157 kN-m

M_{DLT} = 190 kN-m + (0.67 kN-m/°C) * 55 °C = 227 kN-m

Step 4: Compare M_{DLT} to M_y for the pile section.

The moments in the head of the pile are limited to 1.15 * M_y under dead, live, and thermal loading. M_y for each pile section is calculated by multiplying the yield stress (345 MPa) by the section modulus for the plane of bending. Table B.2 compares M_{DLT} and M_y for both pile sections.

Table B.2. Comparison of M_{LT} to M_y for Example Problem

Pile Section	Section Modulus (mm^3)	M_{DLT} (kN-m)	M_y (kN-m)	M_{DLT} / M_y
HP 360x108 (HP 14x73)	586657	198	202.4	98%
HP 360x132 (HP 14x89)	725947	227	250.3	91%

Both sections meet the $M_{DLT} \leq 1.15 * M_y$ criterion. Furthermore, the moment in the most severe loading case for both pile sections will remain below M_y, and therefore yielding of the pile will be less likely to occur.

Step 5: Calculate V_{DT} and V_{DLT}.

The coefficients for the shear at the pile tip calculated from M_{DT} and M_{DLT} are taken from Table 5.5. For a 2.5 m long pile in sand and gravel, β_1 and β_2 are equal to 3.12 and 1.95, respectively.

For HP 360x108:

V_{DT} = (138 kN-m * 3.12) / 2.5 m = 172 kN

V_{DLT} = (198 kN-m * 1.95) / 2.5 m = 154 kN

For HP 360x132:

V_{DT} = (157 kN-m * 3.12) / 2.5 m = 196 kN

V_{DLT} = (227 kN-m * 1.95) / 2.5 m = 177 kN

Step 6: Calculate ratio of shear force to axial load.

For HP 360x108:

V_{DT} / P_D = 172 kN / 430 kN = 0.40

V_{DLT} / P_{DL} = 154 kN / 635 kN = 0.24

For HP 360x132:

V_{DT} / P_D = 196 kN / 430 kN = 0.45

V_{DLT} / P_{DL} = 177 kN / 635 kN = 0.28

For both pile sections, the case where the pile is subjected to dead and thermal loading is the controlling case.

Step 7: Verify assumption of pinned support at pile tip.

Since there is insufficient information about the bedrock in the area of the piles, the factor of safety can be conservatively taken as 1.75. For a steel H-pile with a driving point on intact bedrock, μ can be taken as 0.7.

For HP 360x108:

$0.7 / 1.75 = 0.4 \geq 0.4$ - OK

For HP 360x132:

$0.7 / 1.75 = 0.4 \leq 0.45$ - Not acceptable

Based on the friction criteria at the pile tip, the pinned support assumption at the tip of an HP 360x132 section is not valid. Therefore, a HP 360x108 section should be used

BIOGRAPHY OF THE AUTHOR

The sky on the afternoon of October 1, 1979 was dark and ominous. Amid the cacophony of a merciless thunderstorm in Stoughton, Mass., there was joyous celebration as John G. DeLano sprung forth from his mother's womb. After sending numerous preschool, elementary, and junior high school teachers to an early retirement, John began matriculation at Sacred Heart High School in Kingston, MA. Four years and numerous yardstick ruler beatings later, he graduated with honors in 1998.

Shortly thereafter, a committee escorted him to the northern border of Massachusetts to give him a fond farewell, and to ensure that he would never return. He enrolled at the University of Maine in the formidable Civil Engineering program. Utilizing his ninja training, he was able to infiltrate the Tau Beta Pi and Chi Epsilon honors societies. Defying all logic and laws of thermodynamics, John graduated summa cum laude with a Bachelor's degree in Civil Engineering, as the departmental valedictorian in 2002.

After only having a week to recuperate from his post-graduation hangover, he was kidnapped by Tom Sandford and Bill Davids, and whisked away to Boardman Hall to become a part of the graduate program in Civil Engineering. There, he was chained to a desk until the present time, only being released to attend classes and crash into things on his mountain bike. He plans to use his knowledge of geotechnical engineering to tunnel back into Massachusetts undetected.

John is a candidate for a Master of Science degree in Civil Engineering from The University of Maine in May, 2004.